Proteasomal Degradation of the APP Intracellular Domain (AICD) and Regulation of its Nuclear Signaling

Dissertation

zur
Erlangung der naturwissenschaftlichen Doktorwürde
(Dr. sc. nat.)
vorgelegt der
Mathematisch-naturwissenschaftlichen Fakultät
der
Universität Zürich

von

Manuel Tobias Gersbacher

aus Deutschland

Promotionskomitee
Prof. Dr. Roger M. Nitsch (Vorsitz, Leitung der Dissertation)
Dr. Uwe Konietzko (Leitung der Dissertation)
Prof. Dr. Stephan C.F. Neuhauss

Zürich, 2015

Abstract

Alzheimer's disease is a neurodegenerative disorder and the most common cause of dementia. No treatment to halt or slow the progressive cognitive decline observed in Alzheimer's disease patients is available. A better understanding of the disease mechanism is urgently needed to further improve diagnosis and develop novel treatment strategies. The amyloid precursor protein (APP) and its processing are central to the pathology of Alzheimer's disease. APP is a transmembrane protein that is cleaved into various peptide fragments, including Aβ and the APP intracellular domain (AICD). Increased Aβ secretion and aggregation is thought to trigger a cascade of toxic events that eventually results in the development of Alzheimer's disease. AICD, in turn, is transcriptionally active and is involved in neurogenesis as well as apoptosis, however, its regulation and functional role remain poorly understood.

The aim of this thesis is to gain molecular and mechanistic insights into the regulation and function of AICD and shed light on a potential contribution of AICD to the pathology of Alzheimer's disease.

In the first results part of this thesis, chapter 3, I analyze nuclear localization of the intracellular domains of APP and its homologues, APP-like protein 1 and 2 (APLP1 and APLP2). As APP, APLP1 and APLP2 undergo proteolytic processing and release intracellular domains. I demonstrate that, similar to AICD, the intracellular domain of APLP2 forms, together with the adaptor protein Fe65 and the histone acetyltransferase Tip60, spherical nuclear complexes (AFT-complexes), which are thought to be transcriptionally active. In contrast, the intracellular domain of APLP1, despite binding to Fe65, does not translocate to the nucleus. I further show that the intracellular domains of APP and APLP1 are degraded by the proteasome and that the N-terminal amino acids of the intracellular domains determine its degradation rates. Together, these results suggest that different nuclear signaling capabilities of APP and its homologues are due to different rates of full-length protein processing and proteasomal degradation of intracellular domains. These results provide evidence in support of a common nuclear signaling function for APP and APLP2 that is absent in APLP1.

The results presented in chapter 3 uncover a novel aspect of AICD regulation, the degradation by the ubiquitin-proteasome system. Therefore, I analyze in chapter 4 the proteasomal degradation of different AICD species. AICD species of different lengths are generated by processing of APP. Interestingly, various mutations that result in the development of Alzheimer's disease are known to cause a shift from shorter AICD50 to longer AICD51. Here, I show that AICD species undergo different proteasomal degradations. Extensive biochemical

analyses reveal that the proteasomal degradation of AICD is independent of ubiquitination. These results show that the identity of the N-terminal of AICD is crucial for proteasomal degradation and argue for an N-end rule-like degradation of AICD. Further, I provide evidence for a different proteasomal degradation of AICD species by Alzheimer's disease-causing mutations, which may result in altered transcriptional regulation and may contribute to the disease progression.

In chapter 5, I present a novel transgenic mouse line for studying regulation and function of AICD *in vivo*. This mouse line expresses an APP transgene fused to the Gal4 DNA binding domain (APPGal4 line). After crossing the APPGal4 line to a UAS-reporter mouse line, the spatiotemporal pattern of transcriptional activity of AICD in the mouse brain can be analyzed. Using immunocytochemical analysis of primary neurons, I validate the functionality of the APPGal4 mice. In this course, I also underline nuclear signaling and the transcriptional activity of AICD experimentally.

Zusammenfassung

Die Alzheimer-Krankheit ist eine degenerative Erkrankung des Gehirns und die häufigste Ursache für die Entwicklung von Demenz. Gegenwärtig gibt es keine Behandlungsmöglichkeiten welche die kognitive Verschlechterung der Betroffenen eindämmen oder gar aufhalten. Um eine bessere Diagnose und neue Behandlungswege zu entwickeln, ist es unerlässlich, ein besseres Verständnis des pathologischen Mechanismus der Krankheit zu bekommen. Eine zentrale Rolle in der Pathologie der Alzheimer-Krankheit spielt das amyloid precursor protein (APP). APP ist ein Intermembranprotein, das in mehrere Peptidfragmente zerteilt wird. Diese beinhalten unter anderem Aβ und die Intrazellulardomäne AICD (APP intracellular domain). Es wird angenommen, dass erhöhte Sekretion und Aggregation von Aβ eine Reihe toxischer Effekte bedingt, die letztendlich zu der Entwicklung der Alzheimer-Krankheit führen. AICD hingegen ist ein Regulator von Genexpression, und es wurde aufgezeigt, dass AICD eine Rolle in der Neurogenese und Apoptose spielt. Dennoch ist unser Wissen über die Regulierung und Funktion von AICD nur bruchstückhaft.

Das Ziel dieser Doktorarbeit ist es, ein besseres Verständnis für die Regulierung und Funktion von AICD zu gewinnen. Des Weiteren soll untersucht werden ob AICD möglicherweise zur Pathologie der Alzheimer-Krankheit beitragen könnte.

Im ersten Ergebnisteil dieser Doktorarbeit, dies ist Kapitel 3, untersuche ich die Zellkernlokalisierung der Intrazellulardomänen von APP und der APP homologen Proteine APLP1 (APP-like protein 1) und APLP2 (APP-like protein 2). APLP1 und APLP2 werden ähnlich wie APP geschnitten und setzen ebenfalls Intrazellulardomänen frei. Ich zeige, dass die Intrazellulardomäne von APLP2 ebenso wie jene von APP, gemeinsam mit dem Adaptarprotein Fe65 und der Histonacetyltransferase Tip60, kugelförmige nukleare Komplexe bildet (AFT-Komplexe), von welchen angenommen wird, dass sie transkriptionelle Funktionen erfüllen. Im Gegensatz zu APP und APLP2 wird die Intrazellulardomäne von APLP1 nicht in den Kern transportiert, obwohl auch APLP1 an Fe65 bindet. Des Weiteren zeige ich, dass die Intrazellulardomänen von APP und APLP1 von dem Proteasom abgebaut werden, und dass die N-terminalen Aminosäuren der Intrazellulardomänen die Degradationsrate des jeweiligen Peptids bestimmen. Zusammengenommen deuten diese Resultate darauf hin, dass das unterschiedlichen Vermögen von APP und seinen homologen Proteinen, Kernsignale zu entsenden, durch unterschiedliche Raten der Prozessierung und der Degradation bedingt wird. Diese Resultate unterstützen die Idee einer

gemeinsamen Kernsignalfunktion von APP und APLP2, die nicht in APLP1 vorhanden ist.

Die im Kapitel 3 zum ersten Mal beschriebene Regulierung von AICD durch das Ubiquitin-Proteasom-System veranlassen mich dazu, diese Regulierung weitergehend zu analysieren. Daher untersuche ich in Kapitel 4 die proteasomale Degradation unterschiedlicher AICD Spezies, die von APP abgespalten werden und sich in ihrer Länge unterscheiden. Es ist wichtig anzumerken, dass viele Mutationen die zur Entwicklung der Alzheimer-Krankheit führen auch zu einer veränderten Produktion von AICD Spezies führen. Dies bedeutet, dass vermehrt längeres AICD51 produziert wird, wohingegen die Produktion von kürzerem AICD50 zurückgeht. Ich zeige hier, dass AICD Spezies unterschiedlich von dem Proteasom degradiert werden. Weitergehende biochemischen Analysen machen deutlich, dass die Degradation von AICD nicht abhängig von dessen Ubiquitinierung ist. Diese Resultate zeigen, dass die N-terminalen Aminosäuren entscheidend für die Degradation sind und deuten darauf hin, dass ein N-end-rule-ähnlicher Mechanismus für die Degradation von AICD verantwortlich ist. Des Weiteren präsentiere ich Anhaltspunkte für eine unterschiedliche Degradation von AICD durch Alzheimer-Krankheit auslösende Mutationen. Diese Veränderungen können zu einer veränderten Genregulierung führen und auf diese Weise möglicherweise zum Voranschreiten der Alzheimer-Krankheit beitragen.

In Kapitel 5 präsentiere ich eine neue transgene Mauslinie, die es erlauben soll, die Funktionen von AICD *in vivo* zu untersuchen. Die APPGal4 Mauslinie exprimiert APP, das an die DNA-Bindedomäne Gal4 gekoppelt ist. Nach Verpaarung der APPGal4 Mauslinie mit einer UAS-Reporter Mauslinie soll das raumzeitliche Muster der transkriptionellen Aktivität von AICD im Mausgehirn untersucht werden können. Ich zeige hier die Funktionalität der APPGal4 Mauslinie mit Hilfe von immunozytochemischen Analysen primärer Neuronen auf. In diesem Zusammenhang bekräftige ich auch experimentell die Zellkernlokalisierung und transkriptionelle Funktion von AICD.

Contents

Illustrations

Figures

Tables

Abbreviations

Aβ	amyloid-β
AcD	activation domain
AD	Alzheimer's disease
ADAD	autosomal-dominant Alzheimer's disease
AICD	APP intracellular domain
AL1ICD	APLP1 intracellular domain
AL2ICD	APLP2 intracellular domain
APLP1	amyloid precursor-like protein 1
APLP2	amyloid precursor-like protein 2
APLPs	amyloid precursor-like proteins, i.e., APLP1 and APLP2
APP	amyloid precursor protein
AU	arbitrary unit
bp	base pair
C83	α-secretase processing–derived CTF
C99	β-secretase processing–derived CTF
CTF	C-terminal fragment
DBD	DNA binding domain
DIC	differential interference contrast
DIV	days *in vitro*
DUBs	deubiquitinating enzymes
FAD	familial Alzheimer's disease
ICD	intracellular domain
IDE	insulin degrading enzyme
IDR	intrinsically disordered regions
MEFs	mouse embryonic fibroblasts
NFTs	neurofibrillary tangles
POI	protein of interest
PSEN1	presenilin 1
PSEN2	presenilin 2
PTM	post-translational modification
RIP	regulated intramembrane proteolysis
RT	room temperature
SDM	site-directed mutagenesis
UAS	upstream activating sequence
Ub	ubiquitin
UBL	ubiquitin-like protein
UPS	ubiquitin-proteasome system

1 Introduction

1.1 Alzheimer's disease

Alzheimer's disease (AD) is a chronic and progressive degenerative disorder of the brain. Symptoms of AD are typically impairments of cognitive functions including memory and language deficits in the early stages of the disease. In the course of the disease further symptoms are observed, such as executive dysfunction, behavioral disturbances, and psychiatric symptoms, including depression, together strongly impeding activities of daily living of patients (Alzheimer's Association, 2015). As the disease progresses—diagnostic criteria differentiate three consecutive stages: mild, moderate, and severe disease—activities of daily living of AD patients become increasingly impaired, thus requiring also a increasing amount of assistance. At severe stages, full dependence on assistance is required.

1.1.1 Diagnosis and prevalence of Alzheimer's disease

To identify the development of AD as early as possible, the International Work Group (IWG), a working group of twenty-four clinician-researcher led by Bruno Dubois, has suggested a set of criteria for the diagnosis of AD (Cummings et al., 2013). In addition to the necessary core diagnostic criterion, which is an early and significant episodic memory impairment, one or more supportive features must be met to diagnose probable AD. These supportive features are: (i) presence of medial temporal lobe atrophy, (ii) abnormal cerebrospinal fluid biomarkers including but not restricted to Aβ and tau, (iii) a specific pattern in functional neuroimaging with PET such as glucose metabolism and amyloid imaging, and (iv) proven AD autosomal-dominant mutations. However, a definitive diagnosis of the disease can still only be made post-mortem.

Besides the emotional burden for patients and relatives, AD equally is a financial burden to caregivers and the healthcare system. As of 2012, worldwide prevalence is estimated to be as high as twenty-four million people (Mayeux

and Stern, 2012).[1] More than 5 % of people aged sixty-five years or older are suffering from AD, and the prevalence rises with age, thus affecting nearly one forth of the people aged ninety years or older (Bachman et al., 1992). The latest World Alzheimer report on the global economic impact of AD estimated global cost of AD and other dementias to be approximately US$ 600 billion annually (Wimo and Prince, 2010). The increase in world population accompanied by global population aging is expected to lead to a dramatic increase in AD incidences and related costs in the future. Therefore, it is alarming that currently no treatment for AD is available. Available medications are only symptomatic but do not halt or at least slow disease progression (Broadstock et al., 2014). Over the last decade, multiple compounds have failed in clinical studies because of unacceptable safety profile or lack of beneficial effects (Karran et al., 2011; Doody et al., 2013). A current clinical study of a new compound has shown to be beneficial and thus raised hopes for a treatment within reach.[2] Nevertheless, it is clear that for both, better diagnosis and treatment, a clear understanding of the disease mechanism is required.

1.1.2 Neuropathology of Alzheimer's disease

Cerebral atrophy accompanied by dilation of the lateral ventricles is the characteristic macroscopic abnormality observed in the brains of AD patients (Mott and Hulette, 2005). Loss of brain volume due to neuronal loss predominantly takes place in brain regions responsible for memory functions and thus reflects the clinical symptoms observed. Earliest degeneration is observed in the entorhinal cortex, a region critical for the formation of new memories (Tapiola et al., 2008). As the disease progresses, atrophy in other brain regions, such as hippocampus and cortex, is observed (Perl, 2010). The two cardinal histopathological feature of AD visible in microscopic inspection are extracellular neuritic plaques and neurofibrillary tangles (NFTs). Neuritic plaques—also called senile or amyloid plaques—are protein deposits predominantly composed of aggregated form of amyloid-β (Aβ). Aβ develops a β-pleated sheet conformation in plaques, which is then typically extending to reach a size of 10–160 μm. Amyloid plaques are found in most of the neocortex but, interestingly, entorhinal cortex and hippocampus are relatively spared (Braak and

[1] A report of the Alzheimer's Association estimated that currently (i.e. 2015) approximately 5.3 million people live with AD in the USA (Alzheimer's Association, 2015). More recent estimates of global prevalence are not available.

[2] Results of the clinical phase 1b study of BIIB37 were presented by Jeffrey Sevigny at the 12th International Conference on Alzheimer's and Parkinson's Diseases and Related Neurological Disorders (AD/PD) held in Nice, France (March 18–22, 2015).

Braak, 1997). NFTs are predominantly composed of paired helical filaments of hyperphosphorylated forms of the microtubule-associated protein tau. NFTs are mainly observed in the entorhinal cortex, hippocampus, amygdala, and neocortex (Perl, 2010).

1.1.3 Genetic disposition and risk factors for Alzheimer's disease

The greatest risk factor for developing AD is aging. However, our understanding what aging (and healthy aging) means in a complex biological system and how this influences the development of AD remains fragmentary—and moreover no cure for aging was found (Fontana et al., 2014). Nevertheless, aging alone is not sufficient to cause AD and different factors predispose for the development of AD.

Approximately 300 autosomal-dominant mutations are known that cause AD, which is thus also referred to as autosomal-dominant Alzheimer's disease (ADAD; Bateman et al., 2011). All described mutations are restricted to the coding regions of three genes, which encode the amyloid precursor protein (APP), presenilin 1 (PSEN1), and presenilin 2 (PSEN2), commonly referred to as familial Alzheimer's disease (FAD) mutations.[3] APP, as indicated by the name, is the precursor protein of Aβ, whereas later is derived from former by proteolytic processing. PSEN1 and PSEN2 are aspartic proteases and are the catalytic core of proteolytic-active γ-secretase complexes—shortly referred to as γ-secretase. γ-secretase is a major secretase for regulated intramembrane proteolysis (RIP) and, importantly, responsible for the final cleavage of APP, resulting in the release of Aβ. FAD mutations are characterized by a predominantly early onset of AD symptoms, generally between the age of thirty and fifty years.[4] However, it should be noted that autosomal-dominant mutations are described that have a mean late onset, and the mean age-of-onset of a mutation even within a given family can vary considerably (Ryman et al., 2014). Autosomal-dominant mutations causing AD are rare, and it is estimated that ADAD accounts for less than 1 % of all AD cases (Bateman et al., 2011).

The vast majority of AD (i.e., > 99 %) is not caused by autosomal-dominant mutations. Both genetic and environmental risk-factors have been identified

[3] The term FAD mutations will be used for autosomal-dominant mutations in *APP* and the presenilins. However, it should be noted, as pointed out by Bateman et al. (2011), that FAD may also be caused by other means than autosomal-dominant mutations as for example the ϵ4 allele of *ApoE*.

[4] Early onset of AD is generally defined as appearance of symptoms before the age of sixty-five. Correspondingly, appearance of disease symptoms in people of age sixty-five and older is described as late onset. Accordingly, the terms early-onset AD (EOAD) and late-onset AD (LOAD) are used.

that are causative for these cases of AD. The ϵ4 allele of the apolipoprotein E (*ApoE*) gene is the strongest identified genetic risk factor and also the most repeatedly confirmed one. Heterozygous and homozygous carriers of the ϵ4 allele have a three- and twelve-fold, respectively, increased risk to develop AD compared to ϵ3 allele carriers. However, mechanistically, the role of the ApoE protein remains enigmatic. Besides the ϵ4 allele of *ApoE*, large cohort genome-wide association studies (GWAS) have identified over three dozen potential susceptibility loci for AD (Bertram, 2011). However, the risk conferred by these susceptibility loci is small, and consistent replication of these results is missing (Bertram and Tanzi, 2009).[5] In contrast to mutations in *APP* and the presenilins, genetic risk factors, including the ApoE ϵ4 variant, only increase the risk to develop the disease but are not sufficient to cause it. Other causes that have been reported to increase the risk for AD include environmental factors (e.g., exposure to toxins such as DDT), vascular risk factors, diabetes, and cholesterol levels (Alzheimer's Association, 2014). Similar to the identified genetic risk factors, the list of environmental risk factors is long (and growing) but the conferred susceptibility not high.

Together, our current knowledge suggests that non-ADAD is caused by a combination of multiple genetical and environmental factors that individually have only a small risk but mutually act towards AD. Thus, it is evident that general pathological mechanisms must be identified to allow the development of efficient treatments. Although genetically and etiologically AD appears to be a dichotomous disease—autosomal-dominant mutations on one hand; a multitude of risk factors with low susceptibility on the other—phenotypically and clinically the disease is highly similar, and mostly, except for the age-of-onset, indistinguishable (Selkoe, 2001). Therefore, ADAD is, despite its low incidence, a critically important area of study.

1.1.4 The amyloid cascade hypothesis

The observations that Aβ is the main component of amyloid plaques found in the brains of people suffering from AD, and that mutations in *APP* and its processing enzymes result in autosomal-dominant form of AD have led to the formulation of the amyloid cascade hypothesis (Hardy and Higgins, 1992; Selkoe, 2001; Hardy and Selkoe, 2002). The amyloid cascade hypothesis states that a series of events, starting with Aβ, eventually results in the neuronal degeneration and cognitive decline observed in patients suffering from AD. Increased levels or altered composition of Aβ oligomers act as trigger for

[5] For a regularly updated collection of identified risk factors for AD visit the AlzRisk AD Epidemiology Database under `http://www.alzrisk.org`.

the cascade by exerting its toxicity on synapses. The raised and sustained inflammatory response, by means of activation of microglia and astrocytes, leads to a further progressive synaptic and neuritic injury. In the following, altered neuronal ionic homeostasis sets ground for oxidative injury, which in turn leads to altered kinase activation. Extensive phosphorylation by kinases permits unusual fibrilization of tau and formation of NFTs. These events finally cause a widespread neuritic dysfunction and neuronal cell death, which is clinically reflected by the cognitive impairments observed in AD.

APP processing and thus formation of Aβ takes place also under normal conditions (i.e., in healthy people) without observations of cognitive impairments. Therefore, the amyloid cascade hypothesis further states that a relative increase of longer Aβ42 (i.e., Aβ42-to-Aβ40 ratio), which is more toxic and prone to aggregation than Aβ40, is believed to trigger the cascade. This is also in line with the observation that FAD mutations result in an increased Aβ42-to-Aβ40 ratio. Similarly, AD that is not caused by autosomal-dominant mutations is believed to be also triggered by a relative increase in Aβ42. In this respect, it became evident that also other mechanisms than disturbance of APP processing can results in increased Aβ42-to-Aβ40 ratio, as for example alteration in Aβ metabolism (e.g., decreased degradation of Aβ42). A plethora of studies has supported individual parts of the hypothesis, yet it remains still debated. In particular the role of one of the two cardinal histopathological features of AD and initial premises of the hypothesis, the Aβ plaques, remains elusive.

1.2 The amyloid precursor protein APP

1.2.1 Structure and general features of APP

The amyloid precursor protein (APP), as already lined out, is a central protein in AD, which is also carrying out diverse physiological functions. APP is a type I transmembrane glycoprotein, with a long ectodomain and a short cytoplasmatic domain. The complete structure of APP has yet to be identified, but various distinct folded subdomains in the ectodomain were identified (Müller and Wild, 2013). The N-terminal E1 domain contains a growth-factor-like domain (GFLD), copper-binding domain (CuBD), and Kunitz type protease inhibitor domain (KPI). The more C-terminal, but still extracellular, E2 domain consists of a coiled-coil dimerization motif. Both E1 and E2 domains were shown to play a role in dimerization of APP and might thus influence its processing (Müller and Wild, 2013). APP spans the membrane with a single α-helical

transmembrane domain (TMD), and unlike the ectodomain, the cytoplasmic C-terminus does not fold in a particular structure. In humans APP is encoded by a single gene on chromosome 21q21 (Kang et al., 1987). The eighteen exons of *APP* are alternatively spliced into three major isoforms—APP695, APP751, and APP770.[6] APP is ubiquitously expressed with high expression levels in the brain (Slunt et al., 1994). APP695, which is lacking the KPI domain, is the predominant isoform expressed in neurons. Upon expression APP matures through the constitutive secretory pathway to reach the cell surface (Haass et al., 2012). From the cell surface, APP can be internalized by endocytosis and transported via the endosomal system back to the cell surface or the trans-Golgi network. Degradation of APP can take place via the lysosomal pathway. This complex and manifold trafficking of APP is also closely interconnected with the processing of APP.

1.2.2 Processing of APP

APP is processed by a series of proteolytic cleavage reactions (see figure 1.1 for a schematic presentation of APP processing; Selkoe, 2001). In the non-amyloidogenic pathway, APP is cleaved by α-secretase at the cell surface in the luminal juxtamembrane region, releasing its N-terminal fragment sAPPα into the extracellular space. The remaining membrane-bound C-terminal fragment (CTF) C83, subsequently undergoes RIP by the γ-secretase (Lichtenthaler et al., 2011). This cleavage releases the APP intracellular domain (AICD) into the cytosol and the p3 peptide. Initial cleavage in the amyloidogenic pathway is conducted by the β-secretase BACE1. However, unlike α-secretase cleavage, APP cleavage by BACE1 does not take place at the cell surface, but requires endocytosis of APP. Furthermore, cleavage by BACE1 takes place more distant to the membrane than α-secretase cleavage, thus releasing the slightly shorter sAPPβ. The correspondingly longer CTF C99 then also undergoes RIP by γ-secretase, releasing AICD into the cytosol and the Aβ peptide. It is important to note that, because of different localization of non-amyloidogenic and amyloidogenic processing, cleavage products of the two pathways also differ in their subcellular localization. This applies in particular to AICD, which is identical in the two pathways in terms of its primary sequence, but was shown to exert different functions, likely because of its different localization. Aβ in turn is released into the lumen of endosomes and can subsequently get secreted from the cell. Furthermore, Aβ can form multiple aggregated forms, ranging from dimers to large fibrils, which are part of the amyloid plaques.

[6] The sequence of APP695 isoform will be used as reference for amino acid position throughout this thesis.

Interestingly, γ-secretase cleavage of CTFs displays a certain impreciseness, resulting in the release of Aβ and AICD species of different lengths. For the different Aβ species it was shown that they posses different toxic potential (e.g., Aβ42 is more toxic than Aβ40). In contrast the role of different AICD species remain enigmatic. It also should be noted that even the general processing of APP is not completely understood. In this respect, cleavage by a hitherto unknown enzyme, the η-secretase, was reported recently, which appears to be involved in a novel, different route of APP processing.[7] As yet, it is not clear how η-secretase processing of APP could influence levels of other APP fragments or contribute to AD pathology. However, discovery of the η-secretase clearly emphasizes the complexity of the regulation of APP processing and the need for further research.

1.2.3 Functions of APP and its cleavage products

In addition to the toxic function of Aβ, multiple and diverse physiological functions have been discovered for other APP cleavage products and APP itself (for a comprehensive review of identified APP functions see Zheng and Koo, 2011). In analogy to other type 1 transmembrane proteins such as Notch-1, APP has been proposed to act as a cell surface receptor. Multiple candidate ligands for APP have been identified (e.g., Aβ and F-spondin), and downstream signaling effects of these binding events have been observed, including altered APP processing and binding of downstream molecules to its cytoplasmatic domain. APP can form homo- and hetero-dimers in cis as well as in trans. Particularly, the observed trans-cellular interactions have suggested that APP can act as an adhesion molecule and recent work has shown that this interaction induces presynaptic specialization (Stahl et al., 2014). Multiple studies have shown a role of sAPPα in synaptotrophic and neuroprotective activities (e.g., Mattson et al., 1993). sAPPβ in contrast does not display these functions and could even act toxic (Nikolaev et al., 2009). Analysis of APP knockout mice also underlined the diverse functions of APP and its cleavage products. Loss of APP resulted in various phenotypes in the central and peripheral nervous system. Most notably, APP knockout mice show behavioral deficits and defects in long-term potentiation (LTP; Zheng et al., 1995; Seabrook et al., 1999). Altered spine density was observed in independent studies, although with different outcomes possibly due to different brain regions that were looked at (Bittner

[7] η-secretase processing of APP was presented by Michael Willem at the 12th International Conference on Alzheimer's and Parkinson's Diseases and Related Neurological Disorders (AD/PD) held in Nice, France (March 18–22, 2015), and is as yet (date of submission of this thesis) not published.

et al., 2009; Tyan et al., 2012). Further, APP knockout mice show reduced grip strength, which is likely due to an altered neuromuscular junction that was repeatedly reported. For a comprehensive review of APP knockout mice and their phenotypes see Müller and Zheng (2012).

1.3 The APP intracellular domain AICD

1.3.1 Structure and molecular architecture of AICD

Cleavage of APP by γ-secretase releases its C-terminal domain, also referred to as APP intracellular domain or AICD.[8] AICD is, neither before nor after release by γ-secretase, adopting a stable configuration or structure. However, the forty-eight to fifty amino acid long peptide possesses three well-preserved motifs, which reflect its diverse functions (Müller and Wild, 2013). The most N-terminal motif is the YxxΦ[9] basolateral sorting motif (653YTSI sequence), which was shown to regulate APP trafficking (Kozik et al., 2010). The second motif is the PTE motif within the 667VTPEER sequence. Threonine 668 has been established as the major phosphorylation site of APP and affects processing of APP. Mechanistically, it has been suggested that the prolyl isomerase Pin1 is catalyzing the cis-trans isomerization of the threonine-proline peptide bond. Additionally, binding of 14-3-3γ seems to stabilize binding of other proteins to AICD. The 682YENPTY sequence with a NPxY motif, which is a described internalization signal for membrane proteins is the best studied motif of AICD. The YENPTY domain of AICD is a central protein binding site, which allows binding of adaptor proteins via their phosphotyrosine-binding (PTB) domain. Multiple interactions with PTB-containing proteins have been described, including the Fe65, Mint, Dab, and Jip protein families (Muller et al., 2008). The interaction with the adaptor protein Fe65 has attained special attention because it might execute multiple functions. Fe65 is a multi-domain adaptor protein that is predominantly expressed in the brain, and Fe65 and its family members are essential for brain development (Guenette et al., 2006). Binding of Fe65 to AICD is thought to results in structural changes in both Fe65 and APP, and might thus result in the observed alterations in APP localization and processing and exert transcriptional function. Among the binding partners

[8] Although C-terminal domain and AICD denote the same part of APP, commonly the term *C-terminal domain* is exclusively used for the sequence as long as it is part of APP or CTFs (i.e., before γ-secretase cleavage) while *AICD* commonly denotes the cytoplasmatic protein released after γ-secretase cleavage or the sequence itself.

[9] x denotes any residue and Φ denotes large hydrophobic residue according to Aasland et al. (2002).

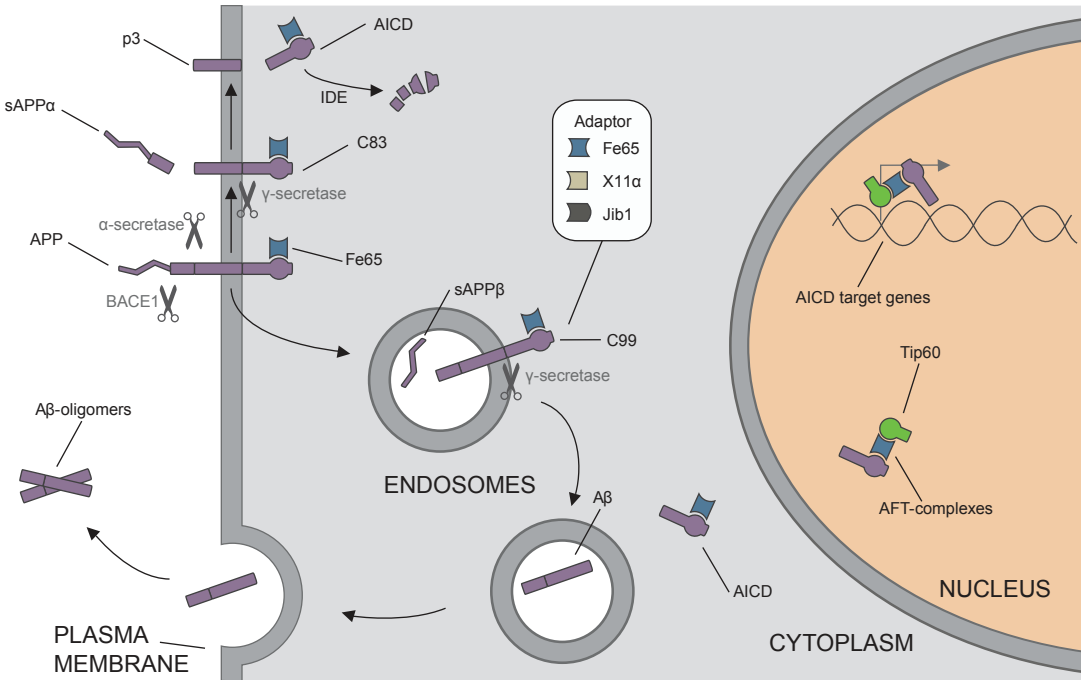

Figure 1.1 Schematic presentation of APP processing, AFT-complex formation, and transcriptional function of AICD. The type 1 transmembrane protein APP is either cleaved by α-secretase and γ-secretase (non-amyloidogenic pathway) or BACE1 and γ-secretase (amyloidogenic pathway). In the non-amyloidogenic pathway that takes place at the membrane, sAPPα is released and the membrane bound C83 is further cleaved to release p3 and AICD. In the amyloidogenic pathway that takes place in endosomes, sAPPβ is released and the membrane bound C99 is further cleaved to release Aβ and AICD. AICD can undergo degradation by the insulin-degrading enzyme (IDE) or form trimeric nuclear complexes with a adaptor protein (e.g., Fe65, X11α or Jib1) and the histone-acetyltransferase Tip60. These AFT-complexes are thought to be transcriptionally active and regulate gene expression.

of AICD, binding to Fe65 is also special because the binding surface stretches along more than the half of the AICD sequence (Radzimanowski et al., 2008).

1.3.2 Functions of AICD

AICD, before and after release by γ-secretase, has been implicated in multiple functions. Binding of Pat1a to AICD for example regulates localization of APP, which in turn was suggested to lead to increased amyloidogenic processing of APP (Kuan et al., 2006). Cao and Sudhof (2001) were the first to show that AICD forms a multimeric complex with Fe65 and the Tat-interacting protein 60 kDa (Tip60) and, importantly, that these complexes are transcriptionally active in luciferase-based UAS/Gal4 assays. Tip60 is a histone-acetyltransferase,

which has been shown to be involved in a variety of signaling pathways including transcriptional regulation, DNA damage repair, and chromatin remodeling (Sapountzi et al., 2006; Sun et al., 2010). Tip60 is predominantly localized in the nucleus, and interaction with AICD-bound Fe65 is believed to take place via the second PTB domain of Fe65. Multiple studies have confirmed the formation of multimeric protein complexes containing AICD, Fe65, and Tip60 (AFT-complexes; von Rotz et al., 2004) and have shown that AFT-complexes co-localize with markers of active transcription (Konietzko et al., 2010). See also figure 1.1 for a schematic presentation of AFT-complex formation and transcriptional function of AICD. The initial observation that AICD is transcriptionally active has triggered the identification of AICD-regulated target genes. To-date approximately thirty genes regulated by AICD have been identified (for a comprehensive list of AICD-regulated genes see Grimm et al., 2013). Some of the identified genes are involved in metabolism of APP and its proteolytic products, such as the β-secretase *BACE1*, the metalloprotease neprilysin (*MME*), which is degrading Aβ, or *APP* itself (Pardossi-Piquard et al., 2005; von Rotz et al., 2004). Regulation of these genes is suggesting that the transcriptional function of AICD is controlling the function of APP and its proteolytic products by various feedback and feedforward mechanisms that could also contribute to the progression of AD. Identification of other genes regulated by AICD, such as the tumor suppressor p53 (*TP53*), the glycogen synthase kinase-3β (GSK3β; *GSK3B*), and the epidermal growth factor receptor receptor (*EGFR*) suggest that AICD has also a function in other signaling pathways as for example apoptosis and cell cycle regulation (Kim et al., 2003; Alves da Costa et al., 2006; Zhang et al., 2007). Nakayama et al. (2008) for example corroborated a role of AICD in apoptosis by showing that AICD expression resulted in increased DNA fragmentation and neuron-specific cell death. Ma et al. (2008) describe also a role of AICD in neurogenesis, but it remains unknown whether this is mediated by the transcriptional function of AICD or by a different mechanism (e.g., inducing structural changes in Fe65). It should be noted that problems have been reported to confirm the regulation of individual genes by AICD, which could partially be explained by usage of different biological systems but might also suggest that AICD transcriptional activity is itself subject to, yet unknown, regulatory mechanism (Hebert et al., 2006; Chen and Selkoe, 2007). Although, it is clear that not all phenotypes reported for APP knockout mice (described above) can be attributed to AICD (because APP knockout mice lack also all other APP-derived proteolytic fragments), an important function of AICD in multiple signaling mechanisms is evident.

1.3.3 Regulation of AICD levels and functions

AICD levels are, as expected for a transcriptional regulator, very low. Half-life was suggested to range from less than 5 min (Cupers et al., 2001) to 35 min (Ring et al., 2007). The fast turnover and its relatively small size have led to technical difficulties in detecting AICD, resulting in mostly usage of AICD overexpression or analysis by usage of *in vitro* assays. Formally, AICD is generated by proteolytic processing by the non-amyloidogenic and amyloidogenic pathway. Since APP processing takes mainly place via the non-amyloidogenic pathway, it is expected that also most AICD is generated from this pathway. However, ample evidence suggests that only AICD generated in the amyloidogenic pathway (β-γ-cleavage) is transcriptional active. Goodger et al. (2009) show that inhibition of β-secretase, but not inhibition of α-secretase, in HEK cells strongly decreases number of AFT-complex-positive cells. Further, they show that BACE KO mouse embryonic fibroblasts (MEFs), in contrast to WT MEFs, fail to produce AFT-complexes. Hoey et al. (2009) similarly show, using a UAS/Gal4-based luciferase assay, that only inhibition of β-secretase activity significantly reduced AICD transcriptional activity. Belyaev et al. (2010) add further functional evidence by showing that regulation of the AICD target-gene NEP is dependent on β-secretase activity and independent of α-secretase activity. Deletion of BACE1 in APP-overexpressing mice resulted in decreased synaptic plasticity as well as performance in learning and memory tasks and AICD was the only APP-derived fragment that correlated with the changes (Ma et al., 2007). So far no study has identified differences in AICD generated from the amyloidogenic and non-amyloidogenic pathways, and we have to assume that the primary AICD sequence generated from the two pathways is the same. Therefore, it is assumed that the functional differences of AICD generated from the two pathways are a result of different sites of generation. In this respect experimental evidence has suggested that retrograde transported of APP in signaling endosomes in the amyloidogenic pathways results in generation of AICD in closer vicinity to the nucleus (Goodger et al., 2009). A second, though not necessarily independent, possibility is that AICD generated from the amyloidogenic pathway is stabilized differently. Indeed, data was presented that AICD is stabilized by Fe65 and that Fe65 shifts APP processing towards the amyloidogenic pathway, but equally, several reports claiming the opposite have been published (Kimberly et al., 2001; Kinoshita et al., 2002; Wiley et al., 2005; Huysseune et al., 2007). Finally, several other PTB-containing proteins could selectively modulate AICD-mediated gene transactivation in the APP processing pathways.

In contrast to production of AICD, only few studies have looked at degradation of AICD. AICD generated *in vitro* is degraded, as Aβ, by the insulin degrading enzyme (IDE), but it remains to be determined whether this degradation takes also place under physiological conditions (Edbauer et al., 2002; Farris et al., 2003; Buoso et al., 2012). Conflicting reports have also been published whether the ubiquitin-proteasome system (UPS) plays a role in AICD degradation (Cupers et al., 2001; Nunan et al., 2003). However, since both reports have used AICD peptides of atypical length, our understanding of the role of the UPS in AICD degradation remains vague. Vingtdeux et al. (2007) also show that AICD is degraded via the endosomal-lysosomal pathway. Clear evidence exists for cleavage of AICD by caspases yielding a fragment called C31 (Lu et al., 2000). However, whether caspase cleavage of AICD takes place before or after γ-secretase cleavage and, thus, whether it directly contributes to degradation of transcriptionally active AICD remains to be determined.

1.4 Scope of this thesis

Processing of APP is a central event in the pathology of AD. Understanding the function of APP and its cleavage products promises to be instrumental to decipher AD pathology and is essential for efficient and save therapeutics. In particular, regulation, physiological function, and a possible pathological contribution of the C-terminal fragment of APP, AICD, remains unclear. Therefore, the general aim of this thesis is to improve our understanding of AICD regulation and function.

In the first results part of this thesis, I present differences in the nuclear signaling capability of the intracellular domains (ICDs) from different APP family members. Based on these observations, I hypothesize that differences in the nuclear signaling capability are due to sequence determinants in the respective ICDs. The specific aim of the experiments presented in the first results part is, therefore, to unveil possible sequence determinants of nuclear signaling of AICD. Knowledge of these sequence determinants will allow to investigate separately APP- and AICD-mediated functions.

The results presented in the first results part of this thesis uncover the regulation of AICD by the ubiquitin-proteasome system and point towards an important role of the N-terminus of AICD is this process. Therefore, I hypothesize that proteasomal degradation of different AICD species is dependent on the identity of their N-terminal residue. The specific aims of the experiments in the second results part are (i) to uncover different proteasomal degradation of AICD species, (ii) to understand the mechanism of proteasomal

degradation of AICD, and (iii) to evaluate a possible contribution of AICD species to AD pathology.

The transcriptional function of AICD and its regulation was predominantly shown *in vitro*. I hypothesize that AICD also posses transcriptional function *in vivo*. The experiments in the third results part aim to explore the regulation and function of AICD *in vivo*. To this end, a novel transgenic mouse line is generated and analyzed.

2 Material and Methods

In this chapter we give detailed descriptions of the materials and experimental procedures used in this thesis. Standard buffers and reagents are listed in table 2.1.

2.1 Molecular methods and reagents

General. Restriction enzymes, antarctic phosphatase, T4 DNA ligase, and Quick Ligation kit were purchased from NEB and used according to the manufacturer's protocol. Oligonucleotides were ordered from Microsynth. DNA was separated in 1 % agarose gels (diluted in TAE and supplemented with 0.1 % ethidium bromide) at 100 V. One Shot Top10 competent bacteria

Table 2.1 Buffer and reagent composition.

Name	Composition
LB media	10 g/l tryptone, 5 g/l yeast extract, 10 g/l NaCl, pH 7.0
LB agar	LB media, 15 g/l agar
Lysis buffers	
RIPA	50 mM Tris-HCl pH 7.6, 150 mM NaCl, 1 % NP40, 0.1 % SDS, 0.5 % sodium deoxycholate, 2 mM EDTA, protease inhibitors (Roche)
Modified RIPA	10 mM Tris Hl pH 7.6, 50 mM NaCl, 0.25 % NP40, 1 % Triton X-100, 2 mM EDTA, protease inhibitors
Pull-down	150 mM KCl, 20 mM HEPES pH 7.2, 10 mM NaCl, 5 % glycerol, 1 % Triton X-100, 2 mM DTT, 5 mM phenanthroline, protease inhibitor
Tail	50 mM Tris-HCl pH 8.0, 20 mM NaCl, 1 % SDS, 1 mM EDTA, 20 mg/ml proteinkinase K (Sigma-Aldrich)
PBS	140 mM NaCl, 2.7 mM KCl, 10 mM Na_2HPO_4, 1.8 mM KH_2PO_4, pH 7.4
Running buffer	1 M Tris-HCl, 1 M tricine, 1 % SDS
TAE	40 mM Tris-acetate, 1 mM EDTA, pH 8.0
TBS	50 mM Tris-HCl, 150 mM NaCl, pH 7.6

Table 2.2 Standard PCR cycler program.

Temperature	Duration	Cycles
95 °C	2 min	1
95 °C	30 s	30
57 °C	30 s	
72 °C	1 min/1.000 bp	
72 °C	10 min	1

(Invitrogen) were used for plasmid transformation by 30 s heat shock at 42 °C. Bacteria were plated on LB agar plates with 100 µg/ml ampicillin or 50 µg/ml kanamycin antibiotics depending on the plasmid backbone. Individual colonies were picked and grown overnight in LB medium with the respective antibiotic. Mini- and maxi-preparation kits as well as DNA purification and DNA agarose extraction kits were purchased from Sigma-Aldrich and used according to the manufacturer's protocol. For DNA sequencing services from GATC or Microsynth were used.

PCR-based cloning methods. For PCR-based cloning primer with desired restriction sites were designed to have a melting temperature of approximately 59 °C of the binding part.[1] PCR reaction mixtures were set up in thin-walled PCR-tubes as following: 10 ng plasmid, 1 µl of 10 mM dNTP mix, 1 µl 10 nmol/ml forward primer, 1 µl 10 nmol/ml reverse primer, 5 µl of 10X Pfu polymerase buffer, 1 µl of 2.5 U PfuTurbo polymerase (Stratagene), filled with H_20 to reach a total volume of 50 µl. Thermocycling of PCR reactions was done according to table 2.2. PCR-driven overlap extension was used to construct scarless protein-fusion constructs and the instructions in Heckman and Pease (2007) were followed.

Site-directed mutagenesis. To mutate base-pairs in plasmids site-directed mutagenesis (SDM) was used. SDM primer containing the desired mutations were designed that both flanking regions of the mutations have a melting temperature of approximately 59 °C. Reaction mixture as for regular PCR was set up and applied to thermocycling according to table 2.3. After thermocycling 1 µl Dpn1 restriction enzyme was added, mixed gently, and incubated in a 37 °C

[1] For calculation of oligonucleotide annealing temperatures the Oligo Calc online tool of the Northwestern University was used, which can be found under `http://www.basic.northwestern.edu/biotools/oligocalc.html`.

Table 2.3 Site-directed mutagenesis cycler program.

Temperature	Duration	Cycles
95 °C	30 s	1
95 °C	30 s	22
55 °C	1 min	
68 °C	1 min/1.000 bp	
68 °C	7 min	1

water bath for one hour. 5 µl of reaction mix were used for transformation of bacteria.

General remarks about used expression constructs. The pUKBK plasmid line, based on an in-house constructed plasmid backbone previously described in Kohli et al. (2012), was used for protein expression, unless plasmids from external sources were obtained—for a graphical representation of the pUKBK plasmid line see figure A.1 in the appendix. The coding sequence of pUKBK plasmids is flanked by SfiI and PmeI cleavage sites. A AscI cleavage site is present in the forty-eight base pair (bp) linker, which allows the C-terminal attachment of different tags or fluorescence proteins. The promoter region is preceded by a SspI cleavage site. The modular character of the pUKBK plasmid line allows simple exchange of regulatory elements and genes by restriction-based and PCR-based cloning. The following abbreviations are used for the individual elements in the plasmid nomenclature. Promoters: C (CMV promoter), G (GAPDH promoter), P (human PGK promoter). Tags: HA (triple HA-tag), myc (triple myc-tag), SBP (streptavidin-binding protein). Fluorescence proteins: Cer (cerulean), Cit (citrine).

Plasmids expressing APP, APLPs, and derivatives thereof. Plasmids expressing C-terminally citrine- and HA-tagged APP (pUKBK-C-APP-Cit, pUKBK-C-APP-HA) have been described previously (von Rotz et al., 2004). pUKBK-G-myc-APP-HA was constructed by inserting a myc-tag coding oligonucleotide after the APP signal peptide (SP) by restriction based cloning. Cerulean- and SBP-tagged plasmids (APP-Cer, APP-SBP) were obtained by restriction-based exchange of citrine. To find sequence determinants of nuclear signaling of APP, *APP* residues were exchanged to corresponding *APLP1* residues (APP-to-APLP1 mutations) by SDM or PCR-driven overlap extension. Citrine- and HA-tagged chimeric APP/APLP1 constructs, APP-AL1ICD and APLP1-AICD were derived from APP and APLP1 constructs by PCR-driven overlap extension.

Lysine-to-arginine exchange and introduction of FAD mutations in APP was achieved by SDM. Plasmids containing *APLP1* (purchased from RZPD) and *APLP2* (obtained from Stefan Kins, TU Kaiserslautern) were used to amplify open reading frames and ICDs and cloned into the pUKBK expression vector system (pUKBK-C-APLP1-Cit, pUKBK-C-APLP2). N-terminally myc-tagged APLP1 and APLP2 constructs were obtained by replacing *APP* in pUKBK-G-myc-APP-HA with *APLP1* and *APLP2* by restriction-based cloning. Cerulean- and HA-tagged plasmids (APLP1-Cer, APLP2-Cer, APLP1-HA, APLP2-HA) were obtained by restriction-based exchange of citrine. For the constructs Cit-AICD, Cit-AL1ICD, Cit-AL2ICD, and Cer-AL2ICD fluorescence proteins were fused to the N-terminus of the respective ICD sequence by PCR-based cloning. AICD-Cit was cloned by PCR-driven overlap extension.

Fe65 and Tip60 plasmids. HA-Fe65 and CFP-Tip60 expressing constructs have been described previously (von Rotz et al., 2004). To generate myc-Tip60, CFP was exchanged with a myc-tag by restriction-based cloning.

Ubiquitin-expressing and ubiquitin-fusion plasmids. The ubiquitin-fusion (Ub-fusion) construct Ub-R-GFP was purchased from Addgene (ID11939; Dantuma et al., 2000). Ha-tagged Ub-fusion constructs of AICD50 and AICD51 (pUKBK-C-Ub-AICD50-HA, pUKBK-C-Ub-AICD51-HA) were constructed by PCR-driven overlap extension. These constructs were used to create EGFP-Ub-fusion constructs (pUKBK-C-EGFP-Ub-AICD50-HA, pUKBK-C-EGFP-Ub-AICD51-HA), in turn used for construction of lentivirus plasmids. A plasmid encoding N-terminally HA-tagged ubiquitin (p-HA-Ub) was obtained from Michael Potente (Goethe University; Guarani et al., 2011).

β-galactosidase assay related constructs. A plasmid expressing APP containing the Gal4-DBD (DNA binding domain) within its C-terminal domain (p-APPGal4) was obtained from Thomas Südhof (Stanford University) and was described in Cao and Sudhof (2001). A plasmid containing four upstream activating sequence (UAS) elements upstream of *lacZ* was used for β-galactosidase assays. A plasmids containing *lacZ* under the control of the CMV-promoter (p-C-lacZ) was obtained from Deniz Gökbuget and Uli Suter (ETH Zurich). By fusing UAS repeats to the N-terminus of a citrine-containing plasmid, the p-UAS-Cit was obtained. Plasmids expressing only Gal4-DBD, Gal4-DBD fused to Gal4-AcD (activation domain), and Gal4-DBD fused to VP16 were obtained from Walter Schaffner (University Zurich).

Lentivirus plasmids. pSicoR-C-MCS, described in Huber et al. (2013), and pCCL-P-EGFP, described in Cusimano et al. (2012), lentivirus plasmids were obtained from Uli Suter (ETH Zurich). EGFP-Ub-fusion constructs of AICD species (pSicoR-C-EGFP-Ub-AICD50-HA and pSicoR-C-EGFP-Ub-AICD51-HA) were obtained by PCR-based cloning into the MCS of pSicoR-C-MCS. By replacing EGFP in pCCL-P-EGFP with a Ub-fusion construct of AICD51 using PCR-based cloning, pCCL-P-Ub-AICD51-HA was obtained.

2.2 Cell culture methods and reagents

Cells. Human embryonic kidney (HEK-293, HEK), HEK293-T, and mouse neuroblastoma N2a (N2a) cells were purchased from DSMZ (Deutsche Sammlung von Mikroorganismen und Zellkulturen). UBR1$^{-/-}$ UBR2$^{-/-}$ (abbreviated to UBR1/2 dKO) mouse embryonic fibroblasts (MEFs) were received from Yong Tae Kwon (University of Pittsburgh) and have been described in Tasaki et al. (2005). Wildtype MEFs were received from Bart De Strooper (University of Leuven). Cells were cultured at 37 °C and 5 % CO_2 in DMEM (Dulbecco's modified eagle medium; Invitrogen) supplemented with 10 % FCS (Gibco) and 1 % penicillin/streptomycin (Invitrogen). For maintenance of cells, confluent cells were washed with PBS (Gibco) detached and dissociated with trypsin/EDTA (Gibco) and plated at a dilution of 1:10. For experiments antibiotic-free media were used. Plastic dishes were coated with poly-D-lysine (Sigma-Aldrich) for experiments with HEK cells. Glass specimen slides were coated with poly-ornithine and fibronectin (both Sigma-Aldrich).

Generation of stable cell lines. The HEK(UAS-Cit) stable cell line was created by antibiotic resistance–mediated selection. The UAS-Cit plasmid, carrying a hygromcin-resistance gene, was transfected into HEK cells (see below for transfection method used). One day after transfection, hygromycin B (300 µg/ml; Sigma-Aldrich) was supplemented to media and media changed every second day. After approximately twenty days, selection pressure was removed and the mixed culture tested for harboring the construct by immunhistochemistry (see results). HEK cells stably expressing HA-tagged EGFP-Ub-fusion constructs of AICD50 and AICD51 (HEK(Ub-AICD50-HA) and HEK(Ub-AICD51-HA)) were generated by lentivirus-mediated genome-integration (see below for virus production). HEK cells were infected by adding virus-containing media (low-titer virus). Efficiency of integration was similar in both cell lines as evaluated by EGFP fluorescence intensity. Cell media was replaced six hours

after infection and cells passaged at least four times before considered to have stably integrated the virus.

Preparation of primary neurons. Primary neuronal cultures were prepared from one-day-old mice as described in Goodger et al. (2009). Briefly, newborn mice were sacrificed and brains removed. Cortices and hippocampi were dissected and cells dissolved mechanically and by enzymatic digestion with papain (Worthington). Cells were counted and plated at a concentration of 54×10^3 cells/cm^2 in laminin- (Invitrogen) and poly-D-lysine-coated cell culture dishes with DMEM supplemented with 10 % horse serum (Invitrogen). Three hours after plating, media were changed to Neurobasal-A (Gibco) medium supplemented with Glutamax (Gibco), sodium pyruvate (sodium pyruvate), and B27 (Invitrogen). Media were changed every three to four days and cells analyzed after ten to fourteen days *in vitro* (DIV).

Delivery of plasmids and virus infection. For transfection Lipofectamine 2000 (Invitrogen) was used according to the manufacturer's protocol. Medium was replaced three hours after transfection and cells fixed or homogenized twenty to twenty-four hours after transfection if not indicated differently. For virus infection with low-titer virus 50 % of cell media was replaced by virus-containing media pre-warmed to 37 °C. High-titer viruses were first mixed with pre-warmed media and then added to cells.

siRNA-mediated knockdown. siRNAs were delivered using Lipofectamine RNAiMAX transfection reagent (Invitrogen) according to the manufacturer's protocol. Three siRNAs recognizing different regions of the same mRNA target were used with final concentration of 10 nM. As control, two negative control siRNAs were used to match the concentration of target siRNAs. The following siRNAs were used (all purchased from Life Technologies): UBA1 (catalogue numbers: 4427038-s599, 4427038-s600, 4427038-s601), UBA6 (catalogue numbers: 4427037-s30515, 4427037-s30516, 4427037-s30517), and *negative control* (catalogue numbers: 4390843, 4390846).

Pharmacological reagents. See table 2.4 for a list of pharmacological compounds used for cell culture experiments in this study. All compounds were diluted in DMSO (Sigma-Aldrich) to stock concentration and DMSO was used as control treatment.

Table 2.4 Pharmacological compounds used for cell culture experiments.

Reagent Name	Supplier (Cat. No.)	Concentration	Duration
Cycloheximide (CHX)	Sigma-Aldrich (66-81-9)	100 µg/ml	0.5–4 h
DAPT	Sigma-Aldrich (D5942)	1 µM	24 h[1]
Epoxomicin (EPX)	Calbiochem (324801)	1 µM[1]	4 h[1]
MG132	Enzo Life Sciences (BML-PI102R)	1 µM[1]	4 h[1]
PYR41	Sigma-Aldrich (N2915)	27 µM	6 h

[1] If not indicated otherwise.

Live antibody incubation. For analysis of APP/APLP endocytosis live antibody incubation was carried out in HEK cells. Twenty-four hours after transfection, cells were incubated with myc-tag antibody (1:100, Roche) at 4 °C for 10 min or 30 min. After washing with ice-cold PBS, cells were fixed and stained for HA- and myc-tags as described below.

Virus production. Lentiviruses were prepared by transfecting HEK293-T plated in 15-cm dishes with 33 µg transfer vector and helper plasmids (7.7 µg pVSVg. 22 µg pDMLG, and 5.5 µg pREV) using 25 kDa polyethylenimine (PEI; Polysciences). Forty-eight hours after transfection supernatants were transferred to Falcon tubes and centrifuged 15 min at 500 rcf and 4 °C to remove cellular debris. Virus containing media was either aliquoted and stored at –80 °C for direct usage (low-titer virus) or applied to virus concentration. For virus concentration, virus-containing media was centrifuged at 25.000 rpm for 2.5 h at 4 °C using a Beckman ultracentrifuge with 70Ti rotor. Supernatant was discarded and the pellet resuspended in 200 µl PBS. High-titer containing solution was aliquoted, frozen using liquid nitrogen, and stored at –80 °C until usage.

2.3 Animals and related methods

All animal experiments were performed according to the Swiss animal protection law (TschG) and approved by the local animal committee (Kantonales Veterinäramt Zürich). Genotyping of mice was done by PCR on DNA extracted from mouse tail tissue with the primers listed in table 2.6. 20 µl tail lysis buffer (table 2.1) were added to tails and incubated 30 min in a 55 °C heat block at maximal agitation. After addition of 200 µl H_2O the suspension was incubated 12 min in a 95 °C heat block at maximal agitation. Suspension was stored at –20 °C and centrifuged 5 min at 14.000 rcf before usage for genotype PCR. PCR

Table 2.5 PCR cycler program for genotyping.

Temperature	Duration	Cycles
95 °C	2 min	1
94 °C	30 sec	
55 °C for APPGal4 & ArcAβ; 64 °C for UAS-lacZ	30 sec	30
72 °C	50 sec	
72 °C	7 min	1

reaction mixtures were set up in thin-walled PCR-tubes as following: 1 µl genomic DNA from lysed tails, 0.4 µl of 10 mM dNTP mix, 0.4 µl 10 nmol/ml forward primer, 0.4 µl 10 nmol/ml reverse primer, 2 µl of 10X RedTaq polymerase buffer, 1 µl of 1 U RedTaq polymerase (Sigma-Aldrich), filled with H_20 to reach a total volume of 20 µl. Thermocycling of PCR reactions was done according to table 2.5.

Generation of APPGal4 transgenic mice. For generation of the APPGal4 transgenic mouse line a APP-Gal4 fusion protein was used, which was originally generated by Cao and Sudhof (2001) and characterized in *in vitro* experiments. The APP-Gal4 fusion protein is composed of the extracellular and transmembrane region of APP (APP residues 1–651), followed by a six amino acid long linker, the 147 amino acid long Gal4-DBD (Gal4 residues 1–147), a nine amino acid long linker, and the remainder of the cytoplasmatic region of APP (APP residues 652–695). The coding sequence of the APP-Gal4 fusion protein was cloned into the pMoPrp plasmid, which is carrying a prion protein promoter (PrP) for protein expression, and which was previously used for the generation the ArcAβ transgenic mouse line (Knobloch et al., 2007). This construct was used by the Institut für Labortierkunde (University Zurich) for generation of APPGal4 transgenic mice by embryo transfer. Three different founder lines were provided and probed for transgene expression by western blotting with an antibody recognizing exclusively human APP (6E10). The founder line with highest transgene expression was chosen for subsequent experiments. Mice were backcrossed to C57BL/6J background.

Other mouse strains used. UAS-lacZ mice, originally generated by Govindarajan et al. (2005), were obtained from Freddy Radtke (EPFL; Smith et al., 2012). The construct used for generation of these mice contains six tandem copies of the UAS element linked to a minimal thymidine kinase promoter and followed by the *lacZ* gene encoding β-galactosidase (see table 2.6 for genotyping primer.

Table 2.6 Genotyping primer.

Genotype	Primer
APPGal4/ArcAβ	5′-CAGAACTGAACCATTTCAACCGAGC-3′
	5′-TCAGTGGGTACCTCCAGCGCCCGAG-3′
UAS-lacZ	5′-ATCCTCTGCATGGTCAGGTC-3′
	5′-CGTGGCCTGATTCATTCC-3′

C57Bl/6J mice, used for preparation of primary neurons, were purchased from The Jackson Laboratory. The ArcAβ mouse line was generated in our laboratory, and mice were genotyped with the same primer and thermocycling program as APPGal4 mice (Knobloch et al., 2007).

2.4 Biochemical methods and reagents

Generation of protein lysates. For generation of protein samples, cells were washed with ice-cold PBS and scraped in RIPA or modified RIPA lysis buffer (see table 2.1 for lysis buffer composition). For detection of ubiquitinated proteins RIPA was supplemented with MG132 (5 µM) and NEM (N-ethylmaleimide; 20 mM; Sigma-Aldrich)—in the following denoted RIPA-Ub—to prevent proteasomal degradation and deubiquitination, respectively. Samples were incubated 15 min on a rotating wheel at 4 °C followed by 5 min centrifugation at 22.000 rcf and 4 °C to remove cellular debris. Supernatants were transferred to fresh Eppendorf tubes and stored at –80 °C until usage.

Western blotting. For western blotting the Novex NuPAGE SDS-PAGE gel system (Invitrogen) was used. Protein samples were mixed with loading buffer (NuPAGE LDS sample buffer (Invitogen) and 5 % β-mercaptoethanol) and placed in a 99 °C heating block for 5 min. Equal amounts of supernatants were separated on 10–20 % Tricine gels (Invitrogen), if not stated otherwise (see table 2.1 for running buffer composition). Protein separation was done at 100 V for approximately 90 min. SeeBlue Plus2 Pre-Stained protein standard (Invitrogen) was used as a molecular weight marker. Proteins were transferred to nitrocellulose transfer membranes (pore size 0.1 µm; Protran) by semi-dry blotting with 2X Tris-Glycine Transfer Buffer (Invitrogen) supplemented with 10 % methanol. Membranes were blocked for one hour at RT with 5 % skim milk diluted in PBS and then washed with PBS. Membranes were incubated overnight at 4 °C with primary antibodies dissolved in PBS—for a list of primary and secondary antibodies used for western blotting see table 2.7. The next

day, membranes were washed, incubated with secondary antibody diluted in blocking buffer.

To increase detection of HA-tagged AICD (derived from full-length APP and Ub-fusion constructs) in western blots with HA-tag antibody a protocol described in Pimplikar and Suryanarayana (2011) was followed. After transfer membranes were dried for approximately half an hour and then incubated with boiling PBS for 5 min. Washing of membranes was done with TBS supplemented with 0.1 % Tween 20 (TBST) and blocking with 10 % FCS in TBST. HA-tag antibody was used at a concentration of 1:250 and secondary antibody was diluted in FCS-based blocking buffer. To increase detection of Aβ in western blots a protocol described in Shankar et al. (2011) was followed. After transfer membranes were boiled in PBS in a microwave at 800 W for 5 min and let then stand for additional 5 min in the hot PBS. Membranes were washed in TBS. Synthetic Aβ42 was purchased from American Peptide.

Protein bands were visualized by ECL (Thermo Scientific) using a LAS 3000 (Fuji) or LAS 4000 (GE Healthcare) imager, both equipped with Fuji CCD cameras. Quantification of protein bands was done by densitometric analysis using Multi Gauge (Fuji) or ImageQuant (GE Healthcare) software. Proteins levels were normalized to α-tubulin levels and expressed in arbitrary unit (AU), unless otherwise stated. Biological replicates loaded to separate western blots were normalized by the sum of the replicates as outlined by Degasperi et al. (2014). Statistical analysis was done with Prism 6 (GraphPad) and the used statistical tests are indicated in the respective experiments.

Dynabeads-streptavidin pull-down. Pull-down of proteins fused to streptavidin-binding protein (SBP) was done as described previously (Kohli et al., 2012). Cells, transfected with APP-SBP and HA-Fe65, were lysed in pull-down lysis buffer and centrifuged for 10 min at 800 rcf (see table 2.1 for lysis buffer composition). Supernatant was incubated with dynabeads-streptavidin M280 (Invitrogen) for four hours at 4 °C. Beads were separated with a magnet and washed four times with homogenization buffer. For protein elution, beads were incubated with a buffer containing 700 nmol biotin for 30 min at 4 °C. Equal amounts of protein elution were loaded on 10–20 % Tricine gels and processed as described above.

Immunoprecipitation. For immunoprecipitation of AICD and detection of its ubiquitination the Dynabeads Protein A Immunoprecipitation kit (Invitrogen) was used according to the manufacturer's protocol. For antibody-to-dynabeads binding, 50 µl dynabeads were transferred to a fresh tube and supernatant

Table 2.7 Antibodies used in this study for western blotting.

Protein/Epitope	Supplier (Cat. No.)	Host	Dilution
Primary antibodies			
AICDneo (AICD50 neo-epitope)	*non-commercial*[1]	rabbit	1:1000
AICD	*non-commercial*[2]	guinea pig	1:1000
APP, C-terminal	Epitomics (1565-1)	rabbit	1:1000
human APP, Aβ-region (6E10)	Covance (39320)	mouse	1:500
c-jun	Santa Cruz Biotechnology (1694)	rabbit	1:1000
c-myc (myc-tag)	Roche (11667149001)	mouse	1:1000
GAPDH	Meridian Life Science (H86504M)	mouse	1:2000
GFP and derivatives (e.g., citrine)	Roche (11814460001)	mouse	1:1000
HA-tag	Roche (11867432001)	rat	1:1000
α-tubulin	Sigma-Aldrich (T-9026)	mouse	1:1000
Ubiquitin	DAKO (Z0458)	rat	1:1000
UBA1	Bethyl (A301-126A)	rabbit	1:1000
UBA6	*non-commercial*[3]	rabbit	1:1000
Secondary antibodies [4]			
mouse IgG	GE Healthcare (NA931V)	sheep	1:2000
guinea pic IgG	Jackson (106-035-003)	goat	1:2000
rabbit IgG	GE Healthcare (NA934V)	donkey	1:2000
rat IgG	GE Healthcare (NA935V)	goat	1:2000

[1] AICDneo antibody was obtained from Patrick May (Eli Lilly) and has been described in Chávez-Gutiérrez et al. (2012).
[2] AICD antibody was raised against a peptide corresponding to the fourteen N-terminal amino acids of AICD by the Institut für Labortierkunde (University Zurich).
[3] UBA6 antibody was obtained from Wade Harper (Harvard University) and has been described in Jin et al. (2007).
[4] All secondary antibodies used in western blot are coupled to horseradish peroxidase (HRP).

removed by retaining beads with a magnet. Antibodies, diluted 1:50 in 200 µl AB Binding & Washing Buffer (PBS with 0.01 % Tween 20), were added to beads and incubated for 10 min at RT. Unbound antibody was discarded by removal of the supernatant and beads washed with AB Binding & Washing Buffer. Cell lysates harvested in RIPA-Ub buffer were added to the antibody-bead-complex, and incubated for one and a half hours at RT. Unbound protein in supernatant was then removed and beads washed three times with washing buffer provided by the kit. Beads were transferred to fresh tubes and eluted with elution buffer (provided by the kit and supplemented with NuPAGE LDS sample buffer and 5 % β-mercaptoethanol) for 10 min in a 99 °C heat block under maximal

Table 2.8 Primary antibodies used for immunocyto- and immunohistochemistry.

Protein/Epitope	Supplier (Cat. No.)	Host	Dilution
β-galactosidase	Abcam (ab9361)	ckicken	1:100
c-myc (myc-tag)	Roche (11667149001)	mouse	1:100
GFP and derivatives (e.g., citrine)	Invitrogen (A11122)	rabbit	1:100
HA-tag	Roche (11867432001)	rat	1:100

agitation. Eluates were loaded directly on SDS-PAGE or stored at –80 °C until further usage.

Immunocytochemistry. Cells were fixed for 20 min with 4 % paraformaldehyde (PFA), washed with TBS containing 0.05 % Triton X-100 and blocked for one hour with TBS containing 0.2 % Triton X-100, 5 % horse serum, and 5 % goat serum. Fixed cells were incubated overnight with primary antibodies (table 2.8) diluted in blocking solution at 4 °C. Cells were washed and incubated one to two hours with secondary antibodies (table 2.9) diluted in blocking solution at room temperature (RT). After subsequent washing, cells were embedded in Mowiol (Sigma-Aldrich) supplemented with Dabco (Sigma-Aldrich) to decrease bleaching. To stain DNA DAPI was added to washing solution in some experiments as indicated. Stained cells were analyzed by confocal microscopy.

β-galactosidase assay. The *lacZ* gene, encoding the enzyme β-galactosidase, is a reporter gene used to visualize and quantify transcriptional activity. Presence of β-galactosidase is visualized by cleavage of the synthetic substrate X-Gal, which is yielding a blue and insoluble product (5,5'-dibromo-4,4'-dichloro-indigo). Staining of cultured cells for β-galactosidase was done with the β-Gal Staining kit (Invitrogen) according to the manufacturer's protocol. Cells grown on coverslips were washed with PBS and fixed with fixative solution for 10 min at RT. After washing staining solution (containing 2 mg/ml X-Gal substrate) was added to cover the cell and incubated one to two hours at 37 °C. Cells were then washed and embedded in Mowiol. Quantification of HEK cells and primary neurons stained for β-galactosidase was done manually. Semiquantitative categories were chosen to classify reporter activity. These categories were: no (= 0) , low (< 10), medium (≥ 10 and < 100), and high (≥ 100 β-galactosidase-positive cells per coverslip). β-galactosidase-positive cells were counted by two researchers independently and blinded.

Table 2.9 Secondary antibodies used for immunocyto- and immunohistochemistry.

Epitope	Fluorophore	Supplier (Cat. No.)	Host	Dilution
chicken IgG	Cy3	Jackson (703-165-155)	donkey	1:250
mouse IgG	Cy3	Jackson (715-165-151)	donkey	1:250
mouse IgG	Cy5	Jackson (715-175-150)	donkey	1:250
rat IgG	Cy2	Jackson (712-225-153)	donkey	1:250
rat IgG	Cy3	Jackson (711-165-153)	donkey	1:250
rat IgG	Cy5	Jackson (712-175-153)	donkey	1:250
rabbit IgG	Alexa 488	Life Technologies (A11008)	goat	1:250

Cytotoxicity assay. For analysis of cytotoxicity of proteasomal inhibitor, release of lactate dehydrogenase (LDH) was measured with the Cytotoxicity Detection kit (Roche) according the manufacturer's protocol. Cells were washed with PBS twice prior to addition of proteasomal inhibitor–containing media. Care was taken that equal amount of media was added to the cells. At the end of treatment, cell media was transferred to Eppendorf tubes and centrifuged 4 min at 400 rcf and 4 °C to remove cellular debris. LDH standards were prepared in fresh media. 75 µl media sample and standard were pipetted to individual wells of a 96-well plate and 75 µl LDH Mastermix added and gently mixed. After approximately one hour incubation in the dark at RT, absorbance was measured with a Tecan workstation at 490 nm. Media from Triton X-100 lysed cells was used as 100 % cytotoxicity. Media from DMSO control-treated cells was set as zero toxicity.

Immunohistochemistry. Immunohistochemical preparation and analysis was done as described previously (Ferretti et al., 2012). Adult APPGal4/UAS-lacZ and APPGal4 mice were deeply anesthetized with ketamine/xylazine and perfused transcardially with PBS for approximately 2 min. Brains were removed and fixed in 4 % PFA for twenty-four hours at 4 °C, followed by incubation in 30 % sucrose for approximately twenty-four hours at 4 °C. Fixed brains were cut coronally into 40 µm thick sections with a freezing sledge microtome (Microm HM 450, Thermo Scientific) at working temperature of approximately –20 °C. Free-floating sections were washed and permeabilized using PBS-T (PBS supplemented with 0.2 % Triton X-100) and blocked for one hour at RT with blocking buffer (5 % goat serum, 5 % donkey serum, 0.2 % Triton X-100 in PBS). Sections were incubated overnight at 4 °C with anti-β-galactosidase antibody (Abcam) diluted 1:500 in blocking buffer. The next day, sections were washed and incubated for two hours in secondary antibody (Cy3-coupled anti-chicken-IgG; Jackson) diluted 1:200 in blocking buffer at RT. Prior to mounting

with Hydromount (National Diagnostics), sections were washed and nuclei stained with DAPI. Analysis was done using a Leica DM 4000 B fluorescence microscope.

2.5 Microscopy and image analysis

Fluorescence microscopy. Fluorescence, brightfield, and differential interference contrast (DIC) images were acquired on inverted DM IRE 2, DM 4000 B, SP2, and SP8 microscopes (all Leica). For confocal images of AFT-complexes, SP2 or SP8 confocal microscope with a 63X water or glycerol immersion objectives were used. The 458-nm and 514-nm lines of the argon laser were used to excite CFP and citrine, respectively. For detection of CFP PMT (photomultiplier tube) window was set to 465–485 nm, for citrine to 525–545 nm. For excitation of Cy3 the 543-nm laser was used and detected in PMT window set to 553–600 nm. DAPI was excited at 405 nm and detected at a PMT window set to 410–430 nm. Approximately ten images were acquired in z-axis and subjected to maximum projection.

FRET measurements. FRET (Förster resonance energy transfer) was used to analyze APP/APLP co-localization and dimerization. For FRET measurements, cerulean was excited with the 458-nm laser and citrine emission was read at 525–555 nm. Expression of fluorophores individually was used to determine cerulean bleach-through and citrine cross-excitation signals. Based on raw FRET values calculation of NFRET was done as described in von Rotz et al. (2004).

3 Regulation of Nuclear Signaling Capability of the Amyloid Precursor Protein Family Members

In this chapter, we investigate nuclear signaling capability of the ICDs from different APP family members. The majority of the results in this chapter have been published in Gersbacher et al. (2013).

3.1 Introduction

APP is a member of a highly conserved family of glycoproteins, which includes APP-like protein 1 (APLP1) and APP-like protein 2 (APLP2) in vertebrates, APPL in *Drosophila*, and APL-1 in *C. elegans*. APP and APLP2 are ubiquitously expressed, with high expression in the brain (Tanzi et al., 1988; Slunt et al., 1994), while APLP1 expression is neuron specific (Lorent et al., 1995). Interestingly, amyloid precursor-like proteins, i.e., APLP1 and APLP2 (APLPs), lack the Aβ-domain, which is a feature unique to APP (Bayer et al., 1999; Thinakaran and Koo, 2008). In humans, APLP2 is located on chromosome 11q23–q25 and exists in two alternatively spliced forms, one of which, similarly to APP, contains a KPI domain (Wasco et al., 1993; Van Nostrand et al., 1994; Bayer et al., 1999). Human APLP1 is located on chromosome 19q13.1 and, as yet, no spliced transcripts have been identified (Wasco et al., 1992; Lenkkeri et al., 1998). All APP family members have been shown to bind zinc and heparin (Bush et al., 1994) and are thought to play an important role in cell adhesion in homo- and heterotypic manner (Coulson et al., 2000; Soba et al., 2005).[1] Furthermore, all APP family members interact with PAT1a (protein interacting with APP tail 1a) via their basolateral sorting signal, and this interaction is promoting their intracellular transport and processing (Kuan et al., 2006).

[1] The term *APP family members* is used in this thesis to denote exclusively the mammalian members of the APP superfamily which are APP, APLP1, and APLP2.

Despite the structural homology and conserved domain structure of APP family members, it has been shown that their subcellular localization differs strikingly. A recent study by Kaden et al. (2009) showed that APP and APLP2 mainly localize within intracellular compartments, such as ER (endoplasmic reticulum) and endosomes, while only minor levels were detected at the plasma membrane. In contrast, APLP1 was found to mainly localize to the plasma membrane, corresponding to an increased tendency to form in trans interactions at cell-cell contacts, highlighting an important role for APLP1 in cell adhesion (Kaden et al., 2009). Further studies investigating the binding of the APP family to adaptor proteins have also identified differences between family members. For example, the binding of JIP1 (JNK interacting protein) to APP has been shown to result in transcriptional activation, whereas expression of JIP1 with APLP1 or APLP2 showed little or no transcriptional activity (Scheinfeld et al., 2003).

Studies using knockout mice have revealed important insights into the relationship between different APP family members. Single knockout of APP, APLP1, or APLP2 cause less pronounced phenotypes, probably due to a redundancy of certain functions within the APP gene family (Zheng et al., 1995; von Koch et al., 1997; Heber et al., 2000). However, it is also clear that the different APP family members exhibit different functions. Mice with disrupted APP and APLP1 are viable and fertile, while those that are double knockout for APP and APLP2 or double knockout for APLP1 and APLP2 die shortly after birth. These findings point to an important developmental role for APLP2, which is essential when either APP or APLP1 are absent. APP/APLP2 double knockout mice exhibit a poorly formed neuromuscular junction and reduced numbers of presynaptic vesicles (Wang et al., 2005), which is in line with findings from *Drosophila* with mutant APPL (Merdes et al., 2004), implicating a role for the APP family in the regulation of synaptogenesis. Triple knockout mice, lacking all three APP family members, were found to die soon after birth and display cortical dysplasia, which resembles human type II lissencephaly, and is characterized by fragmented basal lamina and over-migration of neurons (Herms et al., 2004). This phenotype is very similar to the phenotype reported of Fe65 family knockout mice, highlighting the importance of the AICD-Fe65 interaction in the function of the APP family members (Guenette et al., 2006).

Both APLP1 and APLP2, like APP, are cleaved by α-, β-, and γ-secretase, and intracellular domains (ICDs) are released after γ-secretase cleavage at the ϵ-site (Walsh et al., 2003; Eggert et al., 2004; Pastorino et al., 2004; Yanagida et al., 2009). Furthermore, BACE1 cleavage of APLP1 has recently been shown to result in the release of an Aβ-like peptide, which does not aggregate and could be used as surrogate marker for increased γ-secretase cleavage by cerebrospinal fluid analysis (Yanagida et al., 2009). All three APP family members have been

shown to be cleaved by caspases at their conserved VEVD motif within the C-terminus, but the role of this cleavage is still debated (Galvan et al., 2002; Harris et al., 2010).

Proteolytic processing of APP, APLP1, and APLP2 by γ-secretase at the ϵ-site generates ICDs, which are binding to the adaptor protein Fe65 and, when co-expressed with Fe65, can transactivate Gal4-Tip60 constructs (Scheinfeld et al., 2002; Li and Sudhof, 2004). Transgenic mice expressing AICD and Fe65 were reported to show pathological features of AD (Ghosal et al., 2009). We have previously shown that AICD is transported to the nucleus by Fe65 where, together, they bind Tip60 and form spherical nuclear complexes (AFT-complexes), which localize in transcription factories (von Rotz et al., 2004; Konietzko et al., 2010). Here, we investigate the nuclear localization of APLP1 and APLP2 ICDs upon Fe65 and Tip60 co-expression. Furthermore, we analyze the differences in subcellular localization and turnover of the full-length proteins as well as their ICDs. We identify dramatic differences in subcellular localization and signaling capability of APLP1 compared to APP and APLP2. Our results provide evidence for a nuclear signaling function of ICDs derived from APP and APLP2 and support a distinct functional role for APLP1.

3.2 Results

3.2.1 Nuclear AFT-complex formation of APP family members' ICDs

The members of the APP family—APP, APLP1, and APLP2—show a high degree of sequence homology. In particular, the intracellular domain of APP family members is highly conserved and contains common motifs such as a caspase cleavage site and NPxY motif for binding of adaptor proteins. We have previously shown that AICD bound to Fe65 translocates to the nucleus and forms, together with Tip60, spherical nuclear AFT-complexes (Konietzko et al., 2010). Therefore, we were interested whether APLP1 and APLP2 intracellular domains (subsequently referred to as AL1ICD and AL2ICD) form nuclear AFT-complexes similar to AICD.

Co-expression of Fe65, Tip60, and APP in HEK cells resulted in the retention of Fe65-AICD complexes in the nucleus and the formation of AFT-complexes as reported previously (von Rotz et al., 2004; Goodger et al., 2009; figure 3.1A, top row). For detection of AFT-complexes, Tip60 and APP were fused to citrine and CFP fluorescence proteins, while Fe65 was detected by antibody staining. As already shown in an earlier publication, antibody access to AFT-complexes is restricted due to their density (Goodger et al., 2009). Therefore, the localization of Fe65 to AFT-complexes is sometimes not as clear as observed for the fluorescently-tagged proteins. Similar to AICD, AL2ICD also formed spherical AFT-complexes with Fe65 and Tip60 in the nucleus (figure 3.1A, bottom row). Surprisingly, AL1ICD did not localize to the nucleus and Fe65 was retained in extranuclear compartments, co-localizing with full-length APLP1 (figure 3.1A, middle row). Cytosolic retention of Fe65 prevented the redistribution of Tip60 to nuclear spots, resulting in an accumulation of Tip60 in nuclear speckles.

To exclude the possibility that the observed different nuclear signaling capabilities of APP family members were due to properties of the chosen cell line, experiments were repeated in N2a mouse neuroblastoma cells. Co-expression of Fe65, Tip60, and APP led to the formation of spherical nuclear AFT-complexes (figure 3.1B, top row). Similar to our observations in HEK cells, AL2ICD formed AFT-complexes (figure 3.1B, bottom row), while AL1ICD was not detected in nuclear structures and, due to the sequestration of Fe65 by full-length APLP1, Tip60 was localized to nuclear speckles (figure 3.1B, middle row).

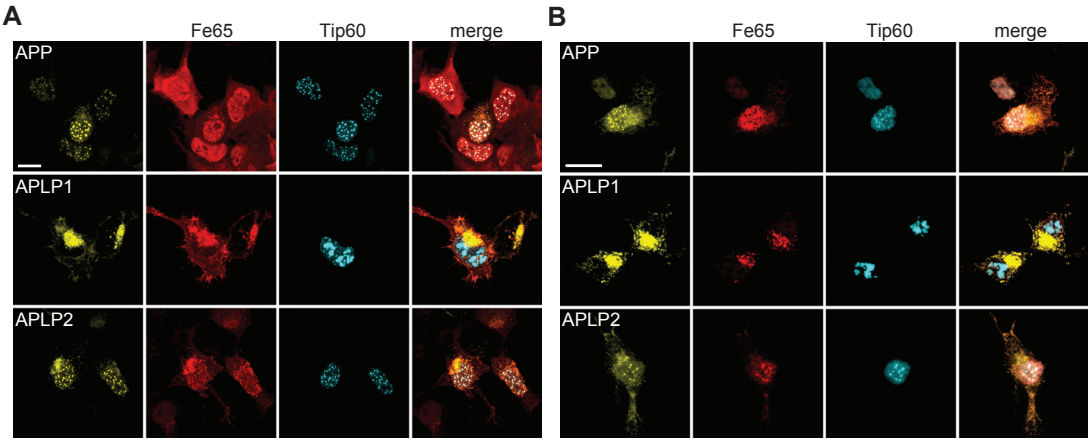

Figure 3.1 ICDs derived from APP and APLP2, but not APLP1, form nuclear AFT-complexes. **A:** Confocal fluorescence images of HEK cells transfected with HA-Fe65, CFP-Tip60, and APP-Cit (top row), APLP1-Cit (middle row), or APLP2-Cit (bottom row). **B:** Confocal fluorescence images of N2a cells transfected with HA-Fe65, CFP-Tip60, and APP-Cit (top row), APLP1-Cit (middle row), or APLP2-Cit (bottom row). Note the formation of spherical AFT-complexes in the nucleus of cells transfected with APP or APLP2 in both cell lines. In contrast expression of APLP1 resulted in accumulation of APLP1 and Fe65 in extranuclear compartments and at the plasma membrane, whereas Tip60 localized to nuclear speckles. Scale bars represent 13 µm.

3.2.2 Protein turnover of APP family members

To further study the subcellular localization of the APP family members we expressed APP/APLP with N-terminal myc-tags, preceded by the APP signal peptide to ensure membrane insertion, and C-terminal HA-tags. A GAPDH promoter was chosen for expression because the GAPDH gene is constitutively expressed at high levels in almost all tissues and expression of transgenes via this mammalian promoter yields good expression, which is weaker than with viral promoters. Expression of APP family members in HEK cells showed a clear intracellular localization to vesicular structures for APP and APLP2, whereas APLP1 was mostly localized to the cell membrane (figure 3.2A). The different subcellular localization of APP and APLP1 was also observed with co-expression of citrine-tagged APP and cerulean-tagged APLP1 proteins (figure 3.3A). Furthermore, a clear FRET signal was observed between APP and APLP2 but not between APP and APLP1 in HEK cells, primary astrocytes, and primary neurons (figure 3.3B–D). Thus, in addition to the co-localization of APP and APLP2, these two family members can form heterodimers.

The N-terminal myc-tagged constructs allowed cell-surface labeling of APP/APLPs on living cells (figure 3.2B). Antibody incubations were performed at 4 °C to inhibit endocytosis that is dependent on the GTPase function.

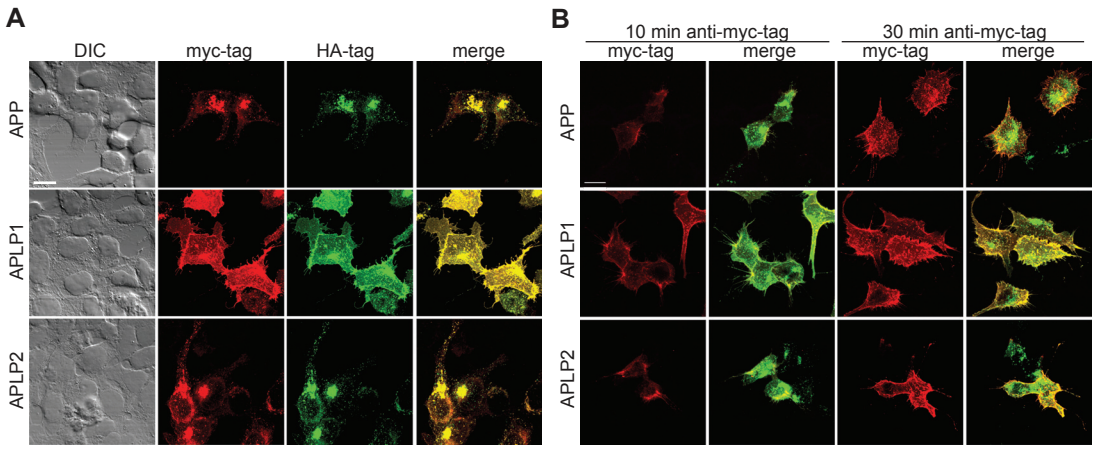

Figure 3.2 APP and APLP2 differ in their subcellular localization from APLP1. **A:** DIC and confocal fluorescence images of HEK cells expressing APP (top row), APLP1 (middle row), or APLP2 (bottom row) and stained with myc- and HA-tag antibodies. APP and APLP2 showed a clear intracellular localization to vesicular structures, whereas APLP1 mostly localized to the cell membrane. **B:** Confocal fluorescence images of HEK cells expressing APP (top row), APLP1 (middle row) or APLP2 (bottom row) after live antibody incubation. Incubation of cells with myc-tag antibody at 4 °C for 10 min resulted in surface labeling, especially of APLP1. After 30 min of myc-tag antibody incubation, cell surface signals of APP and APLP2 reached a similar strength as APLP1. Cells were counter-stained with HA-tag antibody after fixation. Scale bars represent 13 µm.

In contrast, exocytosis, which is promoted by zippering of SNARE proteins mediating vesicle fusion, is still able to occur in the absence of enzymatic activity. After 10 min of myc-tag antibody incubation we detected surface labeling for all three APP family members. The strongest staining was observed for APLP1. However, after 30 min incubation, APP and APLP2 surface staining reached similar levels as APLP1. This points towards a higher turnover of APP and APLP2 compared to APLP1 at the plasma membrane.

To measure the half-lives of the APP family members we inhibited protein synthesis for different durations. HEK cells were transfected with C-terminally HA-tagged APP/APLP constructs, all driven by a GAPDH promoter to ensure comparable expression levels. Twenty-four hours after transfection, protein synthesis was inhibited with cycloheximide. Cells were harvested after the indicated time of cycloheximide incubation and levels of full-length protein determined by western blot (figure 3.4A). APP/APLP full-length levels were normalized to the highly stable α-tubulin. APP and APLP2 displayed short half-lives of 43 min and 53 min, respectively, while half-life of APLP1 was higher than five hours (308 min; figure 3.4B). The much higher stability of APLP1 is also evident in the left column of figure 3.4A: despite the expression

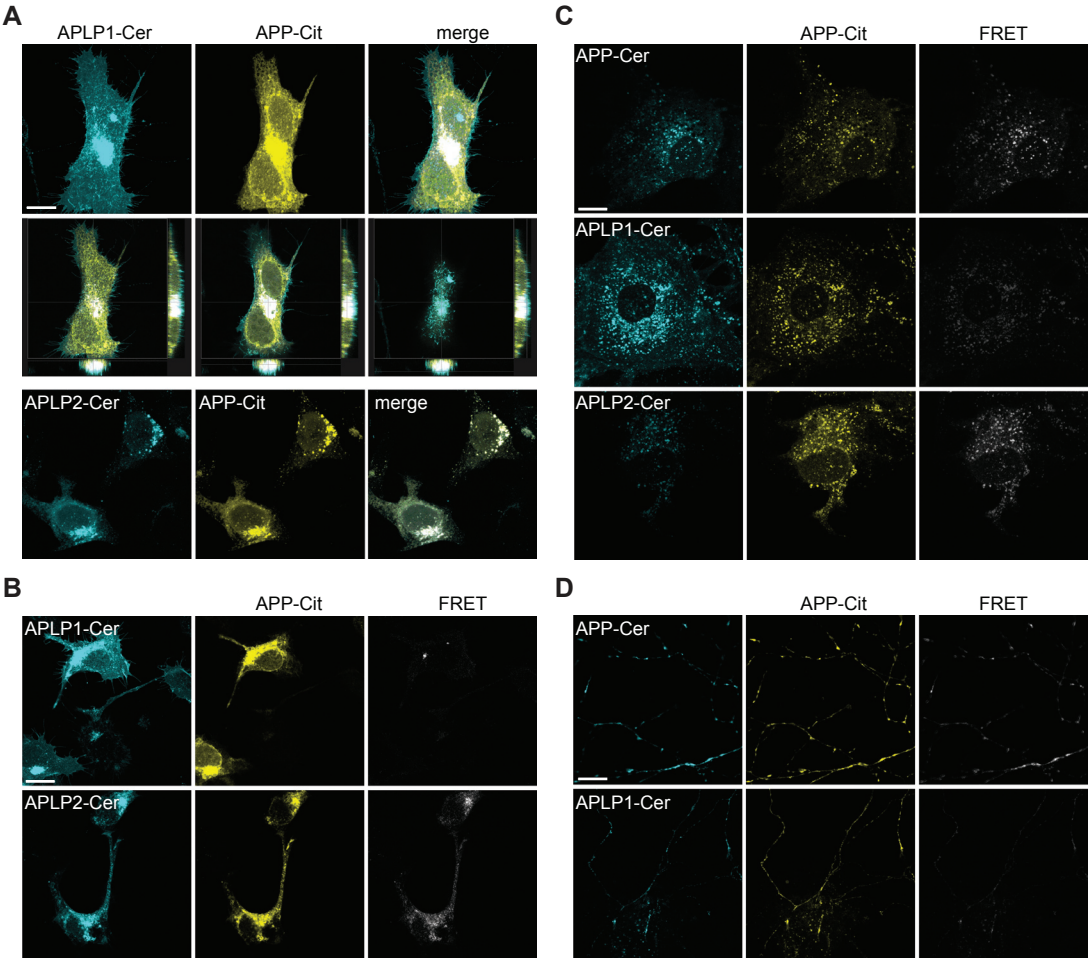

Figure 3.3 APP family members show different subcellular localization and heterodimerization. **A:** Confocal fluorescence images of HEK cells transfected with APLP1-Cer and APP-Cit. Top row shows maximum projection and middle row single sections at different z-positions. Note the intracellular localization of APP and the prominent localization of APLP1 at the plasma membrane. In contrast, the co-expression of APP and APLP2 shows a clear overlap and localization to the same intracellular compartments (bottom row). **B:** Confocal fluorescence images and FRET analysis of HEK cells expressing APLP1-Cer and APP-Cit (top row), APLP2-Cer and APP-Cit (bottom row). **C:** Confocal fluorescence and FRET analysis of primary astrocytes expressing APP family members. APP-Cit was co-expressed with APP-Cer (top row), APLP1-Cer (second row), APLP2-Cer (bottom row). **D:** Confocal fluorescence images and FRET analysis of primary neurons expressing APP-Cer and APP-Cit (top row) and APLP1-Cer and APP-Cit (bottom row). In different cell types (B–D) co-expression of APP-Cit and APP-Cer revealed a strong FRET signal due to the presence of APP homodimers. Similarly, co-expression of APP-Cit and APLP2-Cer generated a FRET signal. In contrast, expression of APLP1-Cer and APP-Cit resulted in minimal FRET signal, indicating the near absence of APP/APLP1 heterodimerization. Scale bars represent 13 μm.

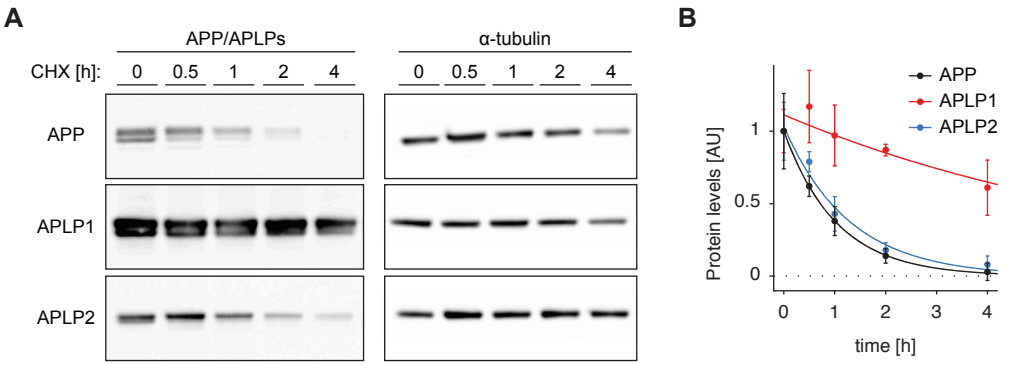

Figure 3.4 APP and APLP2 have a higher protein turnover than APLP1. **A:** Western blot analysis of HEK cells transfected with C-terminally HA-tagged APP/APLPs after indicated times of inhibition of protein synthesis with cycloheximide (CHX). Western blots were probed with HA-tag antibody and full-length APP/APLP displayed. Note the strong accumulation of APLP1 as compared to APP and APLP2. **B:** Quantification of APP/APLP full-length levels from A. Mean ± SEM of n = 3 are shown for each time point. Data was fitted to exponential functions by the least square approach. R^2(APP) = 0.99; R^2(APLP1) = 0.82; R^2(APLP2) = 0.98.

of all three family members under the same promoter, the levels of APLP1 were much higher, again highlighting its slower turnover.

3.2.3 Nuclear signaling capabilities of APP family members' ICDs

To investigate whether differences in nuclear localization capability of AICD and AL1ICD are mediated by properties of their extracellular or intracellular domains, we constructed chimeric APP/APLP1 expression plasmids. ICDs of APP and APLP1 were joined at the ϵ-site of APLP1 and APP, resulting in the chimeric constructs APLP1-AICD and APP-AL1ICD, respectively (figure 3.5A). Chimeric constructs were co-transfected with Fe65 and Tip60 in HEK cells and AFT-complex formation was observed by confocal microscopy. APP-AL1ICD did not form AFT-complexes, despite preserved binding of Fe65 (figure 3.5B top row). In contrast, nuclear AFT-complex formation was observed in cells transfected with APLP1-AICD. These results suggest that the formation of AFT-complexes is determined by the properties of the intracellular domain. Interestingly, the size of AFT-complexes formed from APLP1-AICD appeared to be decreased when compared to AFT-complexes formed from wildtype APP (figure 3.5B top row).

Because the chimeric proteins carry a chimeric ϵ-site it is possible that absent nuclear signaling of ICDs is due to impaired γ-secretase cleavage. To investigate this possibility, HEK cells were transfected with APP, APLP1 or

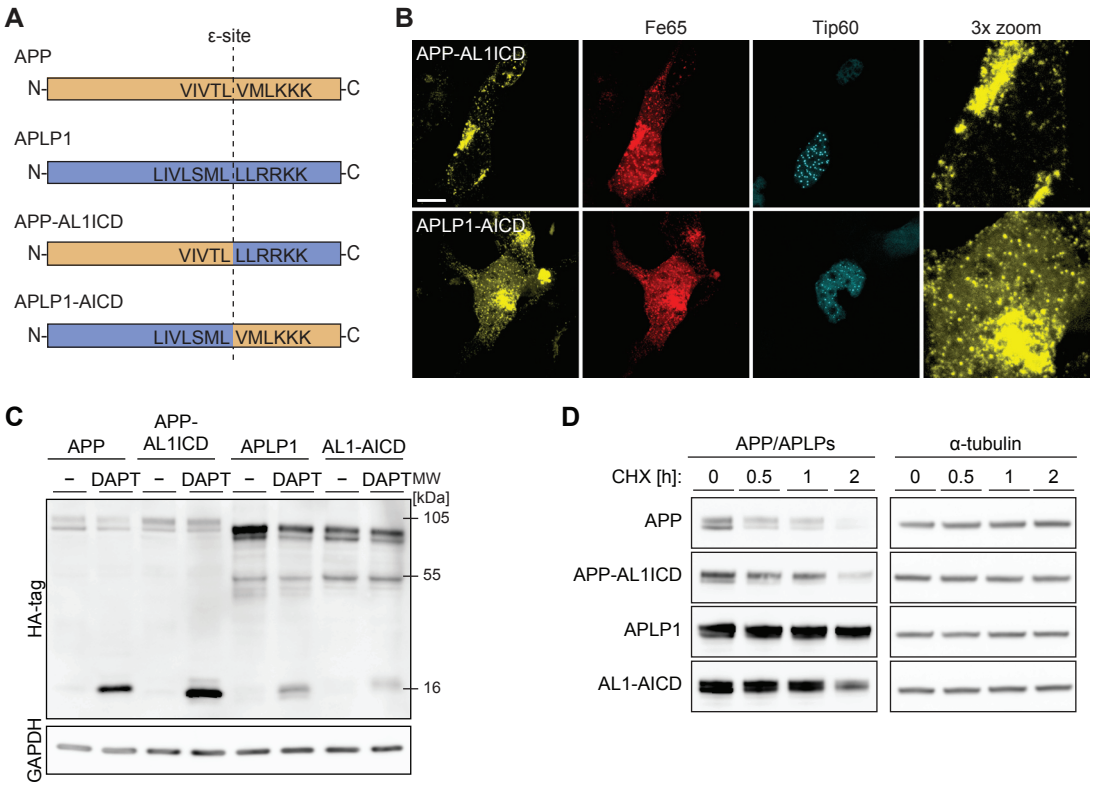

Figure 3.5 Nuclear signaling capability of APP family members is mediated by the intracellular domain. **A:** Schematic presentation of wildtype and chimeric APP/APLP1 constructs. **B:** Confocal fluorescence images of HEK cells co-transfected with HA-Fe65, CFP-Tip60 and the chimeric constructs APP-AL1ICD-Cit (top row) or APLP1-AICD-Cit (bottom row). Note that AFT-complexes formed in cells expressing APLP1-AICD but not APP-AL1ICD. Scale bar represents 13 µm. **C:** Western blot analysis of HEK cells transfected with HA-tagged wildtype or chimeric APP/APLP1 constructs and treated with the γ-secretase inhibitor DAPT or DMSO-control (–) for twenty-four hours. Western blots were probed with HA-tag antibody and accumulation of CTFs was observed with all constructs. **D:** Western blot analysis of HEK cells transfected with HA-tagged APP/APLP after indicated times of inhibition of protein synthesis with cycloheximide (CHX).

the chimeric APP/APLP1 proteins and treated with the γ-secretase inhibitor DAPT (figure 3.5C). DAPT treatment resulted in an accumulation of C-terminal fragments (CTFs) when compared to non-treated cells, demonstrating that γ-secretase cleavage of chimeric proteins is preserved. In line with the previous experiments using cycloheximide, increased full-length levels and decreased CTF levels of APLP1 indicate the slower turnover of APLP1 compared to APP. Furthermore, these results suggest that the extracellular and/or transmembrane regions mediate the differences in protein turnover. To better understand the

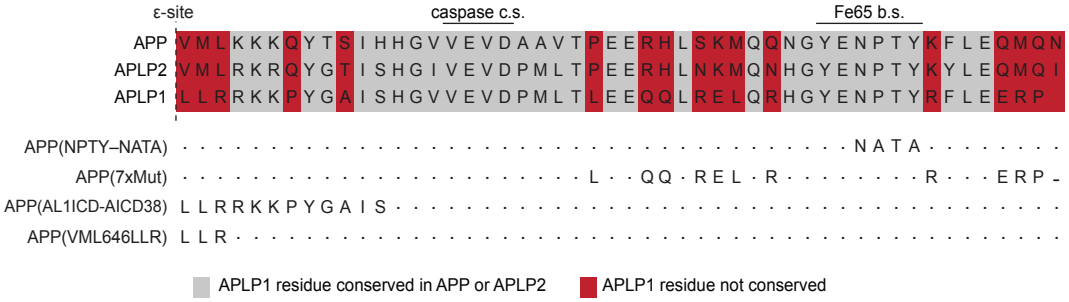

Figure 3.6 APP family members show high sequence homology. Schematic presentation of APP family ICD sequences and APP-to-APLP1 mutations. c.s.: cleavage site; b.s.: binding site.

turnover of APP family members, wildtype and chimeric APP-transfected HEK cells were treated with cycloheximide to monitor the turnover of full-length proteins. As described earlier, APP turnover is much faster than APLP1 turnover (figure 3.5D). Turnover of chimeric proteins was in between those of wildtype proteins but resembled more closely the protein carrying the respective extracellular domain. Together, these results suggest that both extracellular and intracellular regions determine the turnover of APP family members. Moreover, it is likely that the decreased AFT-complex formation for APLP1-AICD as compared to APP is due to the decreased turnover of APLP1-AICD, which would also lead to decreased AICD levels.

Our results show that nuclear signaling by the APP family members is determined by properties of the highly conserved ICDs (figure 3.6). We reasoned that the differences in AFT-complex formation capability between APP/APLP2 and APLP1 must derive from single amino acid or motif differences between the proteins. We identified seventeen conserved residues in AICD and AL2ICD that are not conserved in AL1ICD and could thus be responsible for the observed differences in nuclear signaling (figure 3.6). To test this hypothesis, we exchanged individual or multiple residues of APP by the corresponding residues of APLP1 and investigated AFT-complex formation. APP mutated in the NPxY motif was used as a negative control for AFT-complex formation. NPTY-to-NATA substitution within APP abolished Fe65 binding as previously reported (Cao and Sudhof, 2001) and prevented the nuclear translocation of AICD (figure 3.7, row 2).[2] We subsequently mutated amino acids sequentially, either alone or in combination. (See figures A.2 to A.4 in the appendix for a diagram depicting all APP-to-APLP1 mutations and corresponding confocal fluorescence images.) Changing all seven non-conserved residues in the C-

[2] The APP double substitution PTY685ATA is commonly referred to as NPTY-to-NATA or NPTY–NATA and this nomenclature is also used in this thesis (Cao and Sudhof, 2001).

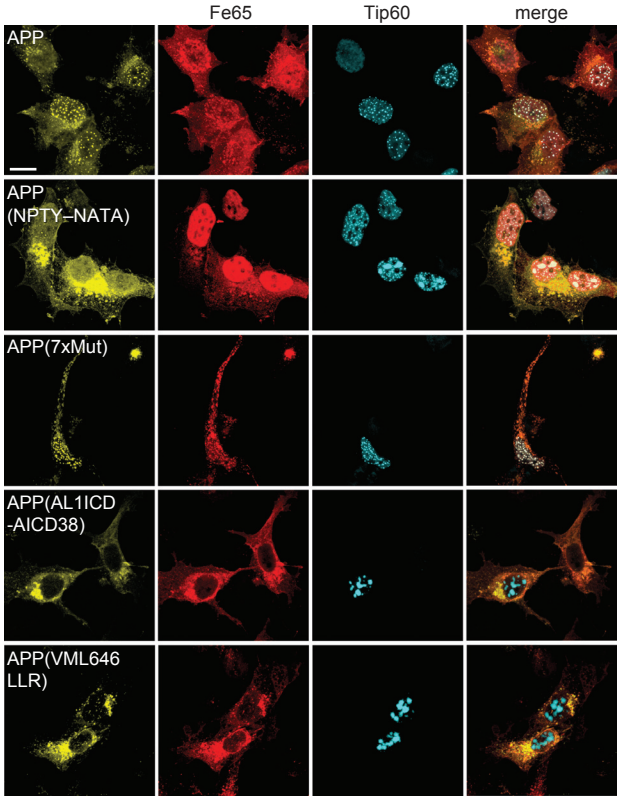

Figure 3.7 N-terminal residues of APP family ICDs are crucial for nuclear signaling capability. Confocal fluorescence images of HEK cells transfected with HA-Fe65, CFP-Tip60 and co-transfected with APP-Cit, APP(NPTY–NATA)-Cit, or indicated citrine-tagged APP-to-APLP1 mutation constructs. See figure 3.6 for abbreviation of APP-to-APLP1 mutation constructs. Scale bar represents 13 µm.

terminal region of AICD that is reported to bind to Fe65 (Radzimanowski et al., 2008) did not disrupt nuclear signaling (figure 3.7, row 3; APP(7xmut)). In contrast, when we inserted the first twelve amino acids of AL1ICD into the APP sequence (APP(AL1ICD-AICD38)), nuclear signaling was completely abolished (figure 3.7, row 4). Further mutagenesis were done to identify the minimal set of amino acids that prevent nuclear localization of AICD (figures A.2 to A.4 in the appendix). By this means we discovered that exchange of the N-terminal residues VML to the corresponding APLP1 residues LLR (APP(VML646LLR)) is sufficient to ablate AFT-complex formation (figure 3.7, row 5).

Co-immunoprecipitation of SBP-tagged APP and APP(VML646LLR) showed that Fe65 binding is not impaired by exchange of N-terminal ICD residues (figure 3.8B). DAPT treatment of cells transfected with APP(VML646LLR) resulted in an accumulation of CTFs. This suggests that absence of nuclear

AFT-complex formation for APP(VML646LLR) is likely not due to disturbed γ-secretase cleavage (figure 3.8A). Interestingly, in DMSO control treated cells, ICDs derived from APP were detected but not from APP(VML646LLR) or APLP1. To unequivocally exclude that the replacement of N-terminal amino acids of AICD has an effect on APP processing, APP and APP(VML646LLR) were cloned to a expression vector with N-terminal myc-tag and C-terminal HA-tag. Cell lysate and culture medium was subjected to western blot and full-length APP, and its cleavage products (i.e., CTFs, AICD, sAPPs, and Aβ) analyzed by densitometry (figure 3.8C–E). The VML646LLR mutation does not change levels of full-length APP and products of the ectodomain shedding, i.e., CTF and sAPP. The products of γ-secretase cleavage, Aβ and AICD are expected to be released in a equimolar ratio. However, the VML646LLR mutation resulted in a significant reduction of AICD levels, but not Aβ levels. These results clearly show that the VML646LLR mutation does not impair the processing of APP and thus suggest that decreased AICD levels are due to faster degradation.

3.2.4 Degradation of APP family members' ICDs

Nunan et al. (2003) have shown that a peptide corresponding to last the twenty amino acids of AICD accumulates after inhibition of the proteasome, pointing to a role of the proteasome in AICD degradation. However, experimental evidence for proteasomal degradation of the complete AICD peptide and AICD derived from APP by γ-secretase cleavage is lacking. Little is also known about the mechanism responsible for degradation of AL1ICD and AL2ICD. We hypothesized that APP family ICDs have a different protein turnover, resulting in different capabilities to form nuclear AFT-complexes. To explore a possible role of the proteasome in the degradation of AICD, we treated HEK cells transfected with APP-Cit with two previously described proteasome inhibitors, epoxomicin and MG132. Treatment with both inhibitors strongly increased AICD levels, thus confirming the hypothesized degradation of AICD by the proteasome. In addition to AICD, an increase of CTF levels was observed by MG132 treatment, suggesting that MG132 inhibits the proteasome as well as γ-secretase when used in higher concentrations, as reported previously (Pinnix et al., 2001; figure 3.9A). To avoid interference with processing of APP, epoxomicin was used for proteasomal inhibition in the following experiments. HEK cells were transfected with APP-Cit, APP(VML646LLR)-Cit, or APLP1-Cit and treated with epoxomicin for six hours. In control treated cells, ICDs generated from APP(VML646LLR) were hardly visible, while clear levels were observed for ICDs derived from wildtype APP (figure 3.9B). Treatment with epoxomicin

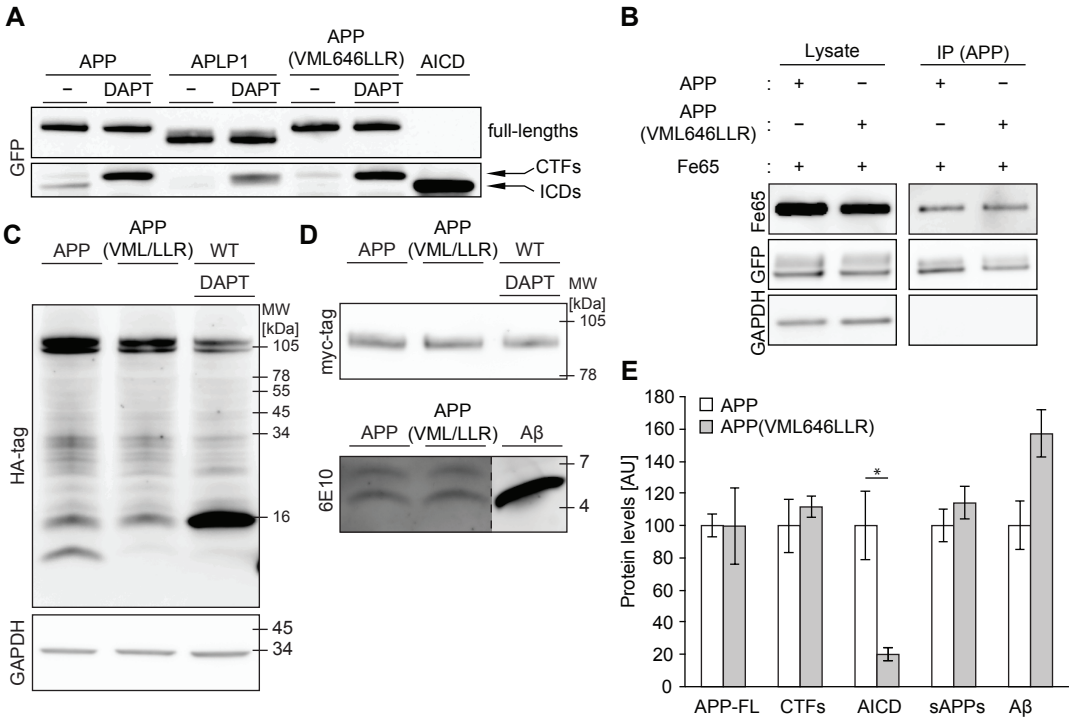

Figure 3.8 Mutation of N-terminal residues of AICD results in reduced levels of AICD but does not impair APP processing. **A:** Western blot analysis of HEK cells transfected with APP-Cit, APLP1-Cit, or APP(VML646LLR)-Cit constructs with 24-hour DAPT or DMSO-control (−) treatment. AICD-Cit transfected cell lysate was loaded to identify ICD bands and the membrane was probed with GFP antibody. **B:** Western blot analysis of co-immunoprecipitation of SBP-tagged APP or APP(VML646LLR) together with HA-tagged Fe65. Binding of Fe65 is not impaired by the VML646LLR mutation. **C:** Western blot analysis of HEK cell lysate transfected with N-terminal myc-tagged and C-terminal HA-tagged APP or APP(VML646LLR) constructs. VML646LLR is abbreviated to VML/LLR. DAPT-treated wildtype APP sample was loaded to identify AICD and CTF bands. **D:** Western blot analysis of the corresponding cell media from C. sAPPs were detected with myc-tag antibody (top panel). 6E10 antibody was used to detect Aβ and 10 ng synthetic Aβ42 were loaded to identify monomeric Aβ (bottom panel). Dashed line indicates removal of western blot lanes; depicted lanes derive from same western blot but different exposure times. **E:** Quantification of protein levels from C and D. Mean ± SEM of n = 3 are shown ($^{*}p < 0.05$, t-test).

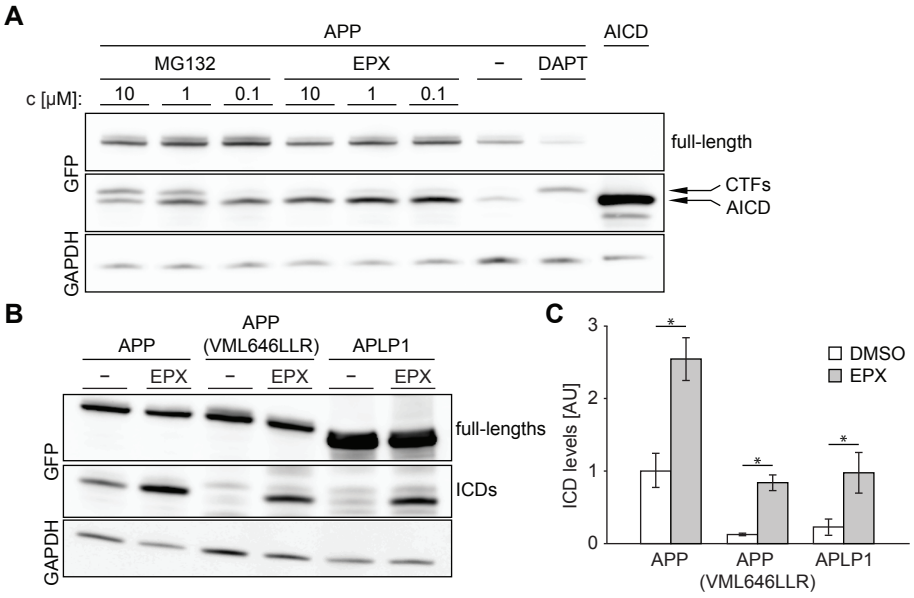

Figure 3.9 APP family ICDs are degraded by the proteasome and N-terminal ICD residues are crucial for their steady-state levels. **A:** Western blot analysis of HEK cells transfected with APP-Cit followed by six hours treatment with indicated concentration of MG132, epoxomicin (EPX), or DMSO-control (−). APP-Cit transfected HEK cells treated with DMSO or DAPT and AICD-Cit transfected cells were loaded to identify CTFs and AICD bands. Membranes were probed with GFP antibody. Note that MG132 inhibits the proteasome and at higher concentrations also γ-secretase, whereas epoxomicin is a specific proteasome inhibitor. **B:** Western blot analysis of HEK cells transfected with APP-Cit, APLP1-Cit or APP(VML646LLR)-Cit constructs followed by six hours of proteasome inhibition with 0.1 µM epoxomicin or DMSO-control (−) treatment. The membrane was probed with GFP antibody and GAPDH was used as a loading control. In the absence of proteasome inhibition ICDs derived from APP are clearly visible, but not ICD derived from APP(VML646LLR) and APLP1. **C:** Quantification of ICD levels from B. GAPDH protein levels were used to normalize ICD protein levels. Mean ± SEM of n = 3 are shown ($^*p < 0.05$, t-test).

significantly increased the ICDs from APP-Cit, APP(VML646LLR)-Cit, and APLP1-Cit to detectable levels (figure 3.9B). To exclude that the observed reduction of ICD derived from APP(VML646)LLR under steady-state conditions is due to the relatively large citrine-tag, we repeated the experiment with HA-tagged constructs. Steady-state levels of ICD from APP(VML646LLR) were clearly reduced (figure 3.10A) and inhibition of the proteasome increased ICD levels derived from both, APP and APP(VML646LLR). To exclude a cell-line specific effect, experiments were repeated in N2a mouse neuroblastoma cells. As in HEK cells, a clear reduction of steady-state levels of ICD from APP(VML646LLR) was observed (figure 3.10B–C). Additionally, inhibition of

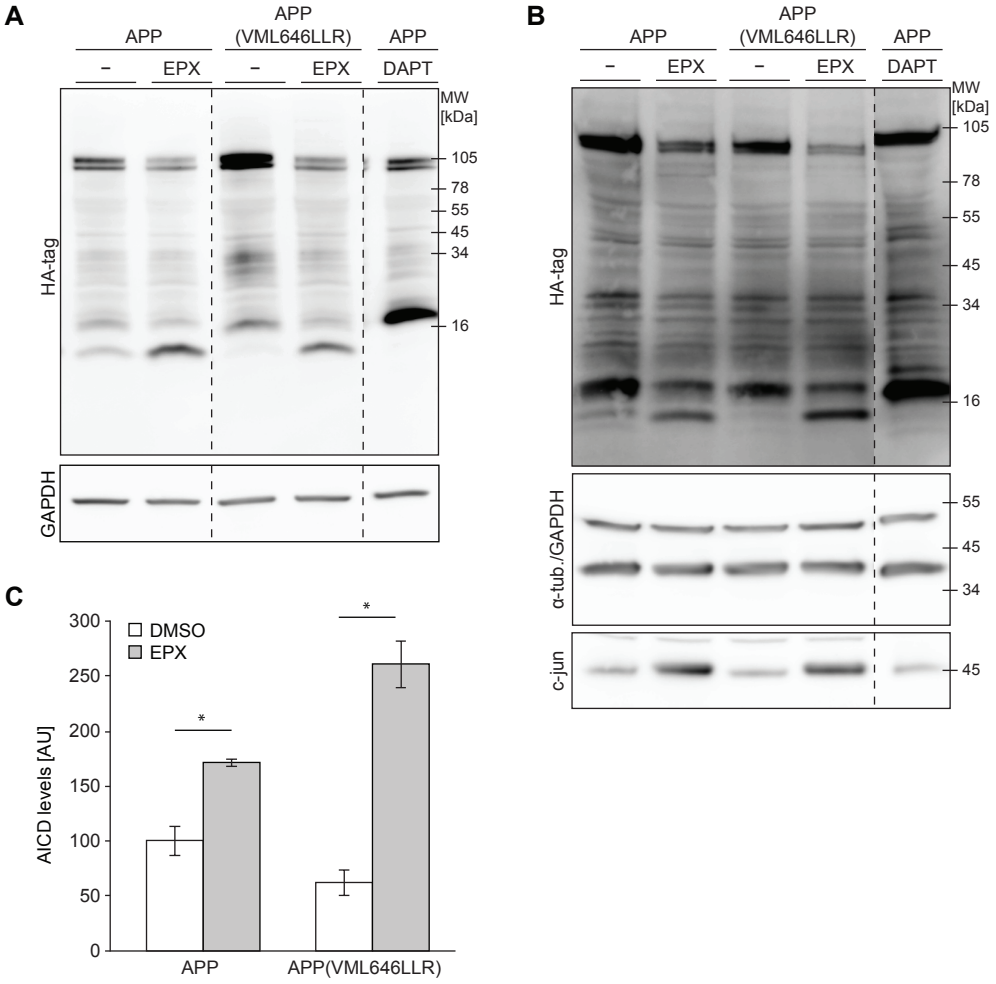

Figure 3.10 Levels of AICD depend on its N-terminal residues. **A:** Western blot analysis of HEK cells transfected with HA-tagged APP or APP(VML646LLR) and treated with 0.1 μM epoxomicin (EPX) or DMSO-control (−) for six hours. **B:** Western blot analysis of N2a cells transfected with HA-tagged APP or APP(VML646LLR) and treated with 1 μM epoxomicin or DMSO-control (−) for six hours. **C:** Quantification of AICD levels from B. Mean ± SEM of n = 4 are shown ($^*p < 0.05$, t-test). DAPT treated samples were loaded to clearly identify CTF and AICD bands. c-jun was detected as positive control for inhibition of the proteasome. Dashed line indicates removal of western blot lanes; depicted lanes derive from same western and same exposure times are displayed.

the proteasome completely restored ICD levels, even above wildtype levels (figure 3.10B–C). In addition to the housekeeping proteins GAPDH and α-tubulin, c-jun was detected as marker for inhibition of the proteasome as used previously (Taylor et al., 2007). It has to be kept in mind that analysis of samples after inhibition of the proteasome allows only indirect conclusions about the rate of proteasomal degradation. Indeed, not proteasomal degradation but protein synthesis is assessed. Incomplete inhibition of the proteasome or too short treatment periods (i.e., before a new steady-state is established) can obstrude result interpretation. Together, our results from HEK and N2a cells using different APP and APP(VML646LLR) constructs clearly show reduced steady-state levels of ICDs derived from APP(VML646LLR). Further, these results suggest that the half-life differs between APP family ICDs due to different proteasomal degradation efficacy that is dependent on the N-terminus generated after γ-secretase cleavage. However, we can not exclude that other mechanism (e.g., lysosomal degradation) have a different effect on AICD with different N-termini.

Next, we asked whether the localization of APP family ICDs that do not form AFT-complexes is changed after inhibition of the proteasome. Both APP(VML646LLR)-Cit and APP-AL1ICD-Cit, co-expressed with Fe65 and Tip60, formed AFT-complexes when treated with epoxomicin (figure 3.11). These results show that both AICD and AL1ICD can be transferred to the

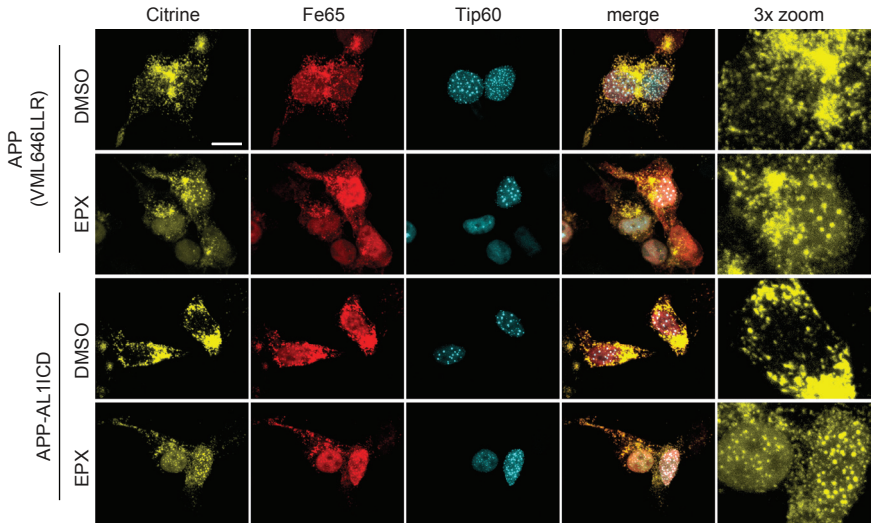

Figure 3.11 Nuclear localization of APP family ICDs is regulated by proteasomal degradation. Confocal fluorescence images of HEK cells transfected with HA-Fe65, CFP-Tip60 and co-transfected with APP(VML646LLR)-Cit (upper rows) or chimeric APP-AL1ICD-Cit (bottom rows) mutation constructs with six hours epoxomicin (EPX; 0.1 µM) or DMSO-control treatment. Note that AFT-complexes are formed after epoxomicin treatment. Scale bar represents 13 µm.

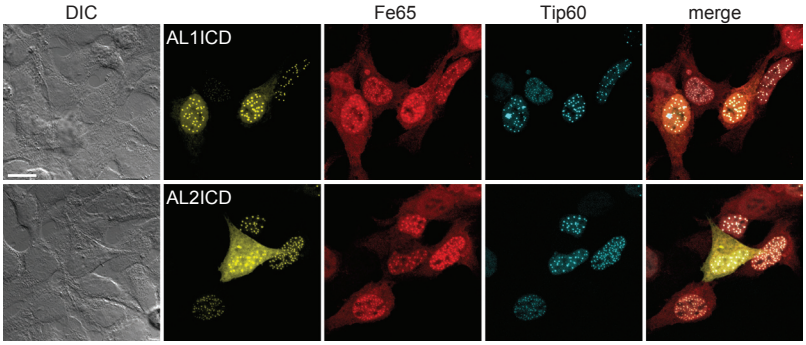

Figure 3.12 AL1ICD and AL2ICD form AFT-complexes. DIC and confocal fluorescence images of HEK cells transfected with HA-Fe65, CFP-Tip60 and Cit-AL1ICD (top row) or Cit-AL2ICD (bottom row). Note the nuclear localization of Al1ICD to nuclear complexes. Scale bars represent 13 µm.

nucleus and form AFT-complexes but under normal conditions AL1ICD is degraded very quickly by the proteasome due to the identity of its N-terminal residue. In line with this, we observe that AL1ICD with an N-terminal citrine-tag—which might prolong its half-life—localizes to AFT-complexes when co-expressed with Fe65 and Tip60 (figure 3.12A).

3.2.5 Regulation of AICD nuclear signaling by APLP1

We have shown that APLP1 does not signal to the nucleus but it nevertheless binds to Fe65. Therefore, investigated the influence of APLP1 expression on the nuclear signaling of AICD. We used a myc-tagged Tip60 to be able to co-express cerulean and citrine-tagged APLP1 and APP. AICD derived from APP again translocated to nuclear AFT-complexes in cells co-expressing Tip60 and Fe65 (figure 3.13). APLP1 bound to Fe65 with higher affinity than Tip60, as seen by the relocalization of Fe65 away from Tip60 in the nucleus. Consequently, co-expression of APLP1 together with APP, Fe65, and Tip60 prevented the formation of nuclear AFT-complexes that are clearly seen in cells not expressing APLP1 (figure 3.13; note that this experiment was performed by Zoë Goodger and previously published in Goodger, 2009 and Gersbacher et al., 2013). These results suggest that, although APLP1 does not directly signal to the nucleus, it influences AICD nuclear signaling via the sequestration of Fe65.

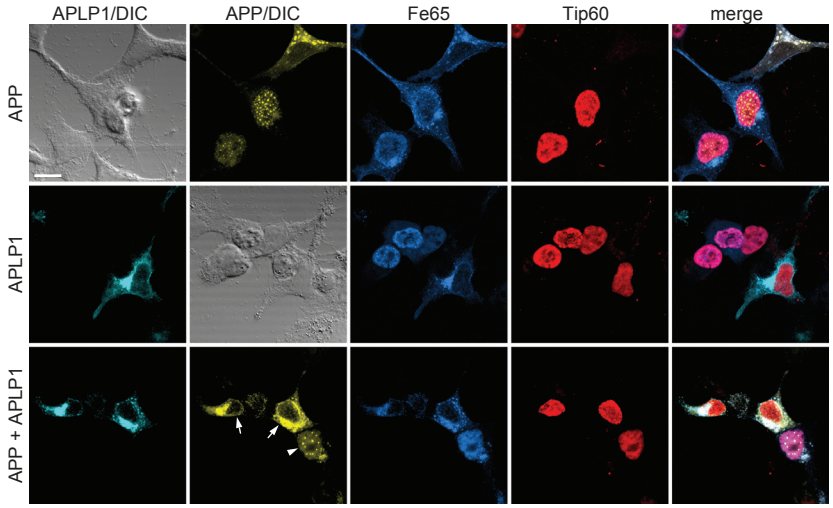

Figure 3.13 APLP1 expression prevents localization of AICD to AFT-complexes. Confocal fluorescence images of HEK cells transfected with HA-Fe65, myc-Tip60 and co-transfected with APP-Cit (top row) APLP1-Cer (middle row) or both (bottom row). Note that AFT-complex formation (arrowhead) was ablated in cells expressing APP as well as APLP1 (arrows). Scale bars represent 13 µm. This image is a courtesy from Zoë Goodger (Goodger, 2009; Gersbacher et al., 2013).

3.3 Discussion

Although the APP family members share a high sequence homology and undergo similar processing, different properties and functions of the three proteins have been described (Kaden et al., 2009). Here, we provide further experimental evidence for a distinct function of APLP1 among APP family members, by reporting a unique nuclear signaling capability for the ICDs of APP and APLP2, but not APLP1. Further, we identify sequence determinants of AICD that are necessary for the formation of AFT-complexes.

We show that the ICDs released from APP and APLP2 localize together with Fe65 and Tip60 to spherical nuclear AFT-complexes. In contrast, the ICD released from APLP1 does not localize to the nucleus, although it is able to bind Fe65. We demonstrate that nuclear localization of AL1ICD is prevented at two steps of APLP1 processing. Firstly, slower turnover of full-length APLP1 compared to APP results in lower levels of CTFs, which are the direct precursors of ICDs. Secondly, sequence analyses of AICD and AL1ICD point towards a increased proteasomal degradation of AL1ICD. Both steps ultimately and independently result in lower levels of AL1ICD. Our results also indicate that, although APLP1 does not signal directly to the nucleus, it has a regulatory function in AICD nuclear localization.

The expression of full-length APP or APLP2, together with Fe65 and Tip60, results in the translocation of their ICDs to nuclear AFT-complexes, which is dependent on cleavage by γ-secretase (von Rotz et al., 2004). In contrast, the ICD derived from APLP1 does not translocate to the nucleus. APLP1 binds and sequesters Fe65 outside of the nucleus, while Tip60 remains localized in nuclear speckles. These speckles represent a different nuclear compartment to that occupied by nuclear AFT-complexes, which themselves are thought to correspond to sites of transcription (Konietzko et al., 2010). Of note, AICD and AL2ICD occupy the same nuclear sites as the transcriptional activator NICD and interactions of AICD and NICD nuclear signaling have been described (data not shown; Kim et al., 2011). This could indicate that similar genes are regulated by the ICDs of APP and APLP2. In fact, the analysis of candidate genes regulated by AICD has shown that neprilysin expression and activity is reduced in fibroblasts derived from APP or APLP2 knockout mice and is dramatically diminished in cells from double knockout mice (Pardossi-Piquard et al., 2005). Likewise, for genes suppressed by AICD, as reported for LRP1, the expression levels were even stronger in APP/APLP2-deficient cells compared to single APP knockout cells (Liu et al., 2007). Taking this combined evidence into account, these results point towards an exclusive function of APP and APLP2 in transcriptional regulation.

Using cell surface labeling of living cells and determination of protein half-life time after cycloheximide-induced inhibition of translation, we show that full-length APP and APLP2 have a clearly faster turnover than APLP1. The stability of APLP1 is evident in different experimental settings and in stark contrast to the rapid turnover of APP and APLP2, whose rapid turnover kinetics have also been reported in vivo (Lyckman et al., 1998). Investigation of the nuclear signaling capabilities of chimeric APP/APLP1 proteins suggested that nuclear signaling capability is an intrinsic property of the ICD sequence that is present in APP but not in APLP1. We aligned the ICD sequences and identified seventeen amino acids that are conserved between APP and APLP2 but differ in APLP1. To identify sequence determinants for nuclear signaling capability we individually or in combination exchanged all amino acids of AICD with the corresponding APLP1 residues. Out of all single amino acid and motif changes, only the exchange of the N-terminal amino acids VML to LLR ablated nuclear signaling of AICD. APP(VML646LLR) binding to Fe65 and processing by secretases were not disturbed, but the resulting ICD levels were significantly lower than for the APP-derived ICDs, suggesting different degradation rates.

It has been reported that AICD is degraded by insulin-degrading enzyme (IDE), the lysosomal pathway, and the proteasome, whereas degradation of ALICDs have hardly been investigated (Buoso et al., 2010; Vingtdeux et al., 2007). Here, we show that the ICDs of both APP and APLP1 are degraded by the proteasome. Inhibition of proteasomal degradation by epoxomicin and the concomitant increase in ICD levels resulted in the translocation of ICDs derived from APP(VML646LLR) and the chimeric construct APP-ALICD to the nucleus. Under normal conditions, the ICDs of these proteins are degraded and do not reach the nucleus. However, ICDs released from APLP1, even with epoxomicin treatment, did not translocate to the nucleus. This is likely because of the slower turnover of APLP1, it accumulates to higher levels that bind and sequester Fe65, making Fe65 thus unavailable for the transport of AL1ICD to the nucleus. Together these results suggest that: (a) nuclear localization is an intrinsic property of all APP family ICDs, (b) a certain threshold level for ICDs has to be reached for nuclear translocation to occur, and (c) slow turnover of full-length APLP1 sequesters Fe65, rendering it unavailable for nuclear translocation of ICDs.

ICDs from APP, APP(VML646LLR), and APLP1 are degraded by the proteasome, and steady-state ICD levels from APP(VML646LLR) and APLP1 are strongly reduced. These results suggest that the proteasomal degradation rate of ICDs is dependent on their N-terminal residues. Interestingly, work by Alexander Varshavsky and colleagues has revealed a proteasomal pathway—the N-end rule pathway of proteasomal degradation—in which the

degradation of a protein is related to the identity of the protein's N-terminal residues (Varshavsky and Byrd, 1996). According to the N-end rule, leucine, the N-terminal residue of APLP1, is a destabilizing residue, whereas valine and methionine, the N-terminal residues of APP, are stabilizing. Since both, APP and APLP1 are degraded by the proteasome and carry multiple lysine residues that could potentially be ubiquitinated, it is possible that APP family ICDs, as suggested previously (De Strooper and Annaert, 2010), are substrates of the N-end rule pathway.

Walsh et al. (2003) reported higher stability for AL1ICD than AICD and AL2ICD when ICDs were expressed as soluble forms. Similarly, we observe nuclear signaling for ICDs of all three APP family members when ICDs are expressed as soluble proteins. The apparent differences in localization for AL1ICD derived from full-length APLP1 and soluble expressed AL1ICD are not surprising since much higher levels of ICDs are obtained from soluble expressed AL1ICD. Furthermore, we have shown that AL1ICD generated by γ-secretase cleavage carries N-terminal residues that influence its degradation rate. However, the expression of soluble ICDs necessitates the addition of a methionine at the N-termini—for the start codon—that is likely to neutralize the different degradation times of AICD and AL1ICD reported here.

Our results help to explain the profound effects seen in knockout mouse lines of the APP protein family members. Animals deficient for APP and APLP2 die shortly after birth (von Koch et al., 1997; Heber et al., 2000). Knock-in mice have been generated to identify the domain of APP responsible for these effects. Mutation of the tyrosine residue preceding the NPxY motif (Tyr-682) abolished Fe65 binding, and thus nuclear signaling by AICD (Barbagallo et al., 2010). APP Y682G knock-in mice crossed to an APLP2 knockout strain were found to be postnatally lethal with neuromuscular synaptic defects, resembling APP/APLP2 double knockouts (Barbagallo et al., 2011). This points towards a requirement for AICD/AL2ICD-mediated nuclear signaling in development, a function that cannot be performed by APLP1. This is further supported by the observation that knock-in of the sAPPα or sAPPβ ectodomains alone is not sufficient to rescue the synaptic deficits of APP/APLP2 knockout mice (Li et al., 2010; Weyer et al., 2011). Although the phenotypes in these mouse lines could also originate from other aspects of APP biology—the Y682G knock-in has a dramatically increased production of sAPPα and the sAPP knock-ins also lack the Aβ sequence in addition to AICD—the current data combined with our experimental evidence strongly supports a role of nuclear signaling by AICD and AL2ICD in synapse formation that cannot be performed by AL1ICD.

We propose that AL1ICD does not have a direct physiological role in transcriptional regulation, but through sequestration of Fe65 by APLP1 this family

member might act as a repressor of AICD-mediated nuclear signaling. We conclude that nuclear signaling is a prime function of the APP and APLP2 ICDs. Our results also caution the use of drugs inhibiting APP processing as treatment for AD because of possible interference with APP/APLP transcriptional function.

4 Characterization of Proteasomal Degradation of AICD Species

In this chapter, we examine proteasomal degradation of different AICD species and evaluate a possible contribution of AICD species to AD pathology.

4.1 Introduction

APP is a central protein in the pathology of AD. Consecutive cleavage of APP by β- and γ-secretase releases Aβ and AICD, which are both short, biologically active peptides. Aβ is the main component of extracellular plaques in the brains of AD patients and is thought to trigger a toxic cascade eventually resulting in the development of AD (Hardy and Selkoe, 2002). For AICD in turn multiple functions have been identified, most prominently its transcriptional activity (Cao and Sudhof, 2001). γ-secretase cleavage of APP emerged to be very complex and different Aβ and AICD species with potentially different functions are produced.

Work pioneered by Yasuo Ihara and colleagues has revealed that γ-secretase is cleaving APP at multiple positions in a regulated sequence, commonly known as *sequential γ-secretase cleavage* (Qi-Takahara et al., 2005; see figure 4.1 for a schematic diagram of γ-secretase cleavage). The first cleavage takes place at the ϵ-site in the juxtamembrane region of APP, resulting in the release of AICD into the cytosol. In the following, γ-secretase moves along the protein stub towards its N-terminus and cleaves after every 3^{rd} to 4^{th} amino acid. Final cleavage takes place at the γ-site, releasing Aβ from the membrane. Importantly, cleavage at the individual sites displays some variety (figure 4.1). As a result AICD and Aβ species of varying lengths are produced. The predominant AICD species found is AICD50 that is produced by γ-secretase cleavage at the ϵ_{49}-site.[1] Additionally, longer AICD51 is produced by cleavage at the

[1] For nomenclature of AICD species, we will use the terms AICD50 and AICD51 which denotes their length in amino acids according to the nomenclature of Aβ-species. Other commonly

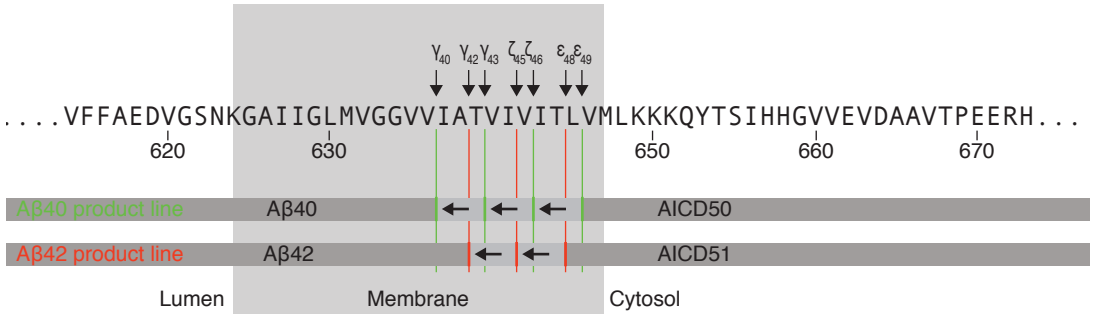

Figure 4.1 Sequential γ-secretase cleavage of APP along different product lines produces AICD and Aβ species of different length. APP peptide sequence surrounding the γ-secretase cleavage sites is depicted. γ-secretase cleavage follows predominantly the Aβ40 product line (green). In this case, initial cleavage at the ϵ_{49}-site releasing AICD50 is followed by cleavages at the ζ_{46}-, γ_{43}-, and γ_{40}-sites, eventually releasing Aβ40. To a lesser extent—albeit an increase is observed by the majority of FAD mutations—γ-secretase cleavage follows the Aβ42 product line (red). Here, initial cleavage at the ϵ_{48}-sites releasing AICD51 is followed by cleavages at the ζ_{45}- and γ_{42}-site, eventually releasing Aβ42. APP amino acids are labeled according to their position in the APP695 isoform. Cleavage sites of γ-secretase follow the commonly used nomenclature according to their position in C99.

ϵ_{48}-site. Multiple shorter AICD species (AICD49, AICD48, and AICD47) were described however their levels were extremely low and subsequent studies have failed to detect them (Gu et al., 2001; Dimitrov et al., 2013). For Aβ, the predominant species detected is Aβ40, produced by γ-secretase cleavage at the γ_{40}-site. Longer Aβ42, which is assumed to be the principal toxic agent in AD, is produced by cleavage at the γ_{43}-site. Additionally, longer Aβ43, which serves as a precursor of Aβ40, as well as shorter Aβ38, Aβ37, and Aβ34 are often detected. Accumulating evidence suggests that the position of the initial γ-secretase cleavage at the ϵ-site determines the positions of the subsequent sequential cleavages. Accordingly, two major product lines, commonly known as *Aβ40 and Aβ42 product lines*, have been identified (Chávez-Gutiérrez et al., 2012). Cleavage along product lines implies that production of AICD and Aβ species are inherently linked, i.e., AICD50 is accompanied by products of the Aβ40 product line, which is foremost Aβ40 but also Aβ43 and Aβ37. AICD51 in turn is accompanied by Aβ42 and its cleavage products Aβ38 and Aβ34. See figure 4.1 for a schematic illustration of sequential γ-secretase cleavage along product lines.

Mutations in the genes encoding APP and the γ-secretase subunits PSEN1 and PSEN2 are known to cause AD. Unsurprisingly, no unifying disease mechanism

found terms are AICD50-99 and AICDϵ49 for AICD50, and AICD49-99 and AICDϵ48 for AICD51 according to their position in C99 and their cleavage site, respectively.

for the approximately 300 described AD-causing mutations has been found. Multiple studies have shown that partial loss-of-function of γ-secretase cleavage at the ε-site is observed in majority of FAD mutations, albeit not all of them. In addition, detailed analyses of γ-secretase processing at the ε-site have revealed that FAD mutations can result in a shift of γ-secretase processing towards the Aβ42 product line (Sato et al., 2003; Chávez-Gutiérrez et al., 2012; Dimitrov et al., 2013). It is well established that AD-causing mutations result in an increase in the Aβ42-to-Aβ40 ratio. Because Aβ42 displays higher aggregation potential and toxicity than Aβ40, increase in the Aβ42-to-Aβ40 ratio is thought to drive disease progression. Interestingly, the described alterations of FAD mutations can also affect AICD. While partial loss-of-function changes AICD quantity (i.e., decreased total AICD levels), shift in product line alters the AICD quality (i.e., increased AICD51). In contrast to Aβ species, metabolism and function of different AICD species have so far been hardly addressed.

Few studies have investigated the mechanisms that result in degradation of AICD. Edbauer et al. (2002) have identified the insulin degrading enzyme (IDE) as a AICD degrading enzyme, which was confirmed by later studies (Farris et al., 2003; Buoso et al., 2012). Degradation by the lysosome was shown by Vingtdeux et al. (2007). Cupers et al. (2001) have shown that synthetic peptides of longer AICD forms (AICD57, AICD59) do not undergo proteasomal degradation. However, the relevance of these findings is not clear because AICD species of these lengths were never detected and are probably not generated by γ-secretase cleavage or any other processing. In contrast, Nunan et al. (2003) show degradation of a peptide corresponding to the last twenty amino acids of APP in *in vitro* proteasome assays. In chapter 3, we show that also AICD derived from APP by physiological γ-secretase cleavage undergoes proteasomal degradation. Our experiments that compare proteasomal degradation of ICDs of APP family proteins, suggest that the N-terminal amino acids are determining proteasomal degradation. Importantly, we further show that regulation of AICD levels by proteasomal degradation is linked to its presumed transcriptional function in AFT-complexes. However, to the best of our knowledge, no study has investigated degradation of specific AICD species separately.

The ubiquitin-proteasome system (UPS) is the major mechanism for selective protein degradation and thus essential for cellular functioning (Ciechanover, 1994). The proteasome is a large, multi-subunit protein complex that is primarily responsible for protein degradation (Ciechanover, 2013). In eukaryotes the proteasome is composed of the 20S core particle and the 19S regulatory particle. The 19S regulatory particle recognizes substrate proteins, unfolds them, and inserts them into the 20S core particle. The 20S core particle is a barrel-like structure with multiple proteolytic sites in its central chamber

that conducts the actual protein degradation. The most prominent substrate recognition signal for the proteasome is polyubiquitination. The seventy-six amino acid peptide ubiquitin is attached to substrate proteins by the interplay of E1 Ub-activating, E2 Ub-conjugating, and E3 Ub-ligase enzymes (Ub abbreviates ubiquitin). Ubiquitin bound to a substrate can itself be ubiquitinated, resulting eventually in the formation of a polyubiquitin chain. Different ubiquitination pathways exist, which are divided according to their mode of substrate recognition (Ravid and Hochstrasser, 2008). In regular ubiquitination, E3 Ub-ligase enzymes recognize substrate proteins via specific structures or specific post-translational modification (PTM) patterns (e.g., phosphorylation). The N-end rule pathway in contrast is a specific proteasomal degradation pathway in which the identity of the N-terminal residue of a protein determines the protein's stability (Bachmair et al., 1986). In the N-end rule pathway the substrate's N-terminus is directly recognized by specific E3 Ub-ligase enzymes, the N-recognins, which ubiquitinate substrate proteins and by this means mark them for degradation. Four functional N-recognins (UBR1, UBR2, UBR4, and UBR5) have been identified in the mammalian genome. N-recognins recognize and bind only specific N-terminal amino acids and, accordingly, the twenty naturally-occurring amino acids have stabilizing or destabilizing function if at the N-terminal position of a protein—see table 4.1 for a list of all amino acids and their function in the N-end rule pathway. Recent studies have indicated that destabilizing residues can be further subdivided in type 1 and type 2 destabilizing residues due to their recognition by structurally different but functionally similar domains of N-recognins. The UBR box, which is present in all four functional N-recognins, binds type 1 residues which are basic amino acids (Sriram et al., 2011). Type 2 residues in contrast are bulky and hydrophobic amino acids and are recognized by the N-domain, which was only found in UBR1 and UBR2. However, experimental evidence has suggested that also UBR4 is important for degradation of proteins with N-terminal type 2 residues, thus cautioning a general residue-to-domain allocation (Tasaki et al., 2005; Sriram et al., 2011). The N-end rule pathway is of particular importance for proteolysis-generated peptides since they can carry other N-terminal residues than the start codon–derived methionine (Varshavsky, 2011). Multiple functions of the N-end rule pathway have been described, including regulation of cardiac signaling and neurogenesis (for review see Tasaki and Kwon, 2007). A recent study has highlighted the role of N-end rule degradation of proteolytic fragments in various neurodegenerative diseases (Brower et al., 2013) and the essential function of the N-end rule pathway is also underlined by the embryonic lethality of mice deficient for the N-recognins UBR1 and UBR2 (An et al., 2006).

Table 4.1 Classification of amino acids according to their function in N-end rule proteasomal degradation. In N-end rule proteasomal degradation the N-terminal amino acid of a protein can have either stabilizing of destabilizing function. Destabilizing residues can be further subdivided into type 1 (basic) and type 2 (bulky, hydrophobic) residues that are recognized by different domain of N-recognins, the UBR-box and N-domain, respectively.

Function	Amino acid
Stabilizing	Alanine, methionine, proline, serine, threonine, valine
Type 1 destabilizing	Arginine, asparagine, aspartic acid, cysteine, glutamic acid, glutamine, glycine, histidine, lysine
Type 2 destabilizing	Isoleucine, leucine, phenylalanine, tryptophan, tyrosine

We have shown in chapter 3 that AICD is degraded by the proteasome and, importantly, that the N-terminus of AICD is crucial for its stability (Gersbacher et al., 2013). Interestingly, the two AICD species generated by γ-secretase processing of APP, AICD50 and AICD51, carry N-terminal residues that fall in different categories of the N-end rule. Valine, the N-terminal residue of AICD50, is a stabilizing residue. Leucine, the N-terminal residue of AICD51, in contrast, is a destabilizing residue and could thus mediate faster proteasomal degradation. However, experimental evidence for a role of the N-end rule pathway in degradation of AICD species is lacking. The aim of this study is, therefore, to investigate whether AICD species are differently regulated by the N-end rule pathway and whether such a regulation could influence transcriptional activity of AICD. We further aimed to explore whether shifting the product line preference of γ-secretase—as it is the case by AD-causing mutations—could result in decreased total AICD levels due to the increased production of a potentially unstable AICD species and influence transcriptional function of AICD.

4.2 Results

4.2.1 Construction and validation of ubiquitin-fusion plasmids

Proteins that undergo degradation by the N-end rule pathway are normally derived from pro-N-end rule substrates by proteolytic cleavage. This cleavage exposes the N-terminus of N-end rule substrates, which are then targeted by N-end rule pathway-specific E3 Ub-ligase enzymes, the N-recognins. For studying N-end rule substrates, it is desirable to examine their catabolism and function independently of preceding proteolytic cleavages. However, protein expression from regular plasmids results in proteins with N-terminal methionine due to the necessity of a start codon for initiation of ribosomal translation. Methionine is a stabilizing residue in terms of the N-end rule, and its N-terminal addition would mask the normal processing of an N-end rule substrate. A way to circumvent the addition of N-terminal methionine is thus needed for expression of N-end rule substrates.

The ubiquitin-fusion (Ub-fusion) technique allows the expression of proteins without N-terminal start codon–derived methionine (Bachmair et al., 1986; Lévy et al., 1996). The technique is based on the way ubiquitin is encoded and processed in most higher eukaryotes (figure 4.2A; Kimura and Tanaka, 2010). Multiple ubiquitin-encoding sequences follow each other in a head-to-tail configuration without interruption, resulting thus in the expression of a linear polyubiquitin chain. However, immediately after translation of the polyubiquitin chain—also referred to as co-translationally—deubiquitinating enzymes (DUBs) recognize and cleave precisely at the border of two ubiquitin moieties, thus releasing separate ubiquitin moieties. Bachmair et al. (1986) show that a protein of interest (POI) fused in frame to the C-terminus of ubiquitin is rapidly separated from ubiquitin. Due to the precise cleavage at the C-terminus of a ubiquitin moiety the technique allows the expression of POIs with desired N-termini.

Ub-fusion constructs of AICD50 and AICD51 were prepared with C-terminal citrine or HA-tag. Ub-AICD50-Cit and Ub-AICD50-Cit constructs were expressed in HEK cells to test expression of Ub-fusion proteins and cleavage by DUBs. Ubiquitin is successfully removed from Ub-AICD-Cit as indicated by a major GFP-positive band at same height as regular-expressed AICD50-Cit (figure 4.2B compare lane two and four). AICD50-Cit from both, regular and Ub-fusion construct, were detected at approximately 7 kDa above GFP, the expected difference by the AICD-linker fusion (figure 4.2B compare lane two and four to lane three). A weak GFP-positive band was observed approximately 9 kDa above AICD-Cit (figure 4.2B lane four), indicating that only a minor

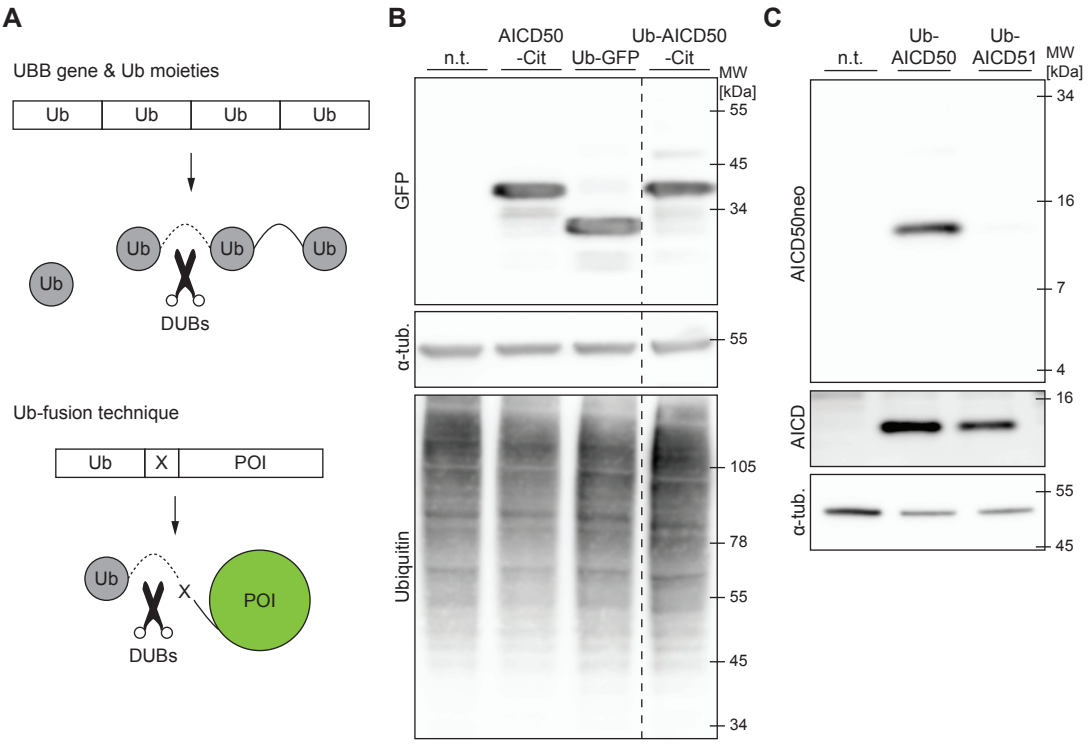

Figure 4.2 Ub-fusion technique allows expression of proteins with desired N-termini. **A:** Schematic illustration of the Ub-fusion techniques. Ubiquitin is encoded in the mammalian genome as tetramer (*UBB*). Upon expression, DUBs co-translationally and precisely separate ubiquitin moieties. Fusion of a POI (e.g., GFP) to the N-terminus of a ubiquitin moiety results in exposure of a desired N-terminal residue of the POI (here X) after removal of ubiquitin. **B:** Western blot analysis of HEK cells non-transfected (n.t.; lane 1), or transfected with citrine-tagged AICD50 with normal N-terminal methionine (AICD50-Cit; lane 2), Ub-fusion construct–derived GFP (Ub-GFP; lane 3), or AICD50-Cit fused at its N-terminus to ubiquitin (Ub-AICD50-Cit; lane 4). For both AICD-expressing constructs major GFP-positive bands were detect on same height, indicating that ubiquitin is successfully removed co-translationally. Dashed line indicates removal of western blot lanes; depicted lanes derive from same western blot and same exposure times are displayed. **C:** Western blot analysis of HEK cells non-transfected (n.t.; lane 1), or transfected with C-terminally HA-tagged Ub-fusion constructs of AICD50 (Ub-AICD50; lane 2) or AICD51 (Ub-AICD51; lane 2). A clear band in the sample expressing Ub-fusion construct of AICD50 with a AICD50neo antibody confirms precise removal of the ubiquitin moiety (upper panel). An antibody recognizing all AICD species (middle panel) and α-tubulin (bottom panel) confirm similar expression of AICD species and similar protein loading, respectively. Western blot was processed to enhance detection of AICD as described in Material and Methods (Pimplikar and Suryanarayana, 2011).

fraction of Ub-AICD-Cit remained uncleaved. Usage of Ub-fusion constructs did not lead to a overt increase in total protein ubiquitination (figure 4.2A bottom panel). These results confirm that AICD expression from Ub-fusion constructs and processing by DUBs is working.

To test whether cleavage ob Ub-fusion constructs by DUBs is precise—and is thus suitable for the expression of specific AICD species—an antibody recognizing exclusively AICD50 (AICD50neo) was used. Previous studies have shown that the AICD50neo antibody does not detect other AICD species, full-length APP, or other APP fragments (Chávez-Gutiérrez et al., 2012). HA-tagged Ub-fusion constructs of AICD50 and AICD51 (Ub-AICD50-HA and Ub-AICD51-HA) were expressed in HEK cells. Western blots were prepared and probed with AICD50neo antibody. A strong band was detected in samples expressing AICD50 at approximately 11 kDa, the expected height of HA-tagged AICD50. No signal was observed in AICD51-expressing samples. An antibody recognizing the C-terminus of AICD was used to show a similar expression of AICD50 and AICD51 (figure 4.2C middle panel). Together, these results show that the Ub-fusion technique allows efficient and reliable expression of specific AICD species. This technique thus allows us to investigate degradation and function of different AICD species separately from APP processing by γ-secretase. Importantly, the AICD Ub-fusion constructs allow us to investigate naturally-occurring AICD species, without a artificial start codon–derived methionine used in previous studies.

4.2.2 Proteasomal degradation of AICD species

We aimed to determine whether AICD species undergo different proteasomal degradation. Ub-fusion constructs of AICD50 and AICD51 were expressed in HEK cells and treated with proteasomal inhibitor (figure 4.3A and B). We observed that AICD51 showed significantly lower levels under DMSO control conditions than AICD50. Both AICD species increased after inhibition of the proteasome with epoxomicin. In contrast to the control conditions, no difference in AICD50 and AICD51 levels was observed after treatment with 1 μM epoxomicin. This means that the apparent differences of AICD50 and AICD51 were repealed by inhibiting the proteasome. In turn we can conclude that AICD51 undergoes faster proteasomal degradation than AICD50. Treatment with a lower concentration of epoxomicin (0.1 μM) resulted in lower levels of AICD50 than treatment with 1 μM, demonstrating that 0.1 μM epoxomicin resulted in an incomplete inhibition of the proteasome. Interestingly, incomplete inhibition with 0.1 μM epoxomicin was not sufficient to restore levels of AICD51 levels to those of AICD50, thus providing further support for a increased proteasomal

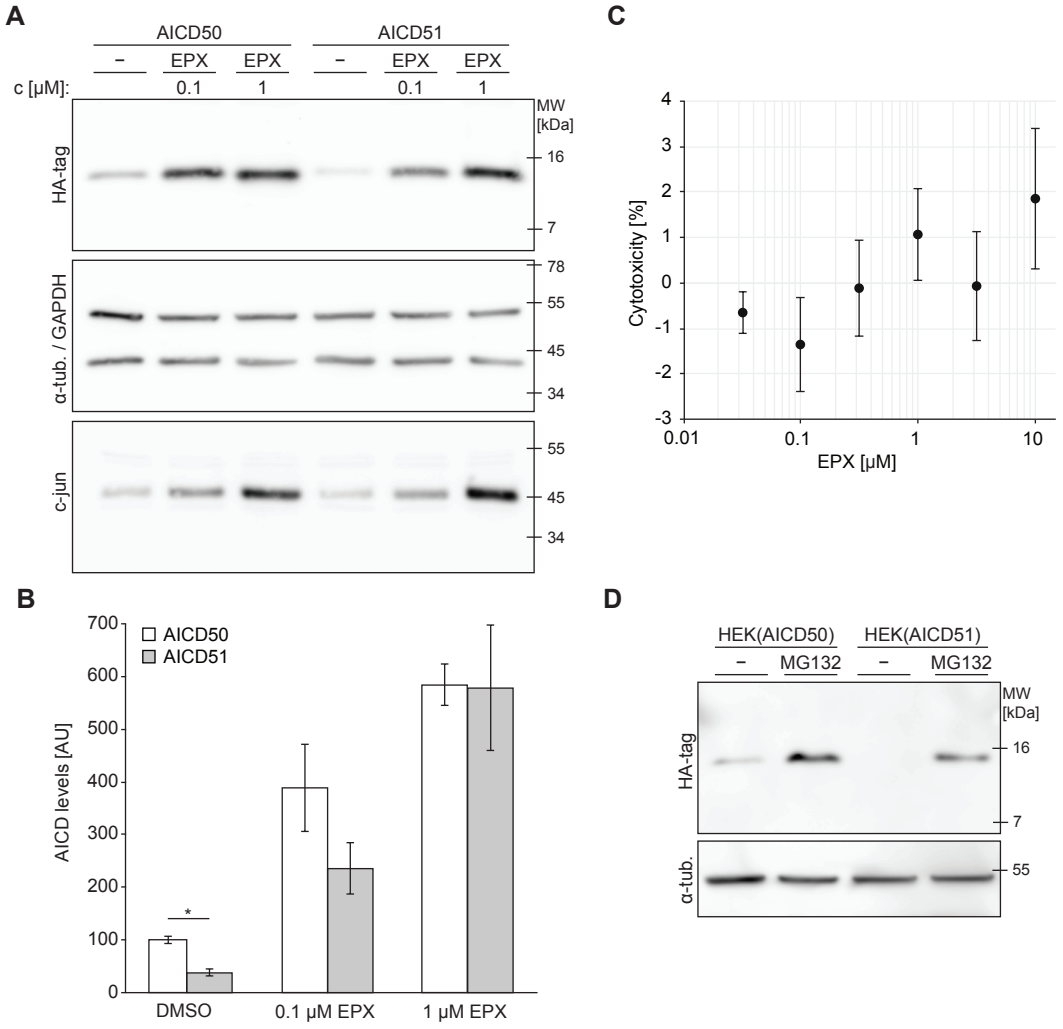

Figure 4.3 AICD51 displays faster proteasomal degradation than AICD50. **A:** Western blot analysis of HEK cells transfected with HA-tagged Ub-fusion constructs expressing AICD50 or AICD51 and treated with the indicated concentration of epoxomicin (EPX) or DMSO-control (−) for four hours. **B:** Quantification of protein levels from A. Mean ± SEM of $n \geq 3$ are shown ($^{*}p < 0.05$, t-test). **C:** Analysis of LDH release from HEK cells treated with different epoxomicin concentrations. LDH release from DMSO-treated cells was set as zero cytotoxicity. **D:** Western blot analysis of HEK cells stably expressing HA-tagged Ub-fusion constructs of AICD50 and AICD51 and treated with MG132 or DMSO-control (−) for four hours.

turnover of AICD51 than AICD50. Incomplete inhibition of the proteasome with 0.1 μM epoxomicin is also evident by levels of the control protein c-jun, which also increase further by the application of 1 μM epoxomicin. Conversely higher rate of proteasomal degradation of AICD51, was thus also resulting under conditions of residual proteasome activity in lower levels of AICD51 than AICD50.

Cytotoxicity of the used concentration of epoxomicin was analyzed to exclude that AICD levels are influenced by cell-death-related mechanisms. Release of the cytosolic lactate dehydrogenase (LDH) from damaged cells was measured as a marker for cytotoxicity and cytolysis. Epoxomicin did not display significantly altered LDH release in the tested range of 3.3 nM to 10 μM (figure 4.3C).

Next, we generated HEK cells stably expressing Ub-fusion constructs of AICD50 and AICD51 by lentivirus-mediated genomic integration. Similar to transiently transfected cells, AICD51 levels were clearly lower than AICD50 levels in DMSO-control conditions (figure 4.3D). Treatment with the proteasomal inhibitor MG132 increased levels of both AICD species, albeit AICD51 levels were not restored entirely. It should be kept in mind that the generally lower AICD species levels are indicative for a slower expression rate of AICD species in stable cells than in transient transfection. Thus, it is possible that the duration of MG132 treatment was not sufficient to restore new AICD species steady-state levels.

Im summary we show that AICD species are degraded by the proteasome. We also show repeatedly reduced AICD51 levels under control conditions, which disappeared after complete blockage of the proteasome. Together our results strongly suggest that AICD51 undergoes faster proteasomal turnover than AICD50 and support our hypothesis that AICD species are degraded by the N-end rule proteasomal degradation.

4.2.3 Mechanism of AICD proteasomal degradation

The role of AICD's lysine residues

To better understand the mechanism of proteasomal degradation of AICD, we aimed to identify potential sites of ubiquitination that are important for proteasomal degradation. Ubiquitination is the most prevalent signal for proteasomal degradation, and lysine residues are the most prevalent sites for ubiquitination (Kravtsova-Ivantsiv and Ciechanover, 2012). The amine group of lysine residues is used in this process by E3 Ub-ligase enzymes to form an isopeptide bond with the carboxyl group of the C-terminal glycine (G76) of ubiquitin (Pickart, 2001). AICD harbors in total five lysine residues

(figure 4.4A). Three lysine residues are clustering in the N-terminal region of AICD (K649–651), of which K650 is conserved in all three APP family members. Interestingly, this lysine-rich stretch is directly following the N-terminal VML sequence that we have previously shown to be important for AICD levels and AFT-complex formation (see chapter 3). The two other lysine residues (K676 and K688) are surrounding the NPxY motif, which is important for binding of adaptor protein such as Fe65. Previous studies have shown ubiquitination of APP at K649–K651 (Morel et al., 2013), K651 (Watanabe et al., 2012), and K688 (El Ayadi et al., 2012). However, no study has related ubiquitination of AICD residues to its proteasomal degradation.

To prevent potential ubiquitination of AICD, lysine residues were substituted by arginine residues that have otherwise similar physiochemical properties (i.e., size, pK, positive charge). We reasoned that APP with lysine-to-arginine substitutions of ubiquitination sites that are indispensable for proteasomal degradation of AICD would result (i) in higher steady-state levels of AICD and (ii) do not show increase in AICD levels upon inhibition of the proteasome. Because of its partial conservation and prior evidence for ubiquitination by Watanabe et al. (2012) and Morel et al. (2013), we started lysine-to-arginine replacements with the N-terminal lysine residues. C-terminal citrine-tagged APP(KKK649-651RRR) was cloned by SDM and expressed in HEK cells. AICD derived from APP(KKK649-651RRR) showed decreased steady-state levels compared to wildtype APP-derived AICD (figure 4.4B). Furthermore, the substitution of N-terminal lysine residues did not ablate AICD accumulation upon inhibition of the proteasome. Thus, despite its prominent position in proximity to the N-terminus, KKK649-651 appears not to play a role in proteasomal degradation of AICD. We next substituted all five lysine residues within the C-terminal domain of APP by arginine residues—APP(KKK649-651RRR, K676R, K688R) abbreviated to APP(5KR). Citrine-tagged APP(5KR) was expressed in HEK cells and treated with epoxomicin (figure 4.4C). Additionally, APP-transfected and DAPT-treated, as well as AICD-transfected protein samples were loaded to western blots to unequivocally identify AICD. Similar to the observations with APP(KKK649-651RRR), APP(5KR)-derived AICD accumulated after treatment with epoxomicin.

Formally, the fluorescence-tag of APP used in the experiments could be ubiquitinated and mediate proteasomal degradation of AICD. Dantuma et al. (2000) have previously shown that GFP accumulates after inhibition of the proteasome, and GFP and derivatives (e.g., citrine) carry multiple lysine residues that could theoretically be ubiquitinated. An Ub-fusion construct of GFP, similar to that used by Dantuma et al. (2000), was expressed in HEK cells and treated with epoxomicin (figure 4.4D). However, we could not observe

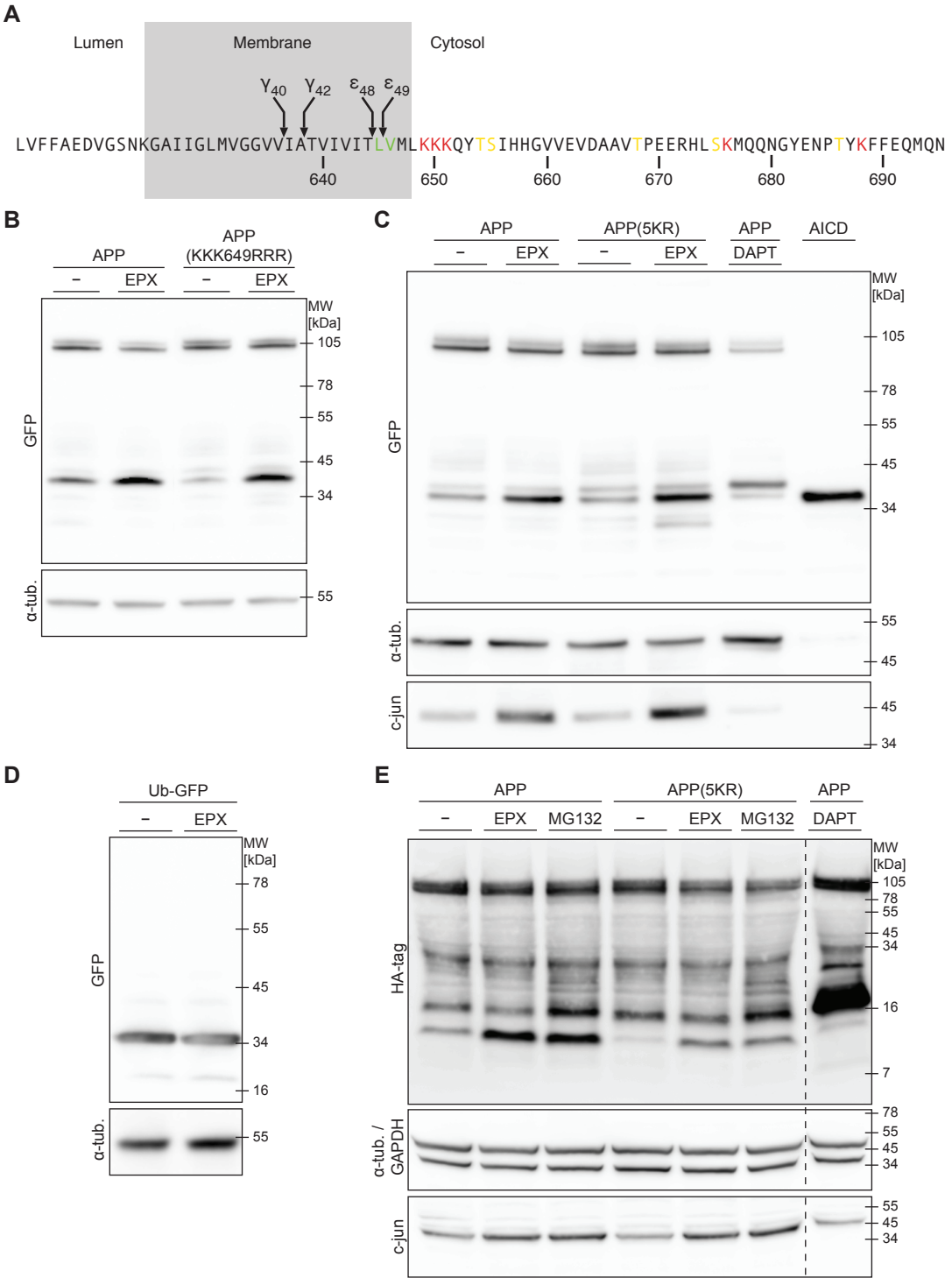
A
Lumen
Membrane
Cytosol
γ40 γ42 ε48 ε49
LVFFAEDVGSNKGAIIGLMVGGVVIATVIVITLVMLKKKQYTSIHHGVVEVDAAVTPEERHLSKMQQNGYENPTYKFFEQMQN
640
650
660
670
680
690
B
APP
APP (KKK649RRR)
– EPX – EPX
MW [kDa]
GFP
105
78
55
45
34
α-tub.
55
C
APP
APP(5KR)
APP
AICD
– EPX – EPX DAPT
MW [kDa]
GFP
105
78
55
45
34
α-tub.
55
45
c-jun
45
34
D
Ub-GFP
– EPX
MW [kDa]
GFP
78
55
45
34
16
α-tub.
55
E
APP
APP(5KR)
APP
– EPX MG132 – EPX MG132 DAPT
MW [kDa]
HA-tag
105
78
55
45
34
16
7
α-tub. / GAPDH
78
55
45
34
c-jun
55
45
34

accumulation of GFP after inhibition of the proteasome. Further, no higher molecular weight forms of GFP—that could be indicative of ubiquitination—were detected, together arguing against a degradation of GFP and derivatives by the UPS. To conclusively exclude that AICD derived from wildtype APP and APP(5KR) is degraded by the proteasome due to an ectopic ubiquitination in the fluorescence-tag, citrine was replaced by an HA-tag, which does not carry lysine residues. HA-tagged APP(5KR) was expressed in HEK cells and treated with two different proteasome inhibitors. Proteins samples were loaded on western blot together with APP-transfected and DAPT-treated samples to identify AICD (figure 4.4E). Similar to our observation with citrine-tagged APP(5KR), inhibition of the proteasome resulted also in accumulation of AICD levels derived from HA-tagged APP(5KR), which is not carrying any lysine residues.

The most prominent function of lysine ubiquitination is to mark proteins for degradation by the proteasome. However, lysine ubiquitination can also modify functions and localization of a protein. For APP, Morel et al. (2013) have shown that ablation of ubiquitination by the KKK649RRR substitution resulted in altered subcellular sorting of APP. Whether these changes in APP localization, subsequently also result in different localization of AICD is not known. Therefore, we asked whether localization of AICD to nuclear AFT-complexes is dependent on a potential ubiquitination on lysine residues. HEK cells were transfected with Fe65, Tip50, and APP(5KR) or wildtype APP and formation of AFT-complexes was analyzed by confocal microscopy (figure 4.5). Similar to wildtype APP-derived AICD, AICD derived from APP(5KR) formed nuclear AFT-complexes and no overt differences in localization were observed.

Figure 4.4 Lysine residues of AICD are dispensable for its proteasomal degradation. **A:** Schematic diagram of AICD peptide sequence and potential ubiquitination sites. Lysine residues are indicated in red. Non-lysine residues and N-terminal residues that can potentially be ubiquitinated are indicated in yellow and green, respectively. **B:** Western blot analysis of HEK cells transfected with citrine-tagged wildtype APP or APP(KKK649RRR) and treated with epoxomicin (EPX) or DMSO-control (−). **C:** Western blot analysis of HEK cells transfected with citrine-tagged wildtype APP and APP(5KR) and treated with epoxomicin or DMSO-control (−). DAPT-treated APP and AICD-Cit samples were loaded to unequivocally identify AICD bands. **D:** Western blot analysis of HEK cells transfected with Ub-fusion construct of GFP and treated with epoxomicin or DMSO-control (−). **E:** Western blot analysis of HEK cells transfected with HA-tagged wildtype APP and APP(5KR) and treated with epoxomicin, MG132, or DMSO-control (−). 16% Tricine gel was used. Dashed line indicates removal of western blot lanes; depicted lanes derive from same western blot and same exposure times are displayed. Epoxomicin (0.1 μM) and MG132 (1 μM) treatment was done for six hours.

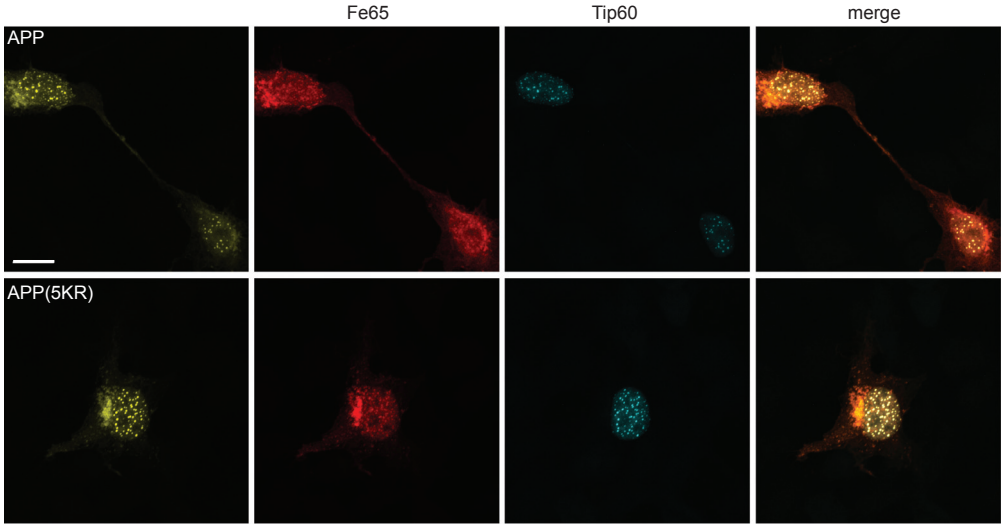

Figure 4.5 Lysine residues of AICD are dispensable for formation of AFT-complexes. Confocal fluorescence images of HEK cells transfected with HA-Fe65, CFP-Tip60, and APP-Cit (top row) or APP(5KR)-Cit (bottom row). Note the formation of spherical AFT-complexes in the nucleus of cells transfected with APP or APP(5KR). Scale bars represent 13 µm.

In summary, our results from lysine-to-arginine substitutions show that lysine residues of AICD are dispensable for its proteasomal degradation, overall localization and the formation of AFT-complexes. Our results explicitly exclude that the mechanism of proteasomal degradation of AICD takes place by ubiquitination of lysine residues.

Ubiquitinated forms of AICD

Ubiquitination of lysine residues is the predominant signal for substrate recognition and degradation by the proteasome (Kravtsova-Ivantsiv and Ciechanover, 2012). However, also other residues have been shown to act as ubiquitin acceptor sites. Described non-lysine ubiquitination sites are cysteine, serine, and threonine residues as well as the α-NH2 group of the N-terminal amino acid of a protein. Although only few reports of non-lysine ubiquitination exist and it is therefore thought to play only a minor role, the possibility of non-lysine-mediated proteasomal degradation of AICD species must be taken into account. AICD harbors five potential non-lysine ubiquitination sites, which are three threonine residues and two serine residues (figure 4.4A). Most of these residues are embedded in the conserved motifs of AICD that mediate several functions of AICD and APP (see section 1.3 for AICD motifs and their function). An arginine replacement approach would likely interfere or disturb these functions and impede result interpretation. Therefore, we decided to

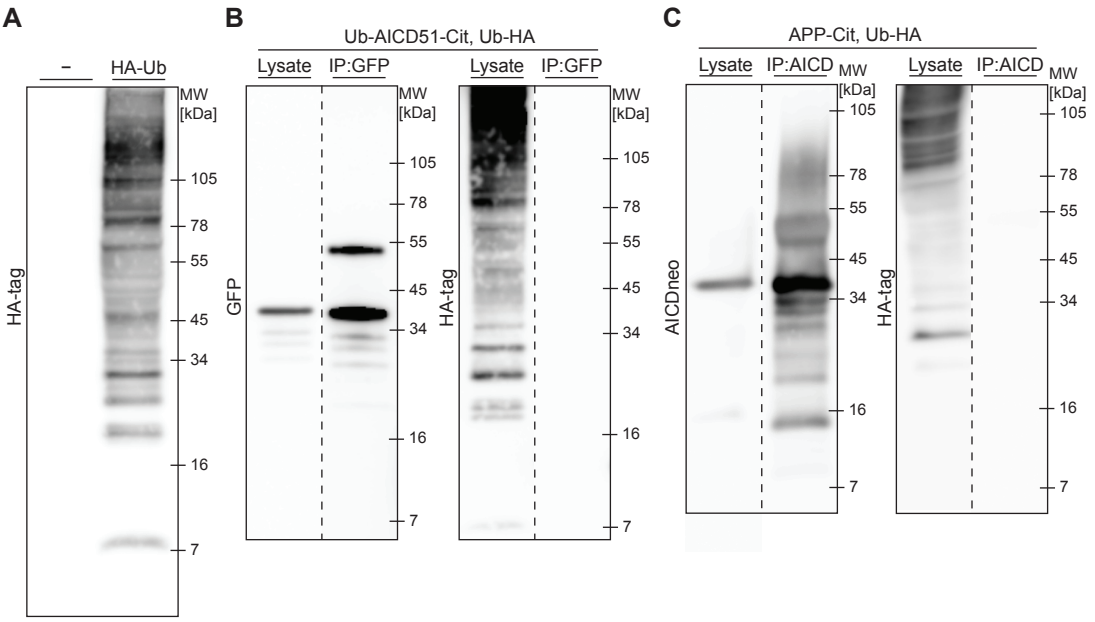

Figure 4.6 AICD is not ubiquitinated. **A:** Western blot analysis of HEK cell lysates transfected with N-terminally HA-tagged ubiquitin (HA-Ub). HA-tagged monoubiquitin is detected at approximately 10 kDa. HA positive bands indicate that HA-tagged ubiquitin is used for protein ubiquitination. **B:** Western blot analysis of HEK cell lysates transfected with citrine-tagged Ub-fusion construct expressing AICD51 and HA-Ub and subjected to immunoprecipitation with GFP antibody. Cells were treated for four hours with MG132 prior to harvest. **C:** Western blot analysis of HEK cell lysates transfected with citrine-tagged APP and HA-Ub and subjected to immunoprecipitation with AICDneo antibody. Cells were treated for four hours with 1 µM epoxomicin prior to harvest. Dashed line indicates removal of western blot lanes; depicted lanes derive from same western blot.

analyze overall AICD ubiquitination—assessing both lysine and non-lysine residue ubiquitination—by immunoprecipitation.

Ubiquitin is bound to substrates by covalent attachment and is thus not removed in SDS-PAGE-based western blots. A plasmid encoding ubiquitin with N-terminal HA-tag (HA-Ub) was used for convenient detection of ubiquitination. Western blot analysis of HA-Ub expressed in HEK cells revealed a band at approximately 10 kDa, corresponding to HA-tagged soluble monoubiquitin (figure 4.6A). Additionally, an HA-tag positive smear, typically observed for protein ubiquitination, was detected, indicating effective expression of HA-Ub and its attachment to target proteins.

Citrine-tagged AICD51 was co-expressed with HA-Ub and treated with MG132 to inhibit proteasomal degradation and accumulate potential ubiquitinated forms of AICD. Samples were harvested in lysis buffer supplemented

with inhibitors of DUBs and the proteasome (RIPA-Ub) to prevent ubiquitin removal and degradation of ubiquitinated forms. AICD51 was immunoprecipitated with an antibody recognizing the fluorescence-tag. Analysis of lysates clearly shows that both proteins, AICD51 and HA-Ub were expressed (figure 4.6B). Eluate probed against AICD51 clearly indicated its successfull immunoprecipitation. However, no HA-tag positive signal was detected in the eluate, indicating that AICD51 is not ubiquitinated.

It is possible that localization and/or proximity to the membrane are necessary for ubiquitination of AICD. To exclude that localization of Ub-fusion construct–derived AICD prevents its ubiquitination, immunoprecipitation was also done with APP-derived AICD. APP-Cit and HA-Ub were expressed in HEK cells and AICD50neo antibody, exclusively recognizing AICD50, used for immunoprecipitation. Although eluate probed with AICD50neo detected a protein smear, no HA-positive signal was observed (figure 4.6C).

In summary, no ubiquitinated forms of AICD were detected in immunoprecipitation experiments. These result suggest that proteasomal degradation of AICD is independent of ubiquitination. However, it should be noted that only minor fractions of a protein are normally ubiquitinated and proteasomal degradation of ubiquitinated proteins is very fast. Therefore, levels of ubiquitinated forms of a protein are often marginal and difficult to detect. Thus the absence of detected ubiquitinated forms is suggestive but not sufficient to refuse a role of ubiquitination and further experiments are required.

The role of E1 ubiquitin-activating enzymes for AICD degradation

To corroborate our findings from immunoprecipitation, we aimed to investigate the role of the ubiquitination machinery in the regulation of AICD. Protein-ubiquitination is mediated by the concerted actions of E1 Ub-activating, E2 Ub-conjugating, and E3 Ub-ligase enzymes. In humans more than fifty E2 Ub-conjugating and more than 500 E3 Ub-ligase enzymes are encoded. In contrast, only eight E1 Ub-activating enzymes are described and, importantly, only two of those activate ubiquitin, while the others activate ubiquitin-like proteins (Schulman and Harper, 2009). UBA1 is the major ubiquitin activating enzyme but in particular in development a second enzyme, UBA6, can activate ubiquitin. The low numerical redundancy of E1 Ub-activating enzymes (in contrast to E2 Ub-conjugating and E3 Ub-ligase enzymes), makes them a suitable target for our investigations. Additionally, previous studies have shown the utility of siRNA-mediated knockdown of E1 Ub-activating enzymes. Lee et al. (2011) for example have shown that siRNA-mediated knockdown of

UBA1/UBA6 results in accumulation of proteins that would otherwise undergo degradation by the UPS.

We have ordered siRNA against UBA1 and UBA6 and transfected them into HEK cells (figure 4.7A). Efficient knockdown of both enzymes, individually and in combination, was observed and reached approximately 94 % and 85 % for UBA1 and UBA6, respectively (figure 4.7A). To test a role of UBA1 and UBA6 in the regulation of AICD, siRNA were transfected into HEK cells transiently expressing different AICD species (figure 4.7B). We reasoned that if proteasomal degradation of AICD is ubiquitin-dependent, knockdown of the E1 Ub-activating enzymes would result in an increase in AICD levels. However, we did not observe an increase for either AICD species, rather a slight reduction of AICD levels after E1 Ub-activating enzyme knockdown was observed, which, however, did not reach significance (figure 4.7C). Our results thus suggest that proteasomal degradation of AICD species is ubiquitination-independent.

To complement genetic ablation of E1 Ub-activating enzymes, pharmacological inhibition was envisaged with the commercially UBA1 inhibitor PYR41 (Yang et al., 2007). However, paradoxically, previous studies have reported an increase in total protein ubiquitination upon PYR41 treatment, which is probably due to off-target inhibition of DUBs (Kapuria et al., 2011). Unfortunately, accumulation of total protein ubiquitination was also observed in our experimental system (figure 4.7D). Because normal function of DUBs is essential for processing of Ub-fusion constructs—used to express AICD species—PYR41 is not suitable for our experiments and hence experiments using this inhibitor were aborted.

4.2.4 The role of N-domain-containing N-recognins in proteasomal degradation of AICD

N-recognins are the central enzymes in the N-end rule pathway. They recognize the N-terminal residues of N-end rule substrates and mediate their proteasomal degradation. N-recognins contain specific domains for substrate recognition, that are the UBR box and the N-domain, which recognize type 1 and type 2 destabilizing residues, respectively (see also table 4.1). The N-domain, which recognizes type 2 destabilizing residues is only conserved in UBR1 and UBR2. To test whether N-recognins mediate proteasomal degradation of AICD species, we obtained UBR1/2 dKO MEFs from Yong Tae Kwon. Lentivirus expressing a Ub-fusion construct of AICD51 was prepared and used for infection of wildtype and UBR1/2 dKO MEFs (figure 4.8A). Cycloheximide was used to inhibit protein synthesis for indicated times and, thus, permit calculation of

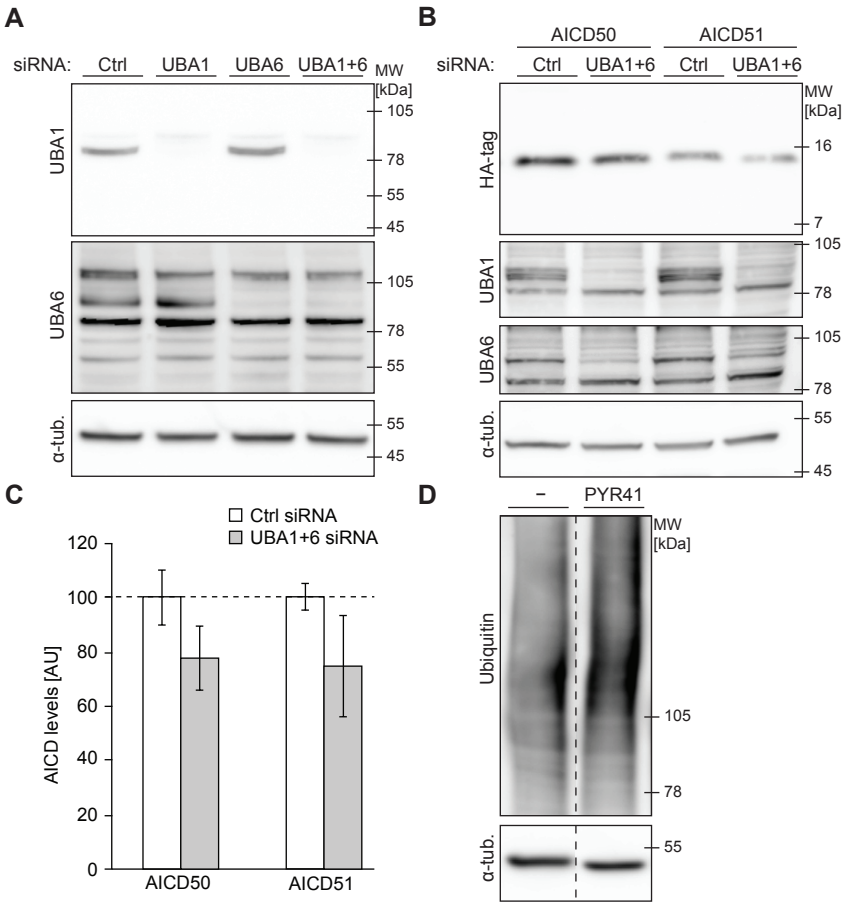

Figure 4.7 Knockdown of E1 Ub-activating enzymes does not stabilize AICD species. **A:** Western blot analysis of HEK cells transfected with siRNAs directed against UBA1 and UBA6 or control siRNA (Ctrl). Both E1 Ub-activating enzymes, UBA1 and UBA6, are efficiently decreased by siRNA-mediated knockdown, individually and combined. **B:** Western blot analysis of HEK cells transfected with Ub-fusion constructs expressing AICD50 and AICD51 and siRNA directed against UBA1 and UBA6 or control-siRNA (Ctrl). **C:** Quantification of AICD levels from B. No significant change in AICD50 and AICD51 was observed after combined knockdown of UBA1 and UBA6. Mean ± SEM of n = 3 are shown ($^*p < 0.05$, t-test). **D:** Western blot analysis of HEK cells treated with the E1 Ub-activating enzyme inhibitor PYR41 or DMSO-control (−). Treatment with PYR41 increased total ubiquitinated protein, likely because of inhibitory function on DUBs. Dashed line indicates removal of western blot lanes; depicted lanes derive from same western blot and same exposure times are displayed.

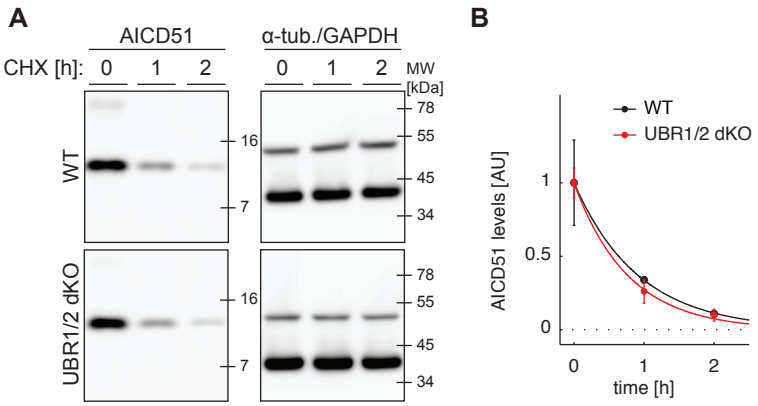

Figure 4.8 Knockdown of N-domain-containing N-recognins does not stabilize AICD species. **A:** Western blot analysis of wildtype and UBR1/2 dKO MEF lysates infected with Ub-fusion construct expressing AICD51 and treated with cycloheximide (CHX) for the indicated time. AICD51 was detected with HA-tag antibody. α-tubulin and GAPDH were probed to show equal protein loading and are detected at approximately 50 kDa and 40 kDa, respectively. **B:** Quantification of AICD51 levels from A. Mean ± SEM of n = 3 are shown for each time point. Data was fitted to exponential functions by the least square approach. R^2(WT) = 1.0; R^2(UBR1/2 dKO) = 0.99.

the half-live of AICD51 in both cell lines. Wildtype and UBR1/2 dKO cells did not display different half-live of AICD51, which was approximately 38 min in wildtype and approximately 38 min in UBR1/2 dKO cells (figure 4.8B). We could also not detect differences in steady-state levels of AICD51 in wildtype and UBR1/2 dKO MEFs—though steady-state comparison between different cell lines have to be considered with caution, because infection efficiency between cell lines could vary considerably. Together, our data suggest that different proteasomal degradation is not mediated by N-domain-containing N-recognins. From the data presented here, we can not exclude that other N-recognins are involved in the degradation of AICD species. Interestingly, Tasaki et al. (2005) show that, in addition to UBR1/2, UBR4 might have a role in degradation of proteins with type 2 destabilizing residues, though UBR4 does not contain an N-domain. Therefore, it is likely that the N-domain is not the only domain mediating degradation of proteins with type 2 destabilizing residues.

4.2.5 The role of AICD binding proteins in AICD degradation

Theoretically, the accumulation of AICD upon proteasomal inhibition that we observed could be a result of decreased proteasomal degradation of a AICD-stabilizing factor. Therefore, we aimed to show that AICD itself is degraded

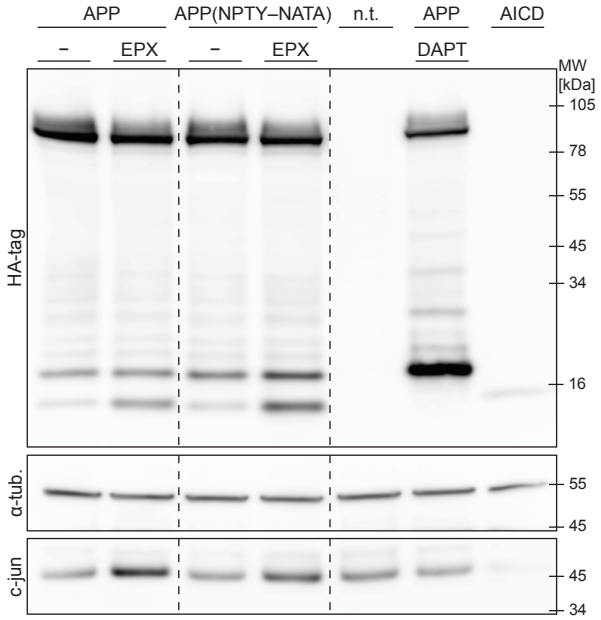

Figure 4.9 Binding of proteins to the YENPTY-domain of AICD is dispensable for its proteasomal degradation. Western blot analysis of HEK cells transfected with HA-tagged wildtype APP or APP(NPTY–NATA) and treated with epoxomicin (EPX; 0.1 μM) or DMSO-control (−) for six hours. Non-transfected sample (n.t.), DAPT-treated APP, and AICD (Ub-AICD50-HA construct) samples were loaded to unequivocally identify CTF and AICD bands. Dashed line indicates removal of western blot lanes; depicted lanes derive from same western blot and same exposure times are displayed.

by the proteasome. Within the C-terminal domain of APP, the majority of described protein interactions takes place at the YENPTY domain harboring the NPxY motif (for a review of AICD binding partners see Muller et al., 2008). These interactions at the YENPTY domain include Fe65 and Fe65-like proteins, which were shown to be ubiquitinated and are suggested to be degraded by the proteasome (Lee et al., 2009). But also other proteins, which were suggested to mediate a function of AICD, as for example the Mint and JIP protein families bind to the YENPTY domain.

To abrogate protein binding and thus investigate a potentially stabilizing function of binding partners, we used a mutation of the NPxY motif. Previous publications have shown that the APP(NPTY-NATA) mutation abrogates protein binding to this site (Cao and Sudhof, 2001; see also figure 3.8A for immunocytochemical analysis of Fe65.) HA-tagged APP(NPTY-NATA) and wildtype APP were transfected into HEK cells and treated with proteasomal inhibitor (figure 4.9). DAPT-treated APP and AICD samples were loaded to identify AICD bands. Similar to wildtype APP, AICD derived from APP(NPTY-

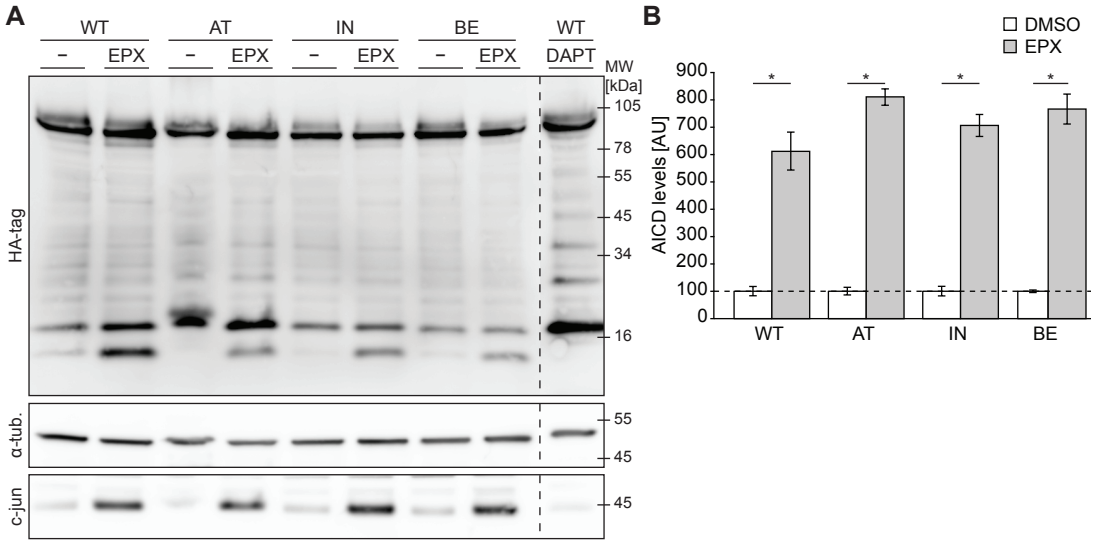

Figure 4.10 APP FAD mutations dramatically decrease AICD levels. **A:** Western blot analysis of HEK cells transfected with wildtype APP (WT) or APP harboring the T639I (Austrian, AT), V639F (Indiana, IN), or K649N (Belgian, BE) mutation (all HA-tagged) and treated with epoxomicin (EPX) or DMSO control (−) for four hours. DAPT-treated APP sample was loaded to identify CTF and AICD bands. Dashed line indicates removal of western blot lanes; depicted lanes derive from same western blot and same exposure times are displayed. **B:** Quantification of AICD levels from A. AICD levels from epoxomicin-treated samples were normalized to AICD levels the from the respective DMSO-control–treated samples. Mean ± SEM of n = 3 are shown ($^*p < 0.05$, t-test).

NATA) displayed accumulation after inhibition of the proteasome. Our results do not permit to exclude stabilization of AICD by binding to other regions. However, considering that most identified binding takes place at the YENPTY domain, a stabilization of AICD by a binding protein that undergoes proteasomal degradation is unlikely. In turn these results suggest that AICD itself is subject to proteasomal degradation.

4.2.6 AICD levels in AD-causing APP mutations

To evaluate a potential role of AICD species in AD, we assessed proteasomal degradation in selected FAD mutants. The T639I (Austrian), V639F (Indiana), and K694N (Belgian) mutations were selected due to their proximity to the ϵ-site. The T639I (Austrian) and V639F (Indiana) mutations were previously also reported to shift processing towards the ϵ_{48}-site, thus increasing the AICD51-to-AICD50 ratio (Chávez-Gutiérrez et al., 2012). APP-expressing plasmids harboring the mutations were cloned, expressed in HEK cells, and

treated with proteasomal inhibitor. DAPT-treated APP sample was loaded to identify AICD bands. Western blot analysis of protein samples revealed strongly decreased steady-state levels of AICD derived from all three mutations under control conditions (figure 4.10A, compare lane three, five, and seven to lane one). This reduction could be due to partial loss-of-function of γ-secretase processing of mutant APP. These different efficiencies of γ-secretase processing should display same fold-changes of AICD levels by inhibition of degradation. Wildtype and FAD mutant–derived AICD levels increased strongly after inhibition of the proteasome. All three FAD mutants displayed increased fold-change of AICD upon inhibition of the proteasome, which can not be explained by decreased γ-secretase cleavage (figure 4.10B). Our data thus point towards an increased proteasomal degradation of AICD from FAD APP mutants, possibly because of a shift of AICD production towards AICD51 that undergoes faster proteasomal degradation.

4.3 Discussion

We have investigated proteasomal degradation of different AICD species. Our data clearly demonstrates that AICD species are degraded by the proteasome and, importantly, that AICD51 displays a faster proteasomal degradation than AICD50. Analysis of the mechanism of degradation points towards an ubiquitination-independent proteasomal degradation of AICD species. Although the different proteasomal turnover of AICD species is reminiscent of N-end rule proteasomal degradation, we could not identify a role of this pathway in AICD species degradation. We further show that AICD levels derived from FAD APP mutations are consistently decreased, possibly due to increased production of unstable AICD species.

4.3.1 Mechanism of different proteasomal degradation of AICD species

Expression of AICD species using Ub-fusion constructs in HEK cells revealed significantly lower levels of AICD51 than AICD50. Inhibition of the proteasome restored AICD51 levels to those of AICD50, clearly indicating that different levels of AICD species are due to different proteasomal degradation. Since AICD50 carries a stabilizing and AICD51 destabilizing residues—while the remaining properties of the proteins are identical—we hypothesized that AICD species undergo N-end rule proteasomal degradation, a specific ubiquitination-dependent branch of proteasomal degradation.

However, our analysis from independent experimental lines argue against an involvement of ubiquitination in the degradation of AICD species. Firstly, we could not detect any ubiquitinated forms of AICD in immunoprecipitation of APP-derived AICD50 and Ub-fusion construct-expressed AICD51. However, enrichment of ubiquitinated forms by inhibition of the proteasome might be counteracted by deubiquitinating activity of DUBs—for which, unfortunately, no broad band inhibitor for cell culture is available. As Jariel-Encontre et al. (2008) pointed out, "ubiquitylation (ubiquitination) usually concerns small fractions of proteins and the assay used may meet with problems of sensitivity" and, thus, absence of detection of ubiquitinated forms is not sufficient to reject ubiquitination of a given protein. Therefore, in a second experimental line, AICD levels were assessed after siRNA-mediated knockdown of E1 Ub-activating enzymes. Combined depletion of both Ub-activating enzymes, UBA1 and UBA6, did not result in increased AICD levels. Given the importance of ubiquitination in multiple cellular processes, an abundance of E1 Ub-activating enzymes is likely and therefore residual enzyme levels could be

sufficient to maintain protein ubiquitination. However, it should be noted that a previous study, which used a similar experimental scheme and achieved similar knockdown efficiencies of E1 Ub-activating enzymes, observed accumulation of proteins that are otherwise degraded by the UPS (Lee et al., 2011). Similar to our results from immunoprecipitation and E1 Ub-activating enzyme knockdown, our investigations concerning a possible ubiquitination site argue against a classical ubiquitin-dependent degradation of AICD. We conclusively show, by lysine-to-arginine substitutions, that lysine residues are dispensable for the proteasomal degradation of AICD. Although, the vast majority of ubiquitination takes place on lysine residues, lysine-independent ubiquitination on cysteine, serine, and threonine residues, as well as on the α-NH2 group of N-terminal amino acids has been described (Kravtsova-Ivantsiv and Ciechanover, 2012). Although, these reports are very rare, and non-lysine dependent ubiquitination has only been described for a handful of proteins, we can formally not exclude ubiquitination on non-lysine residues. Together, our results from AICD immunoprecipitation, E1 Ub-activating enzyme knockdown, and lysine-to-arginine substitutions failed to uncover a involvement of ubiquitination in AICD degradation. Therefore, this combined evidence suggests that AICD undergoes proteasomal degradation independent of ubiquitination. It is worth mentioning that our results are not contradictory to previous studies that have shown ubiquitination of C-terminal lysine residues of APP (Watanabe et al., 2012; El Ayadi et al., 2012; Morel et al., 2013). These studies have only detected ubiquitination of full-length APP and thus allow no conclusion about the ubiquitination status of AICD. Ubiquitinated APP could possibly be degraded or ubiquitin be removed before release of AICD by γ-secretase cleavage. Since, we observe formation of nuclear AFT-complexes with AICD devoid of lysine residues, our results also suggest that the transcriptional function of AICD is no influenced by ubiquitination.

The bulk of proteins that are degraded by the proteasome undergoes prior polyubiquitination, which serves as a recognition signal for the proteasome. However, it must be noted that ubiquitination is not the only way to mark proteins for proteasomal degradation. Two major ubiquitin-independent proteasomal degradation mechanism are known, which are (i) ubiquitin-like protein (UBL)-mediated degradation and (ii) direct substrate recognition by the proteasome without prior PTM (Erales and Coffino, 2014).

UBLs are a family of nearly twenty proteins, which are involved in PTMs and are characterized by a common structural element, the ubiquitin-superfold.[2]

[2] To date known UBLs are—sorted according to van der Veen and Ploegh (2012) in decreasing similarity to ubiquitin: Nedd8, Fub1, Isg15, Fat10, Hub1, Sumo1–3, Ufm1, Urm1, Atg8, and Atg12.

UBLs were shown to be involved in diverse cellular processes such as protein transport, autophagy, and protein translation (for a review see van der Veen and Ploegh, 2012), but presumably many functions remain unexplored. At least three ubiquitin-like modifications—neddylation, fatylation, and sumoylation—were shown to be involved in proteasomal degradation (Schulman and Harper, 2009). Interestingly, AICD can be neddylated at all five lysine residues, which might influence binding of adaptor proteins (Chen et al., 2012). However, among the UBL modification, only attachment of Fat10 was shown to be independent of ubiquitination, while attachment of Nedd8 and Sumo proteins is believed to function as a basis for subsequent ubiquitination. Similar to ubiquitin, absence of detection is not sufficient for denial of PTM by UBL modification, which applies particularly to Fat10, which is rapidly removed from proteins (Buchsbaum et al., 2012). Although, UBLs have their individual E1s (i.e., activating enzymes), UBA6 has dual function in activating ubiquitin and FAT10. In light of the dependency of neddylation and sumoylation on subsequent ubiquitination for proteasomal degradation, the combined knockdown of UBA1 and UBA6 employed here should prevent any described ubiquitin or ubiquitin-like modification that eventually results in proteasomal degradation. Additionally, UBL modification, as ubiquitination, are predominantly taking place on lysine residues. Therefore, lysine-to-arginine substitutions would have equally uncovered a role of UBLs in AICD degradation. Our results thus argue also against a involvement of UBL modification in AICD degradation.

The described evidence thus suggest that AICD undergoes proteasomal degradation independent of modification of ubiquitin or UBL. An increasing number of proteins has been discovered that undergo proteasomal degradation without PTM as recognition signal (see Ben-Nissan and Sharon, 2014 for review and list of proteins). Additionally, multiple proteins (e.g., c-jun and the transcriptional factor Rpn4) can undergo both ubiquitin-dependent and ubiquitin-independent proteasomal degradation (Ju and Xie, 2004). General mechanistic insight how proteins are degraded independent of ubiquitination is missing. Analysis of proteins that undergo ubiquitin-independent proteasomal degradation has revealed that they share a common feature, which are intrinsically disordered regions (IDR; Erales and Coffino, 2014). Whether the IDR is directly recognized by the proteasome or whether IDR folding and binding to interaction partner mediates their proteasomal degradation is not clear. For some proteins experimental evidence has suggested that ubiquitin-independent proteasomal degradation is mediated by the 20S proteasome (Ben-Nissan and Sharon, 2014). Interestingly, NMR and CD experiment have revealed that AICD is intrinsically disordered (Ramelot et al., 2000). Although this feature of AICD has been suggested to play a role for molecular recognition

in intracellular signaling events, investigations of proteasome recognition are missing.

N-end rule degradation is a specific branch of proteasomal degradation. It is distinct from other proteasomal branches in two major points: Firstly, in N-end rule degradation proteins are directly recognized at N-terminal residues by specific E3 Ub-ligase enzymes, the N-recognins, which then ubiquitinate the proteins. In contrast, in other branches of proteasomal degradation, other parts of the protein sequence or a PTM of the protein is recognized by E3 Ub-ligase enzymes (e.g. recognition of phosphorylation by F-box proteins of the SCF E3 Ub-ligase; Winston et al., 1999). Secondly, the identity of the N-terminal amino acids, determines the kinetics of ubiquitination and thus the rate of degradation (Bachmair et al., 1986).[3] Accordingly, the twenty naturally-occurring amino acids have either stabilizing or destabilizing function (see table 4.1), presumingly because of binding specificity of the recognition domains of the N-recognins (Varshavsky, 1992; Choi et al., 2010). Destabilizing residues are further subdivided in type 1 and 2. Type 1 residues are basic amino acids that are recognized by the UBR box of N-recognins. Type 2 residues in contrast are bulky and hydrophobic amino acids and experimental evidence suggest that these residues are recognized by the N-domain, which is present only in the N-recognins UBR1 and UBR2 (Tasaki et al., 2005). Strikingly, we observe a significantly faster proteasomal degradation of AICD51, harboring a type 2 destabilizing N-terminal residue, than AICD50, harboring a stabilizing N-terminal residue. Therefore, we have analyzed AICD species degradation in MEFs deficient for the N-recognins UBR1 and UBR2. Tasaki et al. (2005) have created and used these MEFs to show that N-domain-containing UBRs mediate degradation of proteins bearing type 2 destabilizing residues. However, we could not observe an influence of theses N-recognins on the degradation of AICD51 that has a N-terminal type 2 destabilizing residue. Formally, we can not exclude that other N-recognins play a role in AICD degradation. Indeed, for UBR4 Tasaki et al. (2005) show that, although it does not contain an N-domain, it can contribute to the degradation of proteins with type 2 destabilizing residues, thus suggesting that also other domains than the N-domain mediate the degradation of proteins with type 2 destabilizing residues (Dougan et al., 2012). However, in light of our data that demonstrates that AICD is not ubiquitinated, it is unlikely that proteasomal degradation takes place by N-recognin-mediated N-end rule proteasomal degradation.

[3] Recent studies have shown that in addition to the N-terminal residue, the identity of the following residues can also influence binding to N-recognins and are thus important for the N-end rule pathway (Sriram et al., 2013). Choi et al. (2010) provide also structural inside how residues at the second position of a protein can modulate this binding specificity.

How can the different proteasomal degradation, reminiscent of N-end rule degradation, be explained without the involvement of ubiquitination and N-recognins? It is unlikely that different AICD species adopt different structures, and our experiments, using the expression from Ub-fusion constructs, should also exclude a different localization of AICD species. A direct role of the N-terminal amino acids is more likely and possible mechanisms include: (i) preferential binding of destabilizing factors or the proteasome itself to AICD51 and (ii) preferential binding of stabilizing or shielding factors to AICD50. Preferential binding of destabilizing factors to AICD51 could involve a direct transport to the proteasome. In this respect, a role of the N-terminal region in ubiquitin-independent proteasomal degradation was shown for multiple proteins. Ju and Xie (2004) for example show that ubiquitin-independent degradation of the transcription factor Rpn4 is dependent on its ten N-terminal amino acids, while ubiquitin-dependent degradation depends on a more C-terminal region of the protein. Peña et al. (2006) show that the thymidylate synthase (TS) exclusively undergoes ubiquitin-independent proteasomal degradation and that deletion of the N-terminal residues prevents TS degradation. Whether the identity of the N-terminal residues influences turnover of degradation was not investigated in these studies and also the mechanism how proteins find their way to the proteasome without the ubiquitin-tag remains elusive. Interestingly, in *E.coli*, which lack ubiquitin or ubiquitin-like modifications a N-end-rule-like mechanism mediated by ClpS is well described. Strikingly, the short ClpS protein is homologous to the N-domain, responsible for recognition of type 2 destabilizing residues and sequence relationship analysis between ClpS and N-recognins suggests that they share a common origin (Lupas and Koretke, 2003). In contrast to N-recognins, ClpS mediates N-end rule degradation without prior PTM, by directly escorting a N-terminal bound substrate to the bacterial equivalent of the 26S proteasome (Tasaki et al., 2012). Whether similar, direct degradation mechanism exist also in mammalian cells is not known—at least the two N-domain-containing N-recognins, UBR1 and UBR2, mediate proteasomal degradation via ubiquitination. A potential candidate is the ribosomal protein L7/12, which has substantial structural similarity to ClpS (Lupas and Koretke, 2003). However, experimental evidence whether this structural feature of L7/12 allows recognition of proteins' N-termini and whether L7/12 is involved in proteasomal degradation is missing. In light of the remarkable structural and functional similarities between bacterial proteasome and the mammalian 26S proteasome, it is imaginable that similar or conserved transport mechanism to the proteasome exist (Verma and Deshaies, 2000).

Preferential binding of a stabilizing factor to AICD50 is a second possibility to explain the observed different degradation of AICD species. In this respect

the nanny model for proteins containing intrinsically disordered regions (IDRs) developed by Tsvetkov et al. (2009) is highly interesting. IDRs are often functional domains that allow binding to different binding partners with high specificity and low affinity. Indeed, many IDR-containing proteins are transcription factors or play a role in transcription. At the same time, the IDR-containing proteins are designated to "degradation by default" since the IDR allows a ubiquitination-independent degradation (Tsvetkov et al., 2009). To overcome the paradoxical situation that the functional region of a protein also destines the protein to degradation, and thus prevents its function, a stabilization mechanism—the nanny—is required. The nanny protein shields degradation of the protein after binding to the IDR. Examples for blockage of proteasomal degradation of transcriptional factors include Hdmx binding to N-terminal IDR of p53 and NF-κB shielding of NF-κBα (Tsvetkov et al., 2009). The IDR of AICD, lack of ubiquitination and its role in transcription make a AICD a candidate for nanny model. But—who's AICD's nanny? The only described protein binding to the N-terminus of AICD is SET and an involvement of this complex in apoptosis has been described (Madeira et al., 2005). However, data of differential binding and putative stabilizing (or destabilizing) function is not available. Another interesting candidate, for targeting AICD to the proteasome is ubiquilin-1. Ubiquilin-1 was shown to modulate degradation of proteasome substrates, such as p53 and also to physically interact with the proteasome (Kleijnen et al., 2000; Takalo et al., 2013). Further, ubiquilin-1 can bind to AICD and modulate its aggregation in *in vitro* assays (Stieren et al., 2011) and influence APP processing (Viswanathan et al., 2013). Ubiquilin-1 could be a missing link, by differently shielding AICD species from degradation or transporting them differently to the proteasome.

4.3.2 Function and degradation of AICD species in Alzheimer's disease

Mutations in the genes encoding APP as well as the γ-secretase subunits PSEN1 and PSEN2 result in the development of AD. However, the molecular mechanism by which FAD mutations cause the disease remains heavily debated. A vast number of studies have assessed Aβ production and have revealed that the Aβ42-to-Aβ40 ratio is increased (Wolfe, 2007). In contrast, only few studies have investigated the effects of FAD mutations on the generation of AICD species, although it became evident that FAD mutations affect APP processing in different and multiple ways. The two alterations observed that directly effect

AICD species levels are partial loss-of-function of γ-secretase processing as well as a shift in processing at the ϵ-site.

Loss-of-function of processing at the ϵ-site and hence reduction in AICD levels, has been found for the majority of FAD mutations investigated (for a review see Shen and Kelleher, 2007). All studies have, probably because of the technical difficulties to detect AICD, employed *in vitro* γ-secretase cleavage assays and most have relied on investigation of steady-state levels. To overcome limitations of *in vitro* γ-secretase assays, such as different substrate and/or enzyme concentrations, Chávez-Gutiérrez et al. (2012) have performed detailed kinetic analysis of γ-secretase cleavage with FAD mutations in PSEN1, PSEN2, and APP. Six PSEN1 mutations (Y115H, L166P, ΔE9, I213T, and G384A) and one PSEN2 mutation (N141I) displayed a partial loss-of-function at the ϵ-site as indicated by reduced AICD levels. M139V, was the only PSEN mutation that showed no alteration. Loss-of-function (and hence reduced AICD levels), was also observed for three APP FAD mutations (T639I (Austrian), V640T (German), and I641T). In contrast, no change was observed for the mutations V642F (Indiana) and V644I (London). Overall, this study reflects previous works which show that a partial loss-of-function of γ-secretase activity at ϵ-site and thus corresponding reduction in AICD levels is common in FAD mutations (Moehlmann et al., 2002; Hecimovic et al., 2004; Guardia-Laguarta et al., 2010; Svedružić et al., 2012). In particular FAD mutations in the presenilins show predominantly a partial loss-of-function of γ-secretase activity. However, it is important to emphasize that loss-of-function of γ-secretase activity is not observed in all FAD mutations.

The second observed route how FAD mutations affect AICD species is a shift of γ-secretase cleavage position at the ϵ-site. Sato et al. (2003) were the first to observe an increase in AICD51 while total AICD levels were unchanged for two PSEN1 mutations (M233T and G384A) and the N141I PSEN2 mutation. A shift of γ-secretase cleavage from the ϵ_{49}- to the ϵ_{48}-site was confirmed for PSEN1 G384A mutation and further shown for the mutations Y115H, L166P, and M139V (Chávez-Gutiérrez et al., 2012). However, shifting γ-secretase cleavage at the ϵ-site is not a compulsive property of PSEN mutations since it was not observed for M146L (Sato et al., 2003), ΔE9, and I213T mutations (Chávez-Gutiérrez et al., 2012). For mutations in APP, Chávez-Gutiérrez et al. (2012) observed a shift in all four mutations tested which are T639I (Austrian), V640A (German), V642F (Indiana), and V642I (London). Recent and independent studies have confirmed these results and shown shifts also for the T639A (Iranian), I641V (Florida), and L648P (Australian) mutations (Dimitrov et al., 2013; Olsson et al., 2014). In contrast, APP FAD mutations more distant to the ϵ-site —A617G (Flemish) , E618G (Arctic), and D619N

(Iowa)—did not show a shift (Dimitrov et al., 2013). Similar to the described partial loss-of-function, shifting of cleavage at ϵ-site is no necessary property of FAD mutations. However, it can be excluded that partial loss-of-function and ϵ-site shifting are mutually dependent or exclusive since mutations that result in both but also those which result only in one are described. Interestingly, all mutations that were examined for both properties displayed at least one.

The described studies assessing AICD levels in FAD mutations have almost exclusively relied on *in vitro* systems. Although these approaches are informative, in particular about the kinetics of processing, they do not reflect the physiological situation in the cell. Differences in trafficking and localization and in particular in degradation are not taken into account. Therefore, we have analyzed, for the first time, AICD levels from APP FAD mutations expressed in cells. We placed a particular focus on a possible divergent proteasomal degradation of AICD species due to the described shift in cleavage at ϵ-site. For the three selected APP FAD mutations —T639I (Austrian), V639F (Indiana), and K649N (Belgian)— we observed dramatic decrease in steady-state AICD levels under control conditions. Treatment with epoxomicin levels increased AICD levels in all cases, excluding a complete loss-of-function of γ-secretase processing. If different efficiencies of γ-secretase processing alone were to explain the reduced AICD levels, same fold-changes of AICD levels by inhibition of the proteasome would be expected. However, analysis of fold-changes of AICD levels revealed consistent increases in all three FAD mutations. Thus, our results suggest that FAD APP mutants result in decreased AICD levels by two mechanism, which are a partial loss-of-function of γ-secretase function and a increased degradation by the proteasome. In light of the described processing shift at the ϵ-site for the T639I (Austrian) and V639F (Indiana) mutations—the K649N (Belgian) was not investigated so far—it is tempting to speculate that faster proteasomal degradation of AICD51 contributes to the observed decrease in total AICD levels. However, further analysis, in particular separate and reliable detection of AICD species, are needed to conclusively demonstrate a potential role of different AICD species degradation in FAD mutations.

4.3.3 Conclusion

In summary, the data presented here clearly show for the first time proteasomal degradation of AICD species. We show further that different AICD species undergo different proteasomal degradation and that proteasomal degradation is independent of prior ubiquitination. As discussed, our data suggest a ubiquitination-independent proteasomal degradation of AICD species that is modulated by stabilizing or destabilizing factors in an N-end rule-like

manner. We further analyze for the first time AICD levels from APP FAD mutants from cell culture experiments and show that APP FAD mutations result in consistent reduction of AICD levels. Our results suggest that decreased efficiency of γ-secretase cleavage and shift in processing towards AICD species that is degraded faster by the proteasome results in overall decreased AICD levels. Thus our results imply that alteration in the production of Aβ42/40 is inherently correlated with alterations in the transcriptional regulator AICD. Interestingly, recent genetic analyses have revealed that the UPS is one of four biological network modules with increased genetic association to AD (International Genomics of Alzheimer's Disease Consortium (IGAP), 2014) and multiple studies have shown that the UPS is impaired in AD (Keller et al., 2000; Lam et al., 2000; Riederer et al., 2011). A possible contribution of AICD to the pathological events of FAD—via transcriptional regulation or other— needs therefore further investigations.

5 Towards an *in vivo* Model of AICD Transcriptional Function

In this chapter, we present and analyze a novel mouse model of the transcriptional function of AICD.

5.1 Introduction

Since the first description of the involvement of AICD in gene regulation, the transcriptional function of AICD was repeatedly confirmed *in vitro* (Cao and Sudhof, 2001; Pardossi-Piquard and Checler, 2012). Recent studies have begun to investigate the functional role of AICD also *in vivo*. Using APP knockout as well as knock-in mouse lines, multiple publications, particularly from the laboratories of Luciano D'Adamio and Hui Zheng, have revealed essential functions of APP. Interestingly, binding of Fe65 to the APP C-terminus emerged as particularly important for the role of APP. Tyrosine-to-glycine substitution of the first tyrosine within the YENPTY domain in the C-terminus of APP (APP(Y682G)) abolished binding to Fe65 in an APP knock-in mouse line (Barbagallo et al., 2010). Phenotypical analyses of APP(Y682G) mice revealed an age-dependent cognitive decline and progressive reduction in dendritic spines (Matrone et al., 2012). APP(Y682G) mice crossed to an APLP2 knockout background even displayed postnatal lethality and defects in formation of the neuromuscular junction similar to mice completely deficient in APP and APLP2 (Barbagallo et al., 2011). In an independent mouse line, Weyer et al. (2011) show that ablation of the last ninety-nine amino acids of APP on an APLP2 knockout background resulted in cognitive dysfunction and similar defects at the neuromuscular junction. Although, these mice—in contrast to the APP(Y682G) mice—survived early development, additional defects in hippocampus-dependent learning and memory as well as impaired long-term potentiation were observed. Together, these results demonstrate the importance of the C-terminal domain of APP and its binding to Fe65. Formally, it can not be

excluded that the observed phenotypes are due to other functions of Fe65 than mediating AICD transcriptional signaling (discussed below). However, in light of the well described function of Fe65 for nuclear signaling and transcriptional function of AICD, a role of AICD in the described phenotypes is very likely.

The described mouse lines with ablated AICD signaling have greatly enriched our understanding of the function of AICD *in vivo*. However, no study has so far addressed how the transcriptional function of AICD is regulated *in vivo*. Multiple studies have shown that APP processing as well as Aβ secretion and toxicity are regulated by neuronal activity.[1] Using hippocampal slice cultures, Kamenetz et al. (2003) for example, show that increased neuronal activity increases secreted Aβ levels. They show further, that neuronal activity increases the levels of C83, suggesting that β-cleavage of APP by BACE1 is activity-dependent. In primary cortical neurons, Hoey et al. (2009) observe that activation of synaptic NMDA receptors increased α-secretase processing of APP and decreased Aβ release. Imaging studies indicate that neuronal activity modulates APP processing and/or Aβ deposition also in humans. Buckner et al. (2005) used FDG-PET, to measure glucose metabolism, and PiB-PET, to measure Aβ deposition. Interestingly, highest Aβ plaque levels are found in brain regions with highest synaptic activity reflected by highest metabolic rate. Together, these studies also suggest that AICD—as it is produced hand in hand with Aβ—is regulated by neuronal activity. However, secretion and possible functions of AICD in response to neuronal activity have been hardly addressed. In particular the technical difficulties in detecting AICD, due to its lability but also lack of specific antibodies, have so far not allowed to unequivocally identify nuclear AICD and thus prevented an analysis of AICD regulation in response to neuronal activity. A novel approach to visualize AICD activity is therefore required.

The aim of this project is to establish and analyze an *in vivo* model of AICD transcriptional function. The UAS/Gal4 system allows to study and visualize transcriptional function and has been successfully used for gene expression analysis *in vitro* as well as in animals, such as *Drosophila* and mice (Halpern et al., 2008). The system is based on the modular character of the yeast Gal4 transcription factor. The N-terminal domain of Gal4 contains the DNA binding domain (DBD), which binds to specific DNA sequences, the upstream activating sequence (UAS) elements. Its C-terminal domain contains an acidic domain which activates transcription by interaction with the transcription complex, therefore also called acivation domain (here abbreviated AcD). Binding of complete transactivator Gal4 (i.e., DBD and AcD) to the UAS elements can thus

[1] For a comprehensive review of activity-dependent processing of APP see Haass et al., 2012.

activate expression of a reporter gene of choice present downstream of the UAS elements. Cao and Sudhof (2001) have shown that fusion of AICD to the Gal4-DBD regulates reporter gene expression, thus suggesting that AICD is a transcriptional activator. We reasoned that the UAS/Gal4-system could also be a valuable system for visualization of transcriptional function of AICD *in vivo*. Therefore, we transferred the UAS/Gal4-based AICD transcription assay to an *in vivo* context and describe here the generation of the APPGal4 mouse line. The APPGal4 mouse line promises to allow visualization of the spatiotemporal pattern of the transcriptional function of AICD *in vivo*.

5.2 Results

5.2.1 Characterization of the APP-Gal4 chimeric protein

For the creation of a *in vivo* model for transcriptional activity of AICD, we intended to use a chimeric APP-Gal4 construct. Cao and Sudhof (2001) have cloned and used the APP-Gal4 construct to show that AICD is transcriptionally active in a UAS/Gal4 assay. The construct comprises the insertion of the 147 amino acid long Gal4-DBD (Gal4 residues 1–147) at position 651 of human APP, which is six amino acids C-terminal to the ϵ-site (see also figure 5.1A and section 2.3). Ectodomain shedding of the APP-Gal4 construct produces CTF-Gal4, which is then supposed to be cleaved by γ-secretase to produce AICD-Gal4 (and Aβ). The close proximity of the Gal4-DBD to the γ-secretase cleavage sites have raised concerns about proper cleavage of CTFs (because of e.g., sterical hindrance). Therefore, HEK cells were transfected with APP-Gal4, treated with the γ-secretase inhibitor DAPT, and subjected to western blotting with an antibody recognizing the C-terminus of APP (figure 5.1B). Full-length APP-Gal4 was detected as major band at the expected height of approximately 100 kDa. CTF-Gal4 and AICD-Gal4 were detected in control-treated cells at approximately 30 kDa—the theoretical molecular weight of the primary sequence of α-CTF-Gal4 and AICD-Gal4 are 28 kDa and 24 kDa, respectively. AICD-Gal4 disappeared upon inhibition of γ-secretase, while CTF-

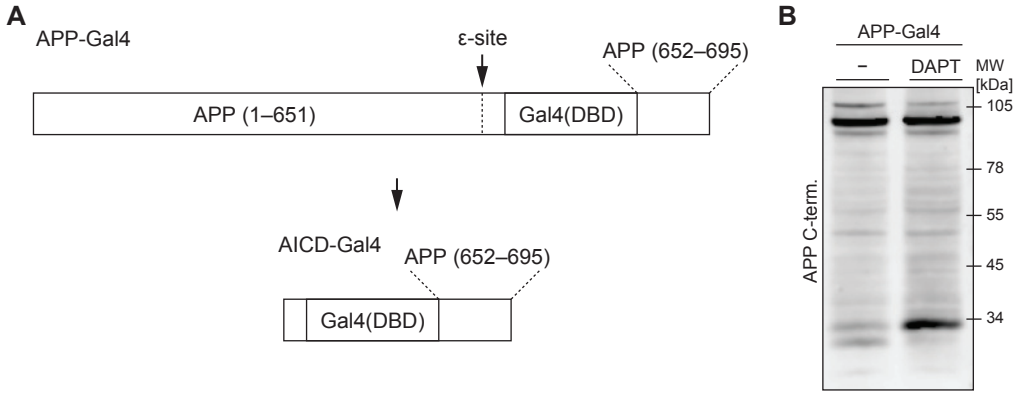

Figure 5.1 The APP-Gal4 chimeric protein undergoes normal APP processing. **A:** Schematic illustration of the APP-Gal4 construct. Cleavage of APP-Gal4 by either α- or β- secretase followed by γ-secretase cleavage at the ϵ-site produces AICD-Gal4. **B:** Western blot analysis of HEK cells transfected with APP-Gal4 and treated with γ-secretase inhibitor DAPT or DMSO-control (−). An antibody recognizing the C-terminus of APP was used to detect APP-Gal4 and its cleavage products.

Gal4 concomitantly accumulated. These results clearly show that γ-secretase is able to cleave APP-Gal4, resulting in the release of AICD-Gal4.

To confirm transcriptional activity of AICD-Gal4 we established a novel, cell based UAS/Gal4 assay. A plasmid expressing citrine under the control of a minimal promoter and nine UAS repeat elements was cloned. Figure 5.2A shows that UAS-Cit construct is only allowing the expression of citrine in the presence of a complete transactivator (i.e., Gal4-DBD fused to an activation domain). To overcome limitations of transient transfection, we prepared a HEK cell line with stable integration of the UAS-Cit element (see section 2.2 for details of preparation of stable cell lines). The HEK(UAS-Cit) cell line displays expression of the citrine reporter gene only upon transfection with a complete transactivator (figure 5.2B). To test transcriptional activity of AICD-Gal4, APP-Gal4 was transfected into the HEK(UAS-Cit) cell line and citrine reporter signal was amplified by immunostaining (figure 5.3). However, no fluorescence signal was observed. Binding of AICD to adaptor proteins such as members of the Fe65 and Jip family of proteins is known to be necessary for nuclear transport of AICD (see e.g., von Rotz et al., 2004). However, Fe65 for example is strongly expressed in neurons, while expression in other cell types is rather low (Sabo et al., 2003). Therefore, nuclear signaling and transcriptional activity of AICD in HEK cells could be limited by low levels of adaptor proteins. Co-transfection of APP-Gal4 and Fe65 into the HEK(UAS-Cit) cell line showed prominent signal

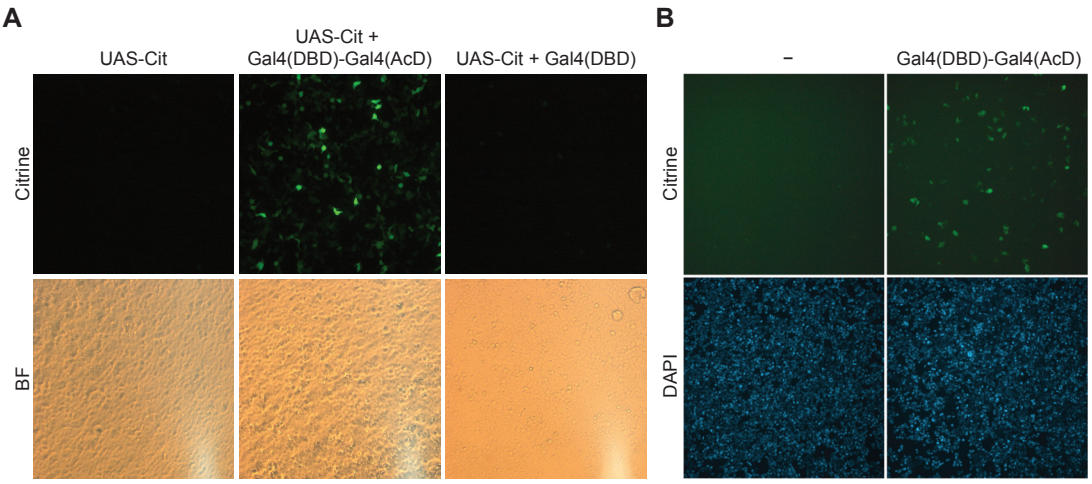

Figure 5.2 The HEK(UAS-Cit) cell line shows reporter activity with a transactivator. **A:** Fluorescence and bright-field (BF) images of HEK cells transfected with the UAS-Cit plasmid and co-transfected with the complete transactivator Gal4(DBD)-Gal4(AcD) or Gal4-DBD alone. **B:** Fluorescence images of HEK(UAS-Cit) cells mock transfected or transfected with or Gal4(DBD)-Gal4(AcD). Nuclei were stained with DAPI.

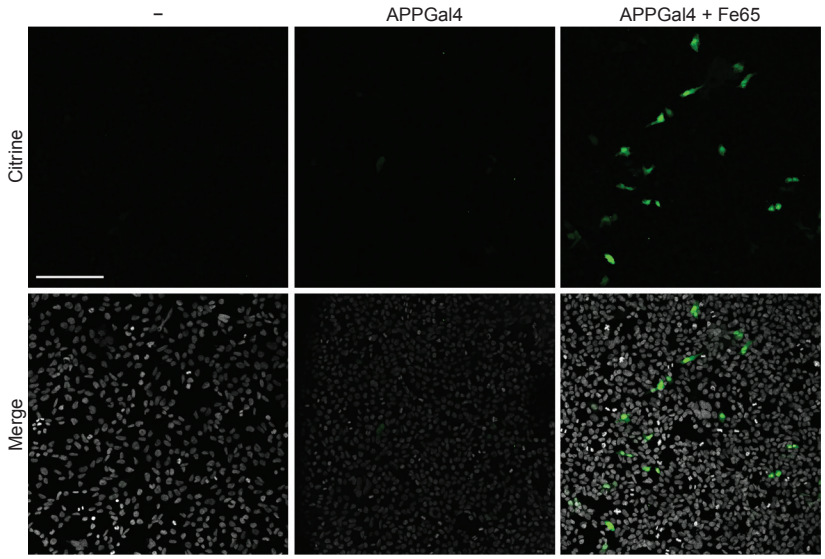

Figure 5.3 APP-Gal4 shows nuclear transcriptional activity with co-transfection of Fe65. Confocal fluorescence images of HEK(UAS-Cit) cells mock transfected (–), transfected with APP-Gal4, or co-transfected with APP-Gal4 and Fe65. Citrine signal was enhanced by immunostaining. Nuclei were stained with DAPI. Merge is DAPI and citrine. Scale bar represents 200 µm.

of reporter activity, indicating that indeed levels of Fe65 are a rate-limiting factor for transcriptional activity of AICD in non-neuronal cells (figure 5.3). In summary, our results from a novel cell-based UAS/Gal4 assay confirm that AICD-Gal4 derived from APP-Gal4 is transcriptionally active. In addition, it is important to note, that because of the stable integration of UAS-Cit in the HEK(UAS-Cit), we show here for the first time unequivocally that nuclear localization of AICD is necessary for its transcriptional activity.

5.2.2 Construction and analysis of the APPGal4 mice

APP-Gal4 was cloned into a pMoPrp plasmid, previously used successfully in our laboratory to generate the ArcAβ mice, a APP transgenic mouse line (Knobloch et al., 2007). Transgenic mice were generated by the Institut für Labortierkunde (University Zurich) by embryo transfer of the APP-Gal4 construct and three different founder lines were provided. Whole brain lysates of founder lines were prepared and probed for expression of the transgene with an antibody recognizing human but not mouse APP (figure 5.4). All three founder lines showed expression of APP-Gal4, however, levels were considerably lower than APP levels in ArcAβ mice. Founder line #3, subsequently called APPGal4 mice, was chosen for subsequent experiments because of highest expression levels.

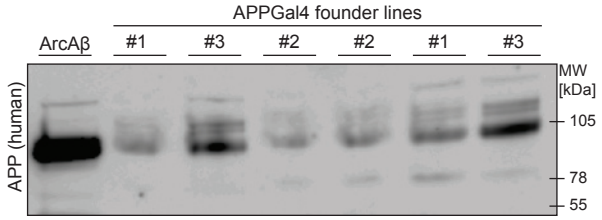

Figure 5.4 APPGal4 founder lines showed moderate expression of the APP-Gal4 protein. Western blot analysis of whole brain lysates were probed with an antibody recognizing exclusively human (here i.e., transgenic) APP. Note that AICD is not recognized by this antibody. Founder line #3 was chosen for subsequent experiments, and hereafter called APPGal4 mice.

For *in vivo* analysis of AICD transcriptional activity, APPGal4 mice were cross-breed with UAS-lacZ mice, which were previously used in Govindarajan et al. (2005) and Smith et al. (2012). UAS-lacZ mice carry the β-galactosidase-encoding gene *lacZ* under the control of a minimal promoter and six UAS elements. In absence of a complete transactivator that is able to bind to the UAS repeats no expression of β-galactosidase takes place. Due to the transcriptional activity of AICD, binding of AICD-Gal4 to the UAS element repeats should induce expression of β-galactosidase. β-galactosidase in-turn can be detected by X-Gal staining, a colorimetric staining of a synthetic product of β-galactosidase enzyme activity. To analyze expression of β-galactosidase by transcriptional activity of AICD, cryosections of wildtype, UAS-lacZ, and APPGal4/UAS-lacZ double transgenic mouse brains were prepared. Sections were fixed with PFA, methanol, or fixative solution (provided by the X-Gal staining Invitrogen kit) and stained for β-galactosidase activity. Sections were analyzed one hour and longer durations of incubation at 37 °C by regular light microscopy. However, we could not detect any formation of insoluble, blue precipitate which is suppose to form by β-galactosidase activity. Due to poor quality of sections after extended incubation with X-Gal (more than forty-eight hours incubation) no images of sections were taken.

We reasoned that detection of potentially low β-galactosidase levels in APPGal4/UAS-lacZ mice could be enhanced by immunohistochemical staining. Free-floating brain sections were prepared from adult wildtype and APPGal4/UAS-lacZ double transgenic mice and stained with an antibody recognizing β-galactosidase. Brain sections of embryonic BATGal transgenic mice were obtained from Bruno Fischer and Olivier Raineteau (University Zurich) and used as positive control for β-galactosidase antibody staining. BATGal mice express nuclear β-galactosidase under the control of β-catenin/T-cell factor responsive elements (Maretto et al., 2003; Al Alam et al., 2011; Azim et al., 2014). Staining of BATGal brain sections displayed clear nuclear β-galactosidase

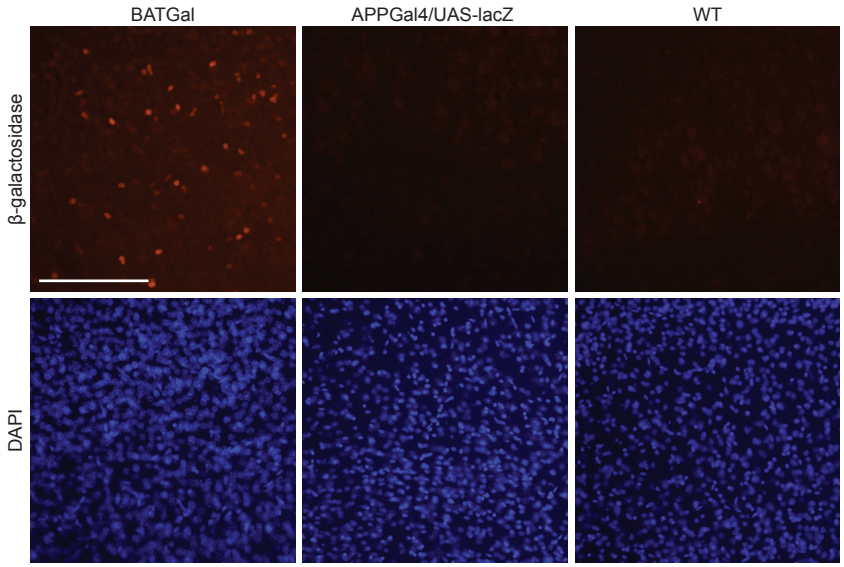

Figure 5.5 β-galactosidase is not detectable in brain sections of APPGal4/UAS-lacZ double transgenic mice. Fluorescence images of brain sections from E14 BATGal (left panel), adult APPGal4/UAS-lacZ double transgenic (middle panel), or adult wildtype mice (right panel) stained with β-galactosidase primary and Cy3-coupled secondary antibody. Nuclei were stained with DAPI. Scale bar represents 150 µm.

staining, demonstrating usability of the employed β-galactosidase staining protocol (figure 5.5). In contrast to sections of BATGal mice, we could not observe β-galactosidase positive cells in sections from APPGal4/UAS-lacZ double transgenic mice (figure 5.5). The weak observed signal observed in APPGal4/UAS-lacZ sections was equally present in sections from wildtype mice and accounts thus as background signal. Together, our results from enzymatic and immunohistochemical staining show no detectable levels of β-galactosidase in APPGal4/UAS-lacZ double transgenic mice. Possible reason for the absence of reporter protein include low sensitivity of the used assays, absence of transcriptional activity of AICD *in vivo*, and dysfunction of the UAS-lacZ reporter mice.

To explore the underlying reason for absence of β-galactosidase signal in APPGal4/UAS-lacZ mice, we envisaged analysis of primary neurons that allow manipulations that are not possible with brain sections. To this end, a β-galactosidase staining protocol for cultured cells was developed. HEK cells were transfected with a plasmid encoding the *lacZ* gene under the control of a CMV promoter, which allows constitutive gene expression. Cells were fixed and stained for enzymatic activity of β-galactosidase as described in section 2.4. A clear β-galactosidase signal was observed in *lacZ* transfected

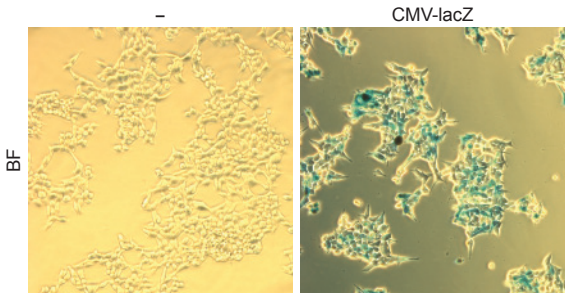

Figure 5.6 β-galactosidase activity can be detected in cultured cells. Bright-field (BF) images of HEK cells transfected with constitutively-expressed *lacZ* or mock transfected (–) and stained for β-galactosidase activity with X-Gal.

cells that was absent in stained but non-transfected control cells (figure 5.6). Next, we prepared primary neurons from one-day-old wildtype, APPGal4, UAS-lacZ, and APPGal4/UAS-lacZ mice. Plasmid transfection of primary neurons was done at DIV 7 and cells fixed and stained for β-galactosidase at DIV 11. Primary neurons from wildtype mice transfected with *lacZ* showed clear and abundant staining of β-galactosidase, confirming the utility of the staining protocol and efficient plasmid transfection also in primary neurons (figure 5.7). Of note, β-galactosidase signal was almost exclusively detected in the cell soma and no signal was observed in dendrites. Similar to the reported observations from brain sections, primary neurons from APPGal4/UAS-lacZ did not show a positive signal. Next, we aimed to analyze functionality of APPGal4 and UAS-lacZ mice separately. For this purpose, the Gal4(DBD)-VP16 plasmid, expressing the potent activation domain VP16 fused to the Gal4-DBD, and the UAS-lacZ plasmid harboring a reporter construct similar to the transgene of UAS-lacZ mice were obtained. Wildtype primary neurons

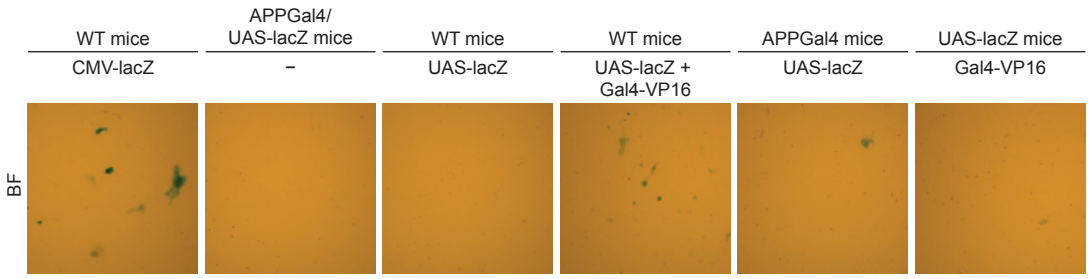

Figure 5.7 UAS-lacZ primary neurons do not show β-galactosidase expression after transfection with a strong transactivator. Representative bright-field (BF) images of primary neurons stained for β-galactosidase with X-Gal staining at DIV 11. Primary neurons were prepared from P1 embryos and transfected with plasmids at DIV 7. Genotypes of mice are indicated above the bar. Plasmid used for transfection are indicated below the bar.

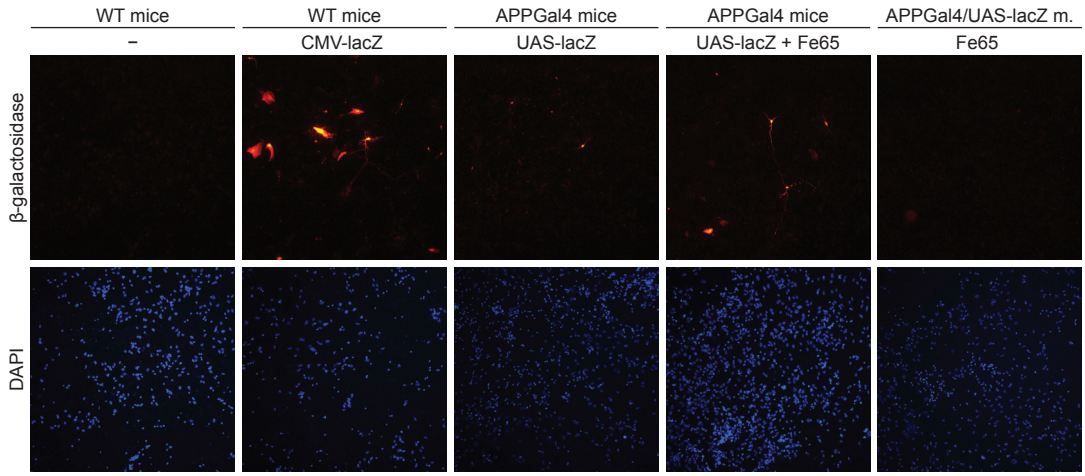

Figure 5.8 Transcriptional activity of AICD-Gal4 in APPGal4 primary neurons is enhanced by expression of Fe65. Representative fluorescence images of primary neurons immunostained for β-galactosidase at DIV 11. Nuclei were stained with DAPI. Primary neurons were prepared from P1 embryos and transfected with plasmids at DIV 7. Genotypes of mice are indicated above the bar. Plasmid used for transfection are indicated below the bar.

transfected with UAS-lacZ and Gal4-VP16 plasmids showed clear positive signal (figure 5.7). No signal in contrast was observed in primary neurons transfected with UAS-lacZ alone , demonstrating that the UAS-lacZ plasmid is not expressing β-galactosidase without complete transactivator. APPGal4 neurons transfected with UAS-lacZ showed any positive signal, albeit in very few cells. In contrast, UAS-lacZ neurons did not show a positive signal when transfected with the strong transactivator Gal4(BDB)-VP16.

As mentioned earlier, immunohistochemical staining for β-galactosidase might display higher sensitivity than enzymatic staining for β-galactosidase activity. Therefore, primary neurons were also analyzed by immunostaining of β-galactosidase. Immunohistochemical staining of wildtype primary neurons showed no signal, indicating very low off-target recognition of both primary and secondary antibody (figure 5.8). In contrast primary neurons transfected with *lacZ* showed strong and abundant fluorescence signal. Similar to staining of enzymatic activity, primary neurons from APPGal4 mice transfected with UAS-lacZ displayed a clear positive signal, albeit in only few cells. As shown earlier, binding of adaptor proteins, such as Fe65, are a rate-limiting factor for transcriptional activity of AICD in non-neuronal cells. We reasoned that levels of adaptor proteins could also be a rate-limiting factor in primary neurons. Co-transfection of UAS-lacZ and Fe65 in APPGal4 primary neurons clearly increased the number of β-galactosidase positive cells compared to transfection with UAS-lacZ alone (figure 5.8). We also transfected APPGal4/UAS-lacZ

primary neurons with Fe65 to test whether increasing nuclear transport of AICD-Gal4 could result in enhancement of its transcriptional activity. However, transfection of Fe65 did also not result in detectable levels of β-galactosidase.

In summary the analysis of primary neurons from APPGal4 and UAS-lacZ mice revealed several interesting findings. Firstly, transfection of UAS-lacZ primary neurons with the strong transactivator Gal4(DBD)-VP16 did not result in expression of β-galactosidase. This observation strongly suggest that the UAS-lacZ element of UAS-lacZ mice is non-functional. Secondly, transfection of APPGal4 primary neurons with a UAS-lacZ plasmid showed positive, albeit little, signal. Further, we show that transcriptional activity of AICD-Gal4 in APPGal4 primary neurons can be strongly increased by transfection of Fe65.

5.3 Discussion

We have generated a novel transgenic mouse line, the APPGal4 line, for analysis of the transcriptional function of AICD *in vivo*. APPGal4 mice were crossed to the UAS-lacZ reporter line and brain lysates, brain sections, and primary neurons analyzed. However, no reporter activity was observed in APPGal4/UAS-lacZ double transgenic mice. By analysis of transgenic mice separately, we discovered that the reporter element of UAS-lacZ mice is non-functional, while APPGal4 mice displayed transcriptional activity as intended by their design.

Our analysis of UAS-lacZ mice demonstrated that the reporter construct is not functional. Primary neurons from UAS-lacZ mice were transfected with the potent transactivator Gal4-VP16 but no reporter activity was detected. It remains unclear why the UAS-lacZ transgene is not functional. Previous studies have successfully used the UAS-lacZ mouse line as a reporter of Notch transcriptional activity (Smith et al., 2012). It is unlikely that UAS-lacZ site is placed in a loci that hinders its accessibility in the here investigated brain-derived tissue because similar tissue was analyzed previously (Smith et al., 2012). A particular difficulty in the maintenance of these mice is that the reporter gene is not expressed, unless crossed to an activator line. Additionally, the number of UAS-lacZ transgene integrations and the actual sites of integration are not known. Therefore, genotyping of mice can only be done by intra-transgenetical PCR and length of the PCR product is the only criterion for selection of offspring. It is possible that UAS-lacZ mice acquired mutations in the UAS regulatory region or *lacZ* coding region that ablate binding of the Gal4(BDB) or impede proper gene expression, respectively.

APPGal4 is a novel mouse line for studying the transcriptional activity of AICD. APP-Gal4 transgene expression is approximately ten fold lower than APP expression in the ArcAβ mouse line, which was established using the same promoter for transgene expression (Knobloch et al., 2007). Because the APPGal4 mouse line is based on the UAS/Gal4 activator/reporter system, its utility is fully dependent on a functional reporter mouse line. In light of the non-functioning of the UAS-lacZ mouse line, analysis of APPGal4 mice was only possible in primary neurons, which can be transfected with UAS-reporter plasmids. Generation of a novel reporter line is therefore obligatory for further investigations using the APPGal4 mouse line. A second critical point of the APPGal4 mouse line are the levels of adaptor proteins that mediate nuclear translocation of AICD-Gal4. We showed that primary neurons from APPGal4 mice transfected with UAS-lacZ plasmid displayed sporadic positive cells, which were greatly increased in number by co-transfection of

the AICD-binding protein Fe65. Though we have not evaluated endogenous Fe65 levels itself, our results suggest that levels of Fe65 are rate-limiting for the transcriptional function of AICD-Gal4 in non-neuronal cells and also primary neurons. However, it is important to emphasize that the data presented here does not allow to claim that AICD has no transcriptional function in these cells at all. Sensitivity of endogenous AICD-binding regulatory elements could be higher than the one of the UAS/Gal4 system. It has also to be kept in mind that AICD levels from transgene expression are probably a multitude higher than endogenous AICD levels. Therefore, levels of Fe65 and other adaptor proteins could be largely sufficient to mediate transcriptional function of endogenous AICD. The observation that APP(Y682G) on a APLP2 knockout background, which have disrupted AICD–Fe65 binding, die perinatally, also emphasizes a important role of this protein complex in mouse development. Therefore, the important question for the utility of the APPGal4 mouse line is, whether levels of adaptor proteins are always the rate-limiting factor for the transcriptional function of transgene-derived AICD-Gal4. Kesavapany et al. (2002) demonstrate that Fe65 levels in late embryonic development and at a birth of mice are barely detectable. However, since Fe65 strongly increases postnatally, we have good reason to believe that levels of adaptor proteins are not generally rate-limiting for the transcriptional function of AICD-Gal4. In summary, our results thus provide proof-of-principle of the APPGal4 mouse line for studying the transcriptional function of AICD. Under the assumption that a functional UAS-reporter mouse can be established, the APPGal4 mouse line constitutes a promising tool for the investigation of transcriptional function of AICD *in vivo*.

6 Conclusions and Outlook

In the first results part of this thesis, we aimed to better understand the mechanism and constraints of nuclear signaling of AICD. We discovered different nuclear signaling and AFT-complex formation capability of ICDs derived from different APP family members. In summary, our subsequent analyses revealed sequence determinants for AFT-complex formation and displays, for the first time, that ICDs from APP family members are subject to proteasomal degradation. Our results suggest a function of APP and APLP2 in transcriptional regulation, which is absent in APLP1. The uncovered sequence determinants for nuclear signaling of AICD can be of great benefit for future analyses of the physiological function of AICD.

APP knockout mice display a variety of phenotypes, including decreased body and brain weight, behavioral deficits, and defects at the neuromuscular junction, which are further aggravated by additional knockout of APLP2 (see also Müller and Zheng, 2012). Whereas these phenotypes first of all clearly demonstrate that APP and its proteolytic products have important physiological functions, they secondly raise the questions which function is mediated by which APP fragment. A prime function of AICD among APP proteolytic fragments was highlighted by the analysis of an APP knock-in mouse line with a single amino acid mutation in vicinity to the NPxY motif (APP(Y682G) mice), which abolished binding of Fe65 (Barbagallo et al., 2010, 2011; Matrone et al., 2012). APP(Y682G) mice crossed to an APLP2 knockout background displayed severe defects in the formation of the neuromuscular junction and perinatal lethality similar to mice completely deficient in APP and APLP2. Binding of Fe65, in addition to its role in nuclear translocation of AICD, was also shown to influence APP processing, which is reflected by clearly increased levels of sAPPα in the brains of APP(Y682G) mice. The observed phenotypes in these mice can therefore not be attributed exclusively to the lack of AICD-mediated transcriptional activity. The discovery of sequence determinants for nuclear signaling of AICD presented here, offers in this respect a unique possibility to investigate the function of AICD. Exchange of the N-terminal

amino acids of AICD VML646 with LLR, did not disrupt binding of Fe65 and, importantly, no differences in APP processing were observed, except for a dramatic reduction in AICD levels. We therefore propose the generation of an APP(VML646LLR) knock-in mouse line. This mouse line—which from a physiological perspective could represent an AICD knockdown model—could allow to investigate unambiguously the physiological functions of AICD *in vivo*. To allow investigation of redundant functions of AICD and AL2ICD, we propose also the construction of a conditional APP(VML646LLR) mouse line to circumvent possible (and likely) perinatal lethality of APP(VML646LLR) mice on an APLP2 knockout background.

In the second results part of this thesis, we aimed to decipher the molecular mechanism of AICD proteasomal degradation. In this analysis, a particular focus was placed on the regulation of different AICD species, generated by variable cleavage of γ-secretase at the ε-site, and a possible contribution of AICD to AD pathology. We clearly show that AICD51 undergoes faster proteasomal degradation than AICD50. This different regulation is reminiscent of the N-end rule proteasomal pathway, a specific ubiquitin-dependent branch of proteasomal degradation, in which the identity of the N-terminal residue of a substrate determines its proteasomal turnover. In summary, our mechanistic analyses, however, show that proteasomal degradation of AICD species is independent of ubiquitination or modification by ubiquitin-like proteins, and we could also not detect any regulation of AICD levels by N-end rule specific E3 Ub-ligase enzymes. Therefore, we suggest that different proteasomal degradation of AICD species is mediated by stabilizing or destabilizing factors in a N-end rule-like manner. Identification of the proposed stabilizing or destabilizing factors that mediate the different degradation of AICD species should, therefore, be a main aim for future experiments. Experiments employing comparative mass spectrometry analysis to identify binding partners of AICD species could build on the already established and efficient immunoprecipitation of AICD species.

In the course of our investigations, we also analyzed, for the first time, AICD levels derived from FAD APP mutants in cell culture experiments and revealed a dramatic reduction of AICD levels. FAD mutants display two well-described, independent phenomena of altered γ-secretase processing, which are partial loss-of-function of γ-secretase activity and shift of γ-secretase cleavage at the ε-site. It is well established that partial loss-of-function results in decreased AICD levels. We suggest that shift of γ-secretase cleavage at the ε-site, by the production of unstable AICD species, similarly results in decreased total AICD levels. Interestingly, such a regulation would imply that production of the principal toxic agent of AD, Aβ42, would be inherently correlated with decreased total levels of AICD, which could in turn point towards a role of AICD

in AD pathology. However, a clear analysis of possible different degradation of AICD species derived from APP, and in particular APP with FAD mutations, is clearly limited by the lack of techniques to separately detect AICD species. Developing means to separately detect AICD species should, therefore, obtain highest priority for future experiments. Two promising techniques that could be employed are usage of urea-based SDS-PAGE, which has been shown to provide higher resolution than regular SDS-PAGE, and detection of AICD by mass spectrometry as performed by Dimitrov et al. (2013) for AICD generated from *in vitro* assays. A better understanding of the regulation of AICD species promises to contribute to our understanding of AD pathology, but will also be essential for developing efficient and save therapeutics.

In the third results part of this thesis, we aimed to explore the regulation and function of AICD *in vivo*. To this end, the APPGal4 mouse line, which harbors a transgenic APP with a Gal4-DBD within the AICD sequence, was generated and analyzed. The APPGal4 mouse line is designed to monitor the transcriptional activity of AICD, after crossing APPGal4 mice with a UAS-reporter mouse line. Our combined analysis from mouse brains and primary neurons revealed a general functionality of the APPGal4 mouse line, but showed, unfortunately, that the UAS-reporter mouse line is not functional. We also showed that the adaptor protein Fe65 is critical for the transcriptional function of AICD in APPGal4 mice. The importance of Fe65 was further underlined in cell-culture based UAS/Gal4 assays. Generation of a novel reporter mouse line is obligatory for future analysis of transcriptional function of AICD with the APPGal4 mouse line. A major problem of the currently available reporter mouse line is the difficulty to monitor integrity of the transgene since it is not expressed unless mice are crossed to activator mice. To ensure better monitoring of transgene integrity in a novel reporter mouse line, we recommend site specific integration of the UAS-reporter element. Usage of fluorescence proteins as reporter—in lieu of β-galactosidase—to allow live *in vivo* analysis of the spatiotemporal patterns of AICD transcriptional activity, should be considered to tap the full potential of the APPGal4 mouse line.

The main challenge to the role of AICD as a transcriptional regulator is the identification of reliable target genes. Regulation of transcription is the most prominent function described for AICD and to date approximately thirty target genes have been identified. However, AICD regulation of several of these genes have been challenged, while other completely lack independent confirmation. Part of these difficulties can be attributed to usage of different biological systems and technical difficulties to manipulate AICD. However, it seems that transcriptional activity by AICD is itself regulated or modulated by hitherto unknown mechanism. This may comprise—but is certainly not restricted

to—regulation by direct binding partners of AICD. Multiple experiments, including results from this thesis, have shown the importance of binding partners, such as Fe65, for nuclear signaling and transcriptional activity, but the identity of these facilitators remain partly unknown and their regulation poorly described. The work presented here will be instrumental to decipher regulation of AICD transcriptional activity and identification of target genes itself. On the one hand, the promises of the APPGal4 mouse line, to uncover the spatiotemporal pattern of transcriptional activity of AICD, could allow us determine constraints of AICD nuclear signaling. Brain regions and cellular networks for example that show transcriptional activity could be identified. On the other hand, identification of nuclear signaling constraints sets the groundwork for a knock-in mouse line that has the physiological properties of a AICD knockout model, and could thus allow the identification of AICD regulated genes.

Appendix

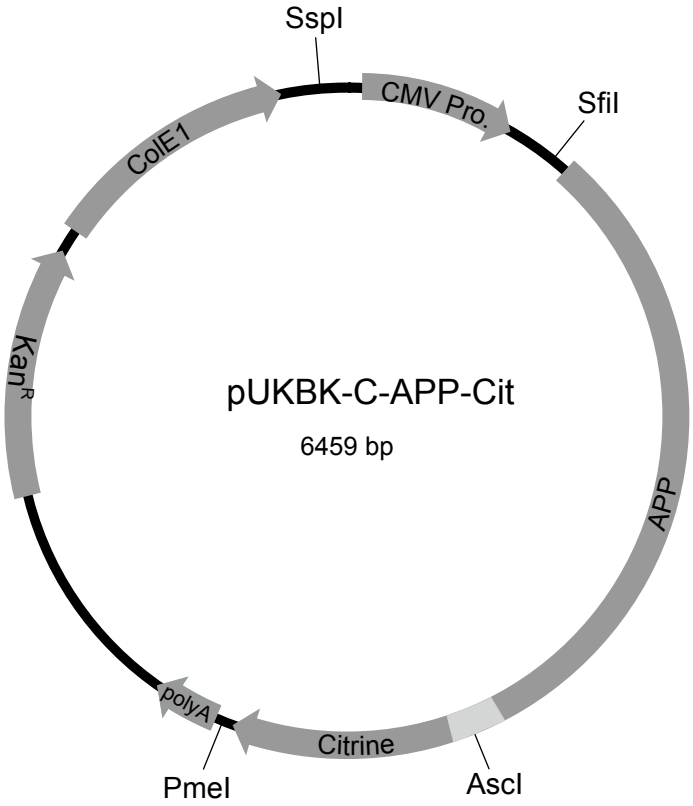

Figure A.1 Plasmid map of pUKBK-C-APP-Cit as representative plasmid for the pUKBK plasmid series. The promoter region (here CMV promoter) of pUKBK plasmids is flanked by a SspI and SfiI cleavage sites for exchange of promoters by restriction-based cloning. The coding sequence (here APP-Cit) is similarly flanked by SfiI and PmeI cleavage sites. An AscI cleavage site is present in the forty-eight bp linker between APP and citrine, which allows simple exchange of the fluorescence proteins or replacement with protein-tags by AscI-PmeI-mediated restriction-based cloning.

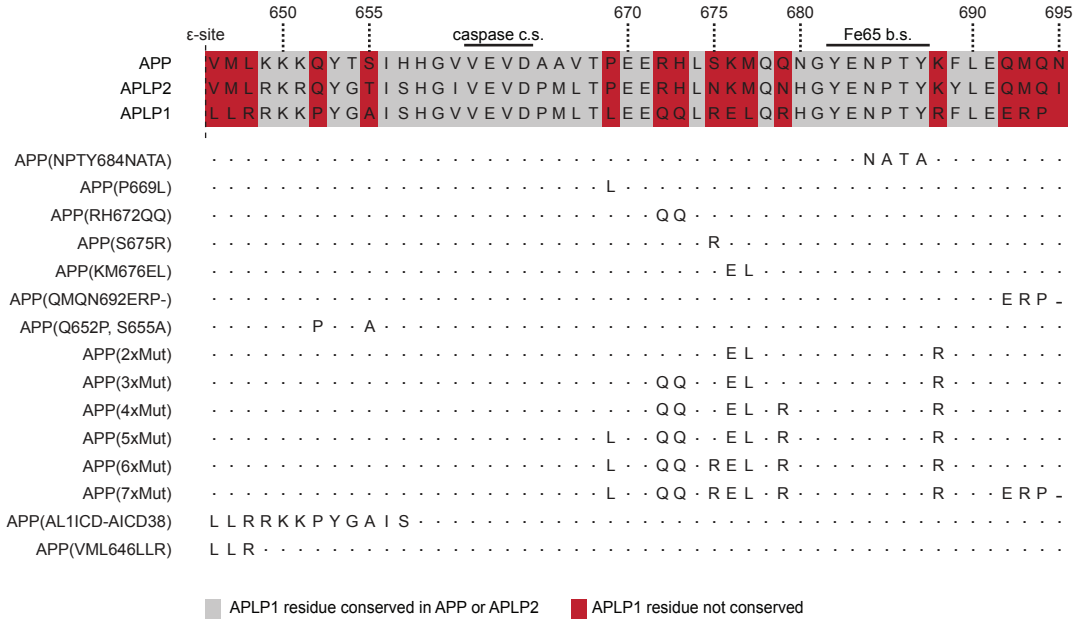

Figure A.2 Schematic presentation of APP family ICD sequences and APP-to-APLP1 substituions used in this study. c.s.: cleavage site; b.s.: binding site.

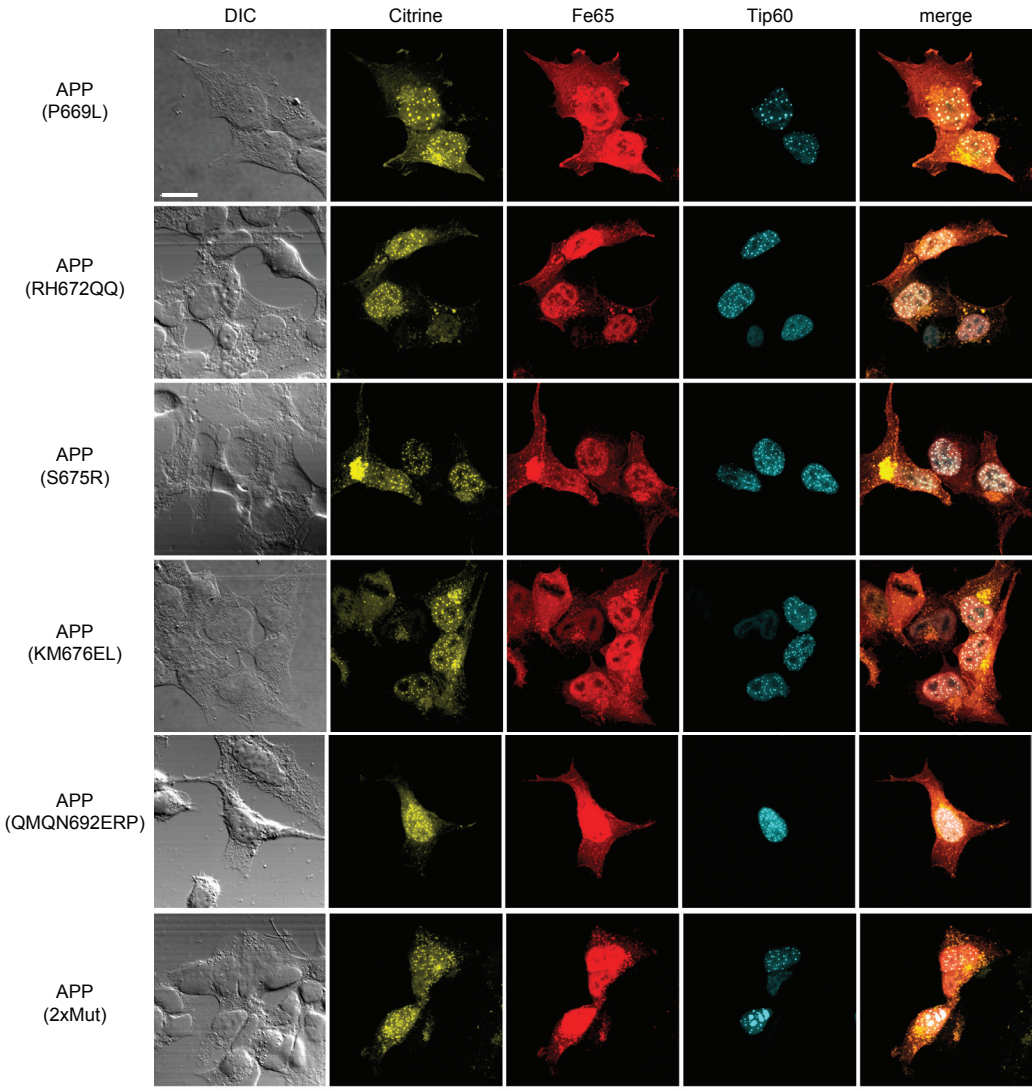

Figure A.3 DIC and confocal fluorescence images of APP with substituted residues, part I. HEK cells were transfected with HA-Fe65, CFP-Tip60 and the indicated citrine-tagged APP-to-APLP1 mutants. See figure A.2 in the appendix for abbreviation of APP-to-APLP1 mutation constructs. Scale bar represents 13 µm.

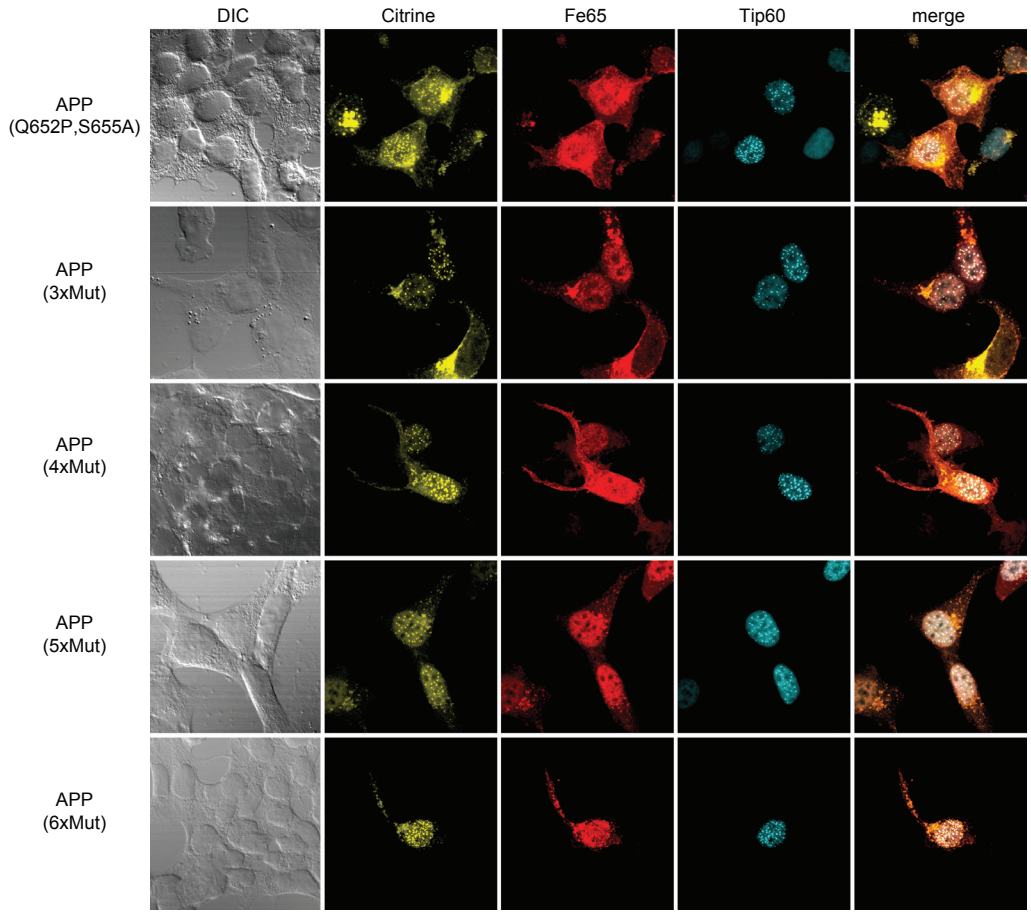

Figure A.4 DIC and confocal fluorescence images of APP with substituted residues, part II. HEK cells were transfected with HA-Fe65, CFP-Tip60 and the indicated citrine-tagged APP-to-APLP1 mutants. See figure A.2 in the appendix for abbreviation of APP-to-APLP1 mutation constructs. Scale bar represents 13 μm.

Acknowledgments

I thank Uwe Konietzko for his guidance and help throughout my doctoral studies. Further, I thank Roger Nitsch for giving me the opportunity to work in his research group and his valuable suggestions and motivation. I am grateful to Stephan Neuhauss for his participation in my steering committee and his scientific advice.

I would like to thank all the past and present members of the Division of Psychiatry Research for help, support, stimulating scientific discussions, and a memorable time both inside and outside the lab. Particular thanks go to Zoë Goodger for initiating an interesting scientific project and Sarina Thöni for excellent technical assistance. Explicitly, I would also like to acknowledge Annette Trutzel for help with preparation of primary neurons, Sonja Grinschgl for preparation of lentiviruses, Maria Teresa Ferretti and Christoph Gericke for help with immunohistochemistry, and Daniel Schuppli for help in preparation, maintenance, and genotyping of mice. I also would like to thank Nico Dantuma, Bart De Strooper, Bruno Fischer, Wade Harper, Stefan Kins, Yong Tae Kwon, Patrick May, Michael Potente, Freddy Radtke, Olivier Raineteau, Walter Schaffner, Thomas Südhof, and Uli Suter for plasmids, cell lines, antibodies, mice, and tissue. Special thanks go to Florian Rau, Patrick Kuppinger, Deniz Gökbuget, and Vinod Udayar for their help with preparation of this doctoral thesis and Doo Yeon Kim for mentorship throughout my doctoral studies.

My deepest gratitude goes to my family and friends. Without the time that I spend with you and your constant support and encouragement this doctoral thesis would not have been possible.

List of publications

Riese F, Grinschgl S, Gersbacher MT, Russi N, Hock C, Nitsch RM, Konietzko U. 2013. Visualization and quantification of APP intracellular domain-mediated nuclear signaling by bimolecular fluorescence complementation. PLoS ONE. 8(9):e76094.

Gersbacher MT*, Goodger ZV*, Trutzel A, Bundschuh D, Nitsch RM, Konietzko U. 2013 Turnover of amyloid precursor protein family members determines their nuclear signaling capability. PLoS ONE. 8(7):e69363.

Kim DY*, Gersbacher MT*, Inquimbert P, Kovacs DM. 2011. Reduced sodium channel Na(v)1.1 levels in BACE1-null mice. J Biol Chem. 286(10):8106-16.

Gersbacher MT*, Kim DY*, Bhattacharyya R, Kovacs DM. 2010. Identification of BACE1 cleavage sites in human voltage-gated sodium channel beta 2 subunit. Mol Neurodegener. 5:61.

Kovacs DM, Gersbacher MT, Kim DY. 2010. Alzheimer's secretases regulate voltage-gated sodium channels. Neurosci Lett. 486(2):68-72.

Madec M, Lallement C, Karstens K, Dittman S, Gersbacher M, Sorg R, Wild M, Muller M, Bourgine P, Donzeau M, Haiech J. 2009. Synthetic biology and microelectronics: a similar design flow. Circuits and System and TAISA Conference Paper

* denotes equal authorship

Curriculum vitae

Personal details

Name:	Manuel Tobias Gersbacher
Date of Birth:	August 24, 1982 in Lörrach (Germany)

Education

09/1993 – 07/2002	Theodor-Heuss Gymnasium Schopfheim (Germany) Degree: Abitur (A-levels)
09/2003 – 09/2005	General Biology, Albert-Ludwigs University Freiburg (Germany) Degree: Vordiplom (Pre-degree)
09/2005 – 09/2006	Neurosciences, University of Leeds (UK)
10/2006 – 10/2009	Biotechnology, Ecole supérieure de Biotechnologie Strasbourg (France) Thesis title: *Characterization of a novel physiological function of BACE1* Degree: M.Sc. Biotechnology
01/2011 – present	Doctoral thesis, University Zurich (Switzerland) Thesis title: *Proteasomal Degradation of the APP Intracellular Domain (AICD) and Regulation of its Nuclear Signaling*

Professional Experience

06/2007 – 08/2007	Internship, Roma Tre University (Italy)
12/2008 – 12/2010	Research Assistant, MGH/Harvard Medical School (USA)

Bibliography

Aasland R, Abrams C, Ampe C, Ball LJ, Bedford MT, Cesareni G, Gimona M, Hurley JH, Jarchau T, Lehto VP, Lemmon MA, Linding R, Mayer BJ, Nagai M, Sudol M, Walter U, Winder SJ (2002) Normalization of nomenclature for peptide motifs as ligands of modular protein domains. FEBS Lett 513:141–4.

Al Alam D, Green M, Tabatabai Irani R, Parsa S, Danopoulos S, Sala FG, Branch J, El Agha E, Tiozzo C, Voswinckel R, Jesudason EC, Warburton D, Bellusci S (2011) Contrasting expression of canonical Wnt signaling reporters TOPGAL, BATGAL and Axin2(LacZ) during murine lung development and repair. PLoS One 6:e23139.

Alves da Costa C, Sunyach C, Pardossi-Piquard R, Sevalle J, Vincent B, Boyer N, Kawarai T, Girardot N, St George-Hyslop P, Checler F (2006) Presenilin-dependent gamma-secretase-mediated control of p53-associated cell death in Alzheimer's disease. J Neurosci 26:6377–85.

Alzheimer's Association (2014) 2014 Alzheimer's disease facts and figures. Alzheimers Dement 10:e47–92.

Alzheimer's Association (2015) 2015 Alzheimer's disease facts and figures. Alzheimers Dement 11:332–84.

An JY, Seo JW, Tasaki T, Lee MJ, Varshavsky A, Kwon YT (2006) Impaired neurogenesis and cardiovascular development in mice lacking the E3 ubiquitin ligases UBR1 and UBR2 of the N-end rule pathway. Proc Natl Acad Sci USA 103:6212–7.

Azim K, Fischer B, Hurtado-Chong A, Draganova K, Cantù C, Zemke M, Sommer L, Butt A, Raineteau O (2014) Persistent Wnt/β-catenin signaling determines dorsalization of the postnatal subventricular zone and neural stem cell specification into oligodendrocytes and glutamatergic neurons. Stem Cells 32:1301–12.

Bachmair A, Finley D, Varshavsky A (1986) In vivo half-life of a protein is a function of its amino-terminal residue. Science 234:179–86.

Bachman DL, Wolf PA, Linn R, Knoefel JE, Cobb J, Belanger A, D'Agostino RB, White LR (1992) Prevalence of dementia and probable senile dementia of the Alzheimer type in the Framingham study. Neurology 42:115–9.

Barbagallo APM, Wang Z, Zheng H, D'Adamio L (2011) A single tyrosine residue in the amyloid precursor protein intracellular domain is essential for developmental function. J Biol Chem 286:8717–21.

Barbagallo APM, Weldon R, Tamayev R, Zhou D, Giliberto L, Foreman O, D'Adamio L (2010) Tyr(682) in the intracellular domain of APP regulates amyloidogenic APP processing in vivo. PLoS One 5:e15503.

Bateman RJ, Aisen PS, De Strooper B, Fox NC, Lemere CA, Ringman JM, Salloway S, Sperling RA, Windisch M, Xiong C (2011) Autosomal-dominant Alzheimer's disease: a review and proposal for the prevention of Alzheimer's disease. Alzheimers Res Ther 3:1.

Bayer TA, Cappai R, Masters CL, Beyreuther K, Multhaup G (1999) It all sticks together–the APP-related family of proteins and Alzheimer's disease. Mol Psychiatry 4:524–8.

Belyaev ND, Kellett KA, Beckett C, Makova NZ, Revett TJ, Nalivaeva NN, Hooper NM, Turner AJ (2010) The transcriptionally active amyloid precursor protein (APP) intracellular domain is preferentially produced from the 695 isoform of APP in a beta-secretase-dependent pathway. J Biol Chem 285:41443–54.

Ben-Nissan G, Sharon M (2014) Regulating the 20S proteasome ubiquitin-independent degradation pathway. Biomolecules 4:862–84.

Bertram L (2011) Alzheimer's genetics in the GWAS era: a continuing story of 'replications and refutations'. Curr Neurol Neurosci Rep 11:246–53.

Bertram L, Tanzi RE (2009) Genome-wide association studies in Alzheimer's disease. Hum Mol Genet 18:R137–45.

Bittner T, Fuhrmann M, Burgold S, Jung CKE, Volbracht C, Steiner H, Mitteregger G, Kretzschmar HA, Haass C, Herms J (2009) Gamma-secretase inhibition reduces spine density in vivo via an amyloid precursor protein-dependent pathway. J Neurosci 29:10405–9.

Braak H, Braak E (1997) Staging of Alzheimer-related cortical destruction. Int Psychogeriatr 9 Suppl 1:257–61; discussion 269–72.

Broadstock M, Ballard C, Corbett A (2014) Latest treatment options for Alzheimer's disease, Parkinson's disease dementia and dementia with Lewy bodies. Expert Opin Pharmacother 15:1797–810.

Brower CS, Piatkov KI, Varshavsky A (2013) Neurodegeneration-associated protein fragments as short-lived substrates of the N-end rule pathway. Mol Cell 50:161–71.

Buchsbaum S, Bercovich B, Ciechanover A (2012) FAT10 is a proteasomal degradation signal that is itself regulated by ubiquitination. Mol Biol Cell 23:225–32.

Buckner RL, Snyder AZ, Shannon BJ, LaRossa G, Sachs R, Fotenos AF, Sheline YI, Klunk WE, Mathis CA, Morris JC, Mintun MA (2005) Molecular, structural, and functional characterization of Alzheimer's disease: evidence for a relationship between default activity, amyloid, and memory. J Neurosci 25:7709–17.

Buoso E, Biundo F, Lanni C, Schettini G, Govoni S, Racchi M (2012) AβPP intracellular C-terminal domain function is related to its degradation processes. J Alzheimers Dis 30:393–405.

Buoso E, Lanni C, Schettini G, Govoni S, Racchi M (2010) β-Amyloid precursor protein metabolism: focus on the functions and degradation of its intracellular domain. Pharmacol Res 62:308–17.

Bush AI, Pettingell J W H, de Paradis M, Tanzi RE, Wasco W (1994) The amyloid beta-protein precursor and its mammalian homologues. Evidence for a zinc-modulated heparin-binding superfamily. J Biol Chem 269:26618–21.

Cao X, Sudhof TC (2001) A transcriptionally [correction of transcriptively] active complex of APP with Fe65 and histone acetyltransferase Tip60. Science 293:115–20.

Chávez-Gutiérrez L, Bammens L, Benilova I, Vandersteen A, Benurwar M, Borgers M, Lismont S, Zhou L, Van Cleynenbreugel S, Esselmann H, Wiltfang J, Serneels L, Karran E, Gijsen H, Schymkowitz J, Rousseau F, Broersen K, De Strooper B (2012) The mechanism of γ-Secretase dysfunction in familial Alzheimer disease. EMBO J 31:2261–74.

Chen AC, Selkoe DJ (2007) Response to: Pardossi-Piquard et al., "Presenilin-dependent transcriptional control of the Abeta-degrading enzyme neprilysin by intracellular domains of betaAPP and APLP." Neuron 46, 541-554. Neuron 53:479–83.

Chen Y, Neve RL, Liu H (2012) Neddylation dysfunction in alzheimer's disease. J Cell Mol Med 16:2583–91.

Choi WS, Jeong BC, Joo YJ, Lee MR, Kim J, Eck MJ, Song HK (2010) Structural basis for the recognition of n-end rule substrates by the ubr box of ubiquitin ligases. Nat Struct Mol Biol 17:1175–81.

Ciechanover A (1994) The ubiquitin-proteasome proteolytic pathway. Cell 79:13–21.

Ciechanover A (2013) Intracellular protein degradation: from a vague idea through the lysosome and the ubiquitin-proteasome system and onto human diseases and drug targeting. Bioorg Med Chem 21:3400–10.

Coulson EJ, Paliga K, Beyreuther K, Masters CL (2000) What the evolution of the amyloid protein precursor supergene family tells us about its function. Neurochem Int 36:175–84.

Cummings JL, Dubois B, Molinuevo JL, Scheltens P (2013) International work group criteria for the diagnosis of Alzheimer disease. Med Clin North Am 97:363–8.

Cupers P, Orlans I, Craessaerts K, Annaert W, De Strooper B (2001) The amyloid precursor protein (APP)-cytoplasmic fragment generated by gamma-secretase is rapidly degraded but distributes partially in a nuclear fraction of neurones in culture. J Neurochem 78:1168–78.

Cusimano M, Biziato D, Brambilla E, Donegà M, Alfaro-Cervello C, Snider S, Salani G, Pucci F, Comi G, Garcia-Verdugo JM, De Palma M, Martino G, Pluchino S (2012) Transplanted neural stem/precursor cells instruct phagocytes and reduce secondary tissue damage in the injured spinal cord. Brain 135:447–60.

Dantuma NP, Lindsten K, Glas R, Jellne M, Masucci MG (2000) Short-lived green fluorescent proteins for quantifying ubiquitin/proteasome-dependent proteolysis in living cells. Nat Biotechnol 18:538–43.

De Strooper B, Annaert W (2010) Novel research horizons for presenilins and gamma-secretases in cell biology and disease. Annual review of cell and developmental biology 26:235–60.

Degasperi A, Birtwistle MR, Volinsky N, Rauch J, Kolch W, Kholodenko BN (2014) Evaluating strategies to normalise biological replicates of western blot data. PLoS One 9:e87293.

Dimitrov M, Alattia JR, Lemmin T, Lehal R, Fligier A, Houacine J, Hussain I, Radtke F, Dal Peraro M, Beher D, Fraering PC (2013) Alzheimer's disease mutations in APP but not γ-secretase modulators affect epsilon-cleavage-dependent AICD production. Nat Commun 4:2246.

Doody RS, Raman R, Farlow M, Iwatsubo T, Vellas B, Joffe S, Kieburtz K, He F, Sun X, Thomas RG, Aisen PS, Alzheimer's Disease Cooperative Study Steering Committee, Siemers E, Sethuraman G, Mohs R, Semagacestat Study Group (2013) A phase 3 trial of semagacestat for treatment of Alzheimer's disease. N Engl J Med 369:341–50.

Dougan DA, Micevski D, Truscott KN (2012) The N-end rule pathway: from recognition by N-recognins, to destruction by AAA+proteases. Biochim Biophys Acta 1823:83–91.

Edbauer D, Willem M, Lammich S, Steiner H, Haass C (2002) Insulin-degrading enzyme rapidly removes the beta-amyloid precursor protein intracellular domain (AICD). J Biol Chem 277:13389–93.

Eggert S, Paliga K, Soba P, Evin G, Masters CL, Weidemann A, Beyreuther K (2004) The proteolytic processing of the amyloid precursor protein gene family members APLP-1 and APLP-2 involves alpha-, beta-, gamma-, and epsilon-like cleavages: modulation of APLP-1 processing by n-glycosylation. J Biol Chem 279:18146–56.

El Ayadi A, Stieren ES, Barral JM, Boehning D (2012) Ubiquilin-1 regulates amyloid precursor protein maturation and degradation by stimulating K63-linked polyubiquitination of lysine 688. Proc Natl Acad Sci USA 109:13416–21.

Erales J, Coffino P (2014) Ubiquitin-independent proteasomal degradation. Biochim Biophys Acta 1843:216–21.

Farris W, Mansourian S, Chang Y, Lindsley L, Eckman EA, Frosch MP, Eckman CB, Tanzi RE, Selkoe DJ, Guenette S (2003) Insulin-degrading enzyme regulates the levels of insulin, amyloid beta-protein, and the beta-amyloid

precursor protein intracellular domain in vivo. Proc Natl Acad Sci USA 100:4162–7.

Ferretti MT, Allard S, Partridge V, Ducatenzeiler A, Cuello AC (2012) Minocycline corrects early, pre-plaque neuroinflammation and inhibits BACE-1 in a transgenic model of Alzheimer's disease-like amyloid pathology. J Neuroinflammation 9:62.

Fontana L, Kennedy BK, Longo VD, Seals D, Melov S (2014) Medical research: treat ageing. Nature 511:405–7.

Galvan V, Chen S, Lu D, Logvinova A, Goldsmith P, Koo EH, Bredesen DE (2002) Caspase cleavage of members of the amyloid precursor family of proteins. J Neurochem 82:283–94.

Gersbacher MT, Goodger ZV, Trutzel A, Bundschuh D, Nitsch RM, Konietzko U (2013) Turnover of amyloid precursor protein family members determines their nuclear signaling capability. PLoS One 8:e69363.

Ghosal K, Vogt DL, Liang M, Shen Y, Lamb BT, Pimplikar SW (2009) Alzheimer's disease-like pathological features in transgenic mice expressing the APP intracellular domain. Proc Natl Acad Sci USA 106:18367–72.

Goodger ZV (2009) Regulation of Nuclear Signalling Mediated by the APP Intracellular Domain (AICD) and its Functional Role. Ph.D. thesis, University Zurich.

Goodger ZV, Rajendran L, Trutzel A, Kohli BM, Nitsch RM, Konietzko U (2009) Nuclear signaling by the APP intracellular domain occurs predominantly through the amyloidogenic processing pathway. J Cell Sci 122:3703–14.

Govindarajan V, Harrison WR, Xiao N, Liang D, Overbeek PA (2005) Intracorneal positioning of the lens in Pax6-GAL4/VP16 transgenic mice. Molecular vision 11:876–86.

Grimm MOW, Mett J, Stahlmann CP, Haupenthal VJ, Zimmer VC, Hartmann T (2013) Neprilysin and Aβ clearance: Impact of the APP intracellular domain in NEP regulation and implications in Alzheimer's disease. Front Aging Neurosci 5:98.

Gu Y, Misonou H, Sato T, Dohmae N, Takio K, Ihara Y (2001) Distinct intramembrane cleavage of the beta-amyloid precursor protein family resembling gamma-secretase-like cleavage of notch. J Biol Chem 276:35235–8.

Guarani V, Deflorian G, Franco CA, Krüger M, Phng LK, Bentley K, Toussaint L, Dequiedt F, Mostoslavsky R, Schmidt MHH, Zimmermann B, Brandes RP, Mione M, Westphal CH, Braun T, Zeiher AM, Gerhardt H, Dimmeler S, Potente M (2011) Acetylation-dependent regulation of endothelial Notch signalling by the SIRT1 deacetylase. Nature 473:234–8.

Guardia-Laguarta C, Pera M, Clarimón J, Molinuevo JL, Sánchez-Valle R, Lladó A, Coma M, Gómez-Isla T, Blesa R, Ferrer I, Lleó A (2010) Clinical, neuropathologic, and biochemical profile of the amyloid precursor protein I716F mutation. J Neuropathol Exp Neurol 69:53–9.

Guenette S, Chang Y, Hiesberger T, Richardson JA, Eckman CB, Eckman EA, Hammer RE, Herz J (2006) Essential roles for the FE65 amyloid precursor protein-interacting proteins in brain development. Embo J 25:420–31.

Haass C, Kaether C, Thinakaran G, Sisodia S (2012) Trafficking and proteolytic processing of APP. Cold Spring Harb Perspect Med 2:a006270.

Halpern ME, Rhee J, Goll MG, Akitake CM, Parsons M, Leach SD (2008) Gal4/UAS transgenic tools and their application to zebrafish. Zebrafish 5:97–110.

Hardy J, Selkoe DJ (2002) The amyloid hypothesis of Alzheimer's disease: progress and problems on the road to therapeutics. Science 297:353–6.

Hardy JA, Higgins GA (1992) Alzheimer's disease: the amyloid cascade hypothesis. Science 256:184–5.

Harris JA, Devidze N, Halabisky B, Lo I, Thwin MT, Yu GQ, Bredesen DE, Masliah E, Mucke L (2010) Many neuronal and behavioral impairments in transgenic mouse models of Alzheimer's disease are independent of caspase cleavage of the amyloid precursor protein. J Neurosci 30:372–81.

Heber S, Herms J, Gajic V, Hainfellner J, Aguzzi A, Rulicke T, von Kretzschmar H, von Koch C, Sisodia S, Tremml P, Lipp HP, Wolfer DP, Muller U (2000) Mice with combined gene knock-outs reveal essential and partially redundant functions of amyloid precursor protein family members. J Neurosci 20:7951–63.

Hebert SS, Serneels L, Tolia A, Craessaerts K, Derks C, Filippov MA, Muller U, De Strooper B (2006) Regulated intramembrane proteolysis of amyloid precursor protein and regulation of expression of putative target genes. EMBO Rep 7:739–45.

Hecimovic S, Wang J, Dolios G, Martinez M, Wang R, Goate AM (2004) Mutations in APP have independent effects on Abeta and CTFgamma generation. Neurobiol Dis 17:205–18.

Heckman KL, Pease LR (2007) Gene splicing and mutagenesis by PCR-driven overlap extension. Nat Protoc 2:924–32.

Herms J, Anliker B, Heber S, Ring S, Fuhrmann M, Kretzschmar H, Sisodia S, Muller U (2004) Cortical dysplasia resembling human type 2 lissencephaly in mice lacking all three APP family members. Embo J 23:4106–15.

Hoey SE, Williams RJ, Perkinton MS (2009) Synaptic NMDA receptor activation stimulates alpha-secretase amyloid precursor protein processing and inhibits amyloid-beta production. J Neurosci 29:4442–60.

Huber N, Guimaraes S, Schrader M, Suter U, Niemann A (2013) Charcot-Marie-Tooth disease-associated mutants of GDAP1 dissociate its roles in peroxisomal and mitochondrial fission. EMBO Rep 14:545–52.

Huysseune S, Kienlen-Campard P, Octave JN (2007) Fe65 does not stabilize AICD during activation of transcription in a luciferase assay. Biochem Biophys Res Commun 361:317–22.

International Genomics of Alzheimer's Disease Consortium (IGAP) (2014) Convergent genetic and expression data implicate immunity in Alzheimer's disease. Alzheimers Dement .

Jariel-Encontre I, Bossis G, Piechaczyk M (2008) Ubiquitin-independent degradation of proteins by the proteasome. Biochim Biophys Acta 1786:153–77.

Jin J, Li X, Gygi SP, Harper JW (2007) Dual E1 activation systems for ubiquitin differentially regulate E2 enzyme charging. Nature 447:1135–8.

Ju D, Xie Y (2004) Proteasomal degradation of RPN4 via two distinct mechanisms, ubiquitin-dependent and -independent. J Biol Chem 279:23851–4.

Kaden D, Voigt P, Munter LM, Bobowski KD, Schaefer M, Multhaup G (2009) Subcellular localization and dimerization of APLP1 are strikingly different from APP and APLP2. J Cell Sci 122:368–77.

Kamenetz F, Tomita T, Hsieh H, Seabrook G, Borchelt D, Iwatsubo T, Sisodia S, Malinow R (2003) APP processing and synaptic function. Neuron 37:925–37.

Kang J, Lemaire HG, Unterbeck A, Salbaum JM, Masters CL, Grzeschik KH, Multhaup G, Beyreuther K, Muller-Hill B (1987) The precursor of Alzheimer's disease amyloid A4 protein resembles a cell-surface receptor. Nature 325:733–6.

Kapuria V, Peterson LF, Showalter HDH, Kirchhoff PD, Talpaz M, Donato NJ (2011) Protein cross-linking as a novel mechanism of action of a ubiquitin-activating enzyme inhibitor with anti-tumor activity. Biochem Pharmacol 82:341–9.

Karran E, Mercken M, De Strooper B (2011) The amyloid cascade hypothesis for Alzheimer's disease: an appraisal for the development of therapeutics. Nat Rev Drug Discov 10:698–712.

Keller JN, Hanni KB, Markesbery WR (2000) Impaired proteasome function in Alzheimer's disease. J Neurochem 75:436–9.

Kesavapany S, Banner SJ, Lau KF, Shaw CE, Miller CCJ, Cooper JD, McLoughlin DM (2002) Expression of the Fe65 adapter protein in adult and developing mouse brain. Neuroscience 115:951–60.

Kim HS, Kim EM, Lee JP, Park CH, Kim S, Seo JH, Chang KA, Yu E, Jeong SJ, Chong YH, Suh YH (2003) C-terminal fragments of amyloid precursor protein exert neurotoxicity by inducing glycogen synthase kinase-3beta expression. FASEB J 17:1951–3.

Kim MY, Mo JS, Ann EJ, Yoon JH, Jung J, Choi YH, Kim SM, Kim HY, Ahn JS, Kim H, Kim K, Hoe HS, Park HS (2011) Regulation of Notch1 signaling by the APP intracellular domain facilitates degradation of the Notch1 intracellular domain and RBP-Jk. J Cell Sci 124:1831–43.

Kimberly WT, Zheng JB, Guenette SY, Selkoe DJ (2001) The intracellular domain of the beta-amyloid precursor protein is stabilized by Fe65 and translocates to the nucleus in a notch-like manner. J Biol Chem 276:40288–92.

Kimura Y, Tanaka K (2010) Regulatory mechanisms involved in the control of ubiquitin homeostasis. J Biochem 147:793–8.

Kinoshita A, Whelan CM, Berezovska O, Hyman BT (2002) The gamma secretase-generated carboxyl-terminal domain of the amyloid precursor protein induces apoptosis via Tip60 in H4 cells. J Biol Chem 277:28530–6.

Kleijnen MF, Shih AH, Zhou P, Kumar S, Soccio RE, Kedersha NL, Gill G, Howley PM (2000) The hPLIC proteins may provide a link between the ubiquitination machinery and the proteasome. Mol Cell 6:409–19.

Knobloch M, Konietzko U, Krebs DC, Nitsch RM (2007) Intracellular Abeta and cognitive deficits precede beta-amyloid deposition in transgenic arcAbeta mice. Neurobiol Aging 28:1297–306.

Kohli BM, Pflieger D, Mueller LN, Carbonetti G, Aebersold R, Nitsch RM, Konietzko U (2012) Interactome of the amyloid precursor protein APP in brain reveals a protein network involved in synaptic vesicle turnover and a close association with Synaptotagmin-1. J Proteome Res 11:4075—4090.

Konietzko U, Goodger ZV, Meyer M, Kohli BM, Bosset J, Lahiri DK, Nitsch RM (2010) Co-localization of the amyloid precursor protein and Notch intracellular domains in nuclear transcription factories. Neurobiol Aging 31:58–73.

Kozik P, Francis RW, Seaman MNJ, Robinson MS (2010) A screen for endocytic motifs. Traffic 11:843–55.

Kravtsova-Ivantsiv Y, Ciechanover A (2012) Non-canonical ubiquitin-based signals for proteasomal degradation. J Cell Sci 125:539–48.

Kuan YH, Gruebl T, Soba P, Eggert S, Nesic I, Back S, Kirsch J, Beyreuther K, Kins S (2006) PAT1a modulates intracellular transport and processing of amyloid precursor protein (APP), APLP1, and APLP2. J Biol Chem 281:40114–23.

Lam YA, Pickart CM, Alban A, Landon M, Jamieson C, Ramage R, Mayer RJ, Layfield R (2000) Inhibition of the ubiquitin-proteasome system in Alzheimer's disease. Proc Natl Acad Sci USA 97:9902–6.

Lee EJ, Hyun S, Chun J, Shin SH, Kang SS (2009) Ubiquitylation of Fe65 adaptor protein by neuronal precursor cell expressed developmentally down regulated 4-2 (Nedd4-2) via the WW domain interaction with Fe65. Exp Mol Med 41:555–68.

Lee PCW, Sowa ME, Gygi SP, Harper JW (2011) Alternative ubiquitin activation/conjugation cascades interact with N-end rule ubiquitin ligases to control degradation of RGS proteins. Mol Cell 43:392–405.

Lenkkeri U, Kestila M, Lamerdin J, McCready P, Adamson A, Olsen A, Tryggvason K (1998) Structure of the human amyloid-precursor-like protein gene APLP1 at 19q13.1. Hum Genet 102:192–6.

Lévy F, Johnsson N, Rümenapf T, Varshavsky A (1996) Using ubiquitin to follow the metabolic fate of a protein. Proc Natl Acad Sci USA 93:4907–12.

Li H, Wang B, Wang Z, Guo Q, Tabuchi K, Hammer RE, Sudhof TC, Zheng H (2010) Soluble amyloid precursor protein (APP) regulates transthyretin and Klotho gene expression without rescuing the essential function of APP. Proc Natl Acad Sci USA 107:17362–7.

Li Q, Sudhof TC (2004) Cleavage of amyloid-beta precursor protein and amyloid-beta precursor-like protein by BACE 1. J Biol Chem 279:10542–50.

Lichtenthaler SF, Haass C, Steiner H (2011) Regulated intramembrane proteolysis–lessons from amyloid precursor protein processing. J Neurochem 117:779–96.

Liu Q, Zerbinatti CV, Zhang J, Hoe HS, Wang B, Cole SL, Herz J, Muglia L, Bu G (2007) Amyloid precursor protein regulates brain apolipoprotein E and cholesterol metabolism through lipoprotein receptor LRP1. Neuron 56:66–78.

Lorent K, Overbergh L, Moechars D, De Strooper B, Van Leuven F, Van den Berghe H (1995) Expression in mouse embryos and in adult mouse brain of three members of the amyloid precursor protein family, of the alpha-2-macroglobulin receptor/low density lipoprotein receptor-related protein and of its ligands apolipoprotein e, lipoprotein lipase, alpha-2-macroglobulin and the 40,000 molecular weight receptor-associated protein. Neuroscience 65:1009–25.

Lu DC, Rabizadeh S, Chandra S, Shayya RF, Ellerby LM, Ye X, Salvesen GS, Koo EH, Bredesen DE (2000) A second cytotoxic proteolytic peptide derived from amyloid beta-protein precursor. Nat Med 6:397–404.

Lupas AN, Koretke KK (2003) Bioinformatic analysis of ClpS, a protein module involved in prokaryotic and eukaryotic protein degradation. J Struct Biol 141:77–83.

Lyckman AW, Confaloni AM, Thinakaran G, Sisodia SS, Moya KL (1998) Post-translational processing and turnover kinetics of presynaptically targeted amyloid precursor superfamily proteins in the central nervous system. J Biol Chem 273:11100–6.

Ma H, Lesne S, Kotilinek L, Steidl-Nichols JV, Sherman M, Younkin L, Younkin S, Forster C, Sergeant N, Delacourte A, Vassar R, Citron M, Kofuji P, Boland LM,

Ashe KH (2007) Involvement of beta-site APP cleaving enzyme 1 (BACE1) in amyloid precursor protein-mediated enhancement of memory and activity-dependent synaptic plasticity. Proc Natl Acad Sci USA 104:8167–72.

Ma QH, Futagawa T, Yang WL, Jiang XD, Zeng L, Takeda Y, Xu RX, Bagnard D, Schachner M, Furley AJ, Karagogeos D, Watanabe K, Dawe GS, Xiao ZC (2008) A TAG1-APP signalling pathway through Fe65 negatively modulates neurogenesis. Nat Cell Biol 10:283–94.

Madeira A, Pommet JM, Prochiantz A, Allinquant B (2005) SET protein (TAF1beta, I2PP2A) is involved in neuronal apoptosis induced by an amyloid precursor protein cytoplasmic subdomain. FASEB J 19:1905–7.

Maretto S, Cordenonsi M, Dupont S, Braghetta P, Broccoli V, Hassan AB, Volpin D, Bressan GM, Piccolo S (2003) Mapping Wnt/beta-catenin signaling during mouse development and in colorectal tumors. Proc Natl Acad Sci USA 100:3299–304.

Matrone C, Luvisetto S, La Rosa LR, Tamayev R, Pignataro A, Canu N, Yang L, Barbagallo APM, Biundo F, Lombino F, Zheng H, Ammassari-Teule M, D'Adamio L (2012) Tyr682 in the Aβ-precursor protein intracellular domain regulates synaptic connectivity, cholinergic function, and cognitive performance. Aging Cell 11:1084–93.

Mattson MP, Cheng B, Culwell AR, Esch FS, Lieberburg I, Rydel RE (1993) Evidence for excitoprotective and intraneuronal calcium-regulating roles for secreted forms of the beta-amyloid precursor protein. Neuron 10:243–54.

Mayeux R, Stern Y (2012) Epidemiology of Alzheimer disease. Cold Spring Harb Perspect Med 2:a006239.

Merdes G, Soba P, Loewer A, Bilic MV, Beyreuther K, Paro R (2004) Interference of human and Drosophila APP and APP-like proteins with PNS development in Drosophila. Embo J 23:4082–95.

Moehlmann T, Winkler E, Xia X, Edbauer D, Murrell J, Capell A, Kaether C, Zheng H, Ghetti B, Haass C, Steiner H (2002) Presenilin-1 mutations of leucine 166 equally affect the generation of the Notch and APP intracellular domains independent of their effect on Abeta 42 production. Proc Natl Acad Sci USA 99:8025–30.

Morel E, Chamoun Z, Lasiecka ZM, Chan RB, Williamson RL, Vetanovetz C, Dall'Armi C, Simoes S, Point Du Jour KS, McCabe BD, Small SA, Di Paolo G (2013) Phosphatidylinositol-3-phosphate regulates sorting and processing of amyloid precursor protein through the endosomal system. Nat Commun 4:2250.

Mott RT, Hulette CM (2005) Neuropathology of Alzheimer's disease. Neuroimaging Clin N Am 15:755–65, ix.

Muller T, Meyer HE, Egensperger R, Marcus K (2008) The amyloid precursor protein intracellular domain (AICD) as modulator of gene expression, apoptosis, and cytoskeletal dynamics-relevance for Alzheimer's disease. Prog Neurobiol 85:393–406.

Müller U, Wild K (2013) Structure and Function of the APP Intracellular domain in Health and Disease. In: Understanding Alzheimer's Disease. InTech.

Müller UC, Zheng H (2012) Physiological functions of APP family proteins. Cold Spring Harb Perspect Med 2:a006288.

Nakayama K, Ohkawara T, Hiratochi M, Koh CS, Nagase H (2008) The intracellular domain of amyloid precursor protein induces neuron-specific apoptosis. Neurosci Lett 444:127–31.

Nikolaev A, McLaughlin T, O'Leary DDM, Tessier-Lavigne M (2009) APP binds DR6 to trigger axon pruning and neuron death via distinct caspases. Nature 457:981–9.

Nunan J, Williamson NA, Hill AF, Sernee MF, Masters CL, Small DH (2003) Proteasome-mediated degradation of the C-terminus of the Alzheimer's disease beta-amyloid protein precursor: effect of C-terminal truncation on production of beta-amyloid protein. J Neurosci Res 74:378–85.

Olsson F, Schmidt S, Althoff V, Munter LM, Jin S, Rosqvist S, Lendahl U, Multhaup G, Lundkvist J (2014) Characterization of intermediate steps in amyloid beta (Aβ) production under near-native conditions. J Biol Chem 289:1540–50.

Pardossi-Piquard R, Checler F (2012) The physiology of the beta-amyloid precursor protein intracellular domain AICD. J Neurochem 120 Suppl 1:109–24.

Pardossi-Piquard R, Petit A, Kawarai T, Sunyach C, Alves da Costa C, Vincent B, Ring S, D'Adamio L, Shen J, Müller U, St George Hyslop P, Checler F (2005) Presenilin-dependent transcriptional control of the Abeta-degrading enzyme neprilysin by intracellular domains of betaAPP and APLP. Neuron 46:541–54.

Pastorino L, Ikin AF, Lamprianou S, Vacaresse N, Revelli JP, Platt K, Paganetti P, Mathews PM, Harroch S, Buxbaum JD (2004) BACE (beta-secretase) modulates the processing of APLP2 in vivo. Mol Cell Neurosci 25:642–9.

Peña MMO, Xing YY, Koli S, Berger FG (2006) Role of N-terminal residues in the ubiquitin-independent degradation of human thymidylate synthase. Biochem J 394:355–63.

Perl DP (2010) Neuropathology of Alzheimer's disease. Mt Sinai J Med 77:32–42.

Pickart CM (2001) Mechanisms underlying ubiquitination. Annu Rev Biochem 70:503–33.

Pimplikar SW, Suryanarayana A (2011) Detection of APP intracellular domain in brain tissue. Methods in molecular biology 670:85–91.

Pinnix I, Musunuru U, Tun H, Sridharan A, Golde T, Eckman C, Ziani-Cherif C, Onstead L, Sambamurti K (2001) A novel gamma-secretase assay based on detection of the putative C-terminal fragment-gamma of amyloid beta protein precursor. J Biol Chem 276:481–7.

Qi-Takahara Y, Morishima-Kawashima M, Tanimura Y, Dolios G, Hirotani N, Horikoshi Y, Kametani F, Maeda M, Saido TC, Wang R, Ihara Y (2005) Longer forms of amyloid beta protein: implications for the mechanism of intramembrane cleavage by gamma-secretase. J Neurosci 25:436–45.

Radzimanowski J, Simon B, Sattler M, Beyreuther K, Sinning I, Wild K (2008) Structure of the intracellular domain of the amyloid precursor protein in complex with Fe65-PTB2. EMBO Rep 9:1134–40.

Ramelot TA, Gentile LN, Nicholson LK (2000) Transient structure of the amyloid precursor protein cytoplasmic tail indicates preordering of structure for binding to cytosolic factors. Biochemistry 39:2714–25.

Ravid T, Hochstrasser M (2008) Diversity of degradation signals in the ubiquitin-proteasome system. Nat Rev Mol Cell Biol 9:679–90.

Riederer BM, Leuba G, Vernay A, Riederer IM (2011) The role of the ubiquitin proteasome system in Alzheimer's disease. Exp Biol Med (Maywood) 236:268–76.

Ring S, Weyer SW, Kilian SB, Waldron E, Pietrzik CU, Filippov MA, Herms J, Buchholz C, Eckman CB, Korte M, Wolfer DP, Muller UC (2007) The secreted beta-amyloid precursor protein ectodomain APPs alpha is sufficient to rescue the anatomical, behavioral, and electrophysiological abnormalities of APP-deficient mice. J Neurosci 27:7817–26.

Ryman DC, Acosta-Baena N, Aisen PS, Bird T, Danek A, Fox NC, Goate A, Frommelt P, Ghetti B, Langbaum JBS, Lopera F, Martins R, Masters CL, Mayeux RP, McDade E, Moreno S, Reiman EM, Ringman JM, Salloway S, Schofield PR, Sperling R, Tariot PN, Xiong C, Morris JC, Bateman RJ, Dominantly Inherited Alzheimer Network (2014) Symptom onset in autosomal dominant Alzheimer disease: a systematic review and meta-analysis. Neurology 83:253–60.

Sabo SL, Ikin AF, Buxbaum JD, Greengard P (2003) The amyloid precursor protein and its regulatory protein, FE65, in growth cones and synapses in vitro and in vivo. J Neurosci 23:5407–15.

Sapountzi V, Logan IR, Robson CN (2006) Cellular functions of TIP60. Int J Biochem Cell Biol 38:1496–509.

Sato T, Dohmae N, Qi Y, Kakuda N, Misonou H, Mitsumori R, Maruyama H, Koo EH, Haass C, Takio K, Morishima-Kawashima M, Ishiura S, Ihara Y (2003) Potential link between amyloid beta-protein 42 and C-terminal fragment gamma 49-99 of beta-amyloid precursor protein. J Biol Chem 278:24294–301.

Scheinfeld MH, Ghersi E, Laky K, Fowlkes BJ, D'Adamio L (2002) Processing of beta-amyloid precursor-like protein-1 and -2 by gamma-secretase regulates transcription. J Biol Chem 277:44195–201.

Scheinfeld MH, Matsuda S, D'Adamio L (2003) JNK-interacting protein-1 promotes transcription of A beta protein precursor but not A beta precursor-like proteins, mechanistically different than Fe65. Proc Natl Acad Sci USA 100:1729–34.

Schulman BA, Harper JW (2009) Ubiquitin-like protein activation by E1 enzymes: the apex for downstream signalling pathways. Nat Rev Mol Cell Biol 10:319–31.

Seabrook GR, Smith DW, Bowery BJ, Easter A, Reynolds T, Fitzjohn SM, Morton RA, Zheng H, Dawson GR, Sirinathsinghji DJ, Davies CH, Collingridge GL, Hill RG (1999) Mechanisms contributing to the deficits in hippocampal synaptic plasticity in mice lacking amyloid precursor protein. Neuropharmacology 38:349–59.

Selkoe DJ (2001) Alzheimer's disease: genes, proteins, and therapy. Physiol Rev 81:741–66.

Shankar GM, Welzel AT, McDonald JM, Selkoe DJ, Walsh DM (2011) Isolation of low-n amyloid beta-protein oligomers from cultured cells, CSF, and brain. Methods Mol Biol 670:33–44.

Shen J, Kelleher r R J (2007) The presenilin hypothesis of Alzheimer's disease: evidence for a loss-of-function pathogenic mechanism. Proc Natl Acad Sci USA 104:403–9.

Slunt HH, Thinakaran G, Von Koch C, Lo AC, Tanzi RE, Sisodia SS (1994) Expression of a ubiquitous, cross-reactive homologue of the mouse beta-amyloid precursor protein (APP). J Biol Chem 269:2637–44.

Smith E, Claudinot S, Lehal R, Pellegrinet L, Barrandon Y, Radtke F (2012) Generation and characterization of a Notch1 signaling-specific reporter mouse line. Genesis 50:700–10.

Soba P, Eggert S, Wagner K, Zentgraf H, Siehl K, Kreger S, Lower A, Langer A, Merdes G, Paro R, Masters CL, Muller U, Kins S, Beyreuther K (2005) Homo- and heterodimerization of APP family members promotes intercellular adhesion. Embo J 24:3624–34.

Sriram S, Lee JH, Mai BK, Jiang Y, Kim Y, Yoo YD, Banerjee R, Lee SH, Lee MJ (2013) Development and characterization of monomeric N-end rule inhibitors through in vitro model substrates. J Med Chem 56:2540–6.

Sriram SM, Kim BY, Kwon YT (2011) The N-end rule pathway: emerging functions and molecular principles of substrate recognition. Nat Rev Mol Cell Biol 12:735–47.

Stahl R, Schilling S, Soba P, Rupp C, Hartmann T, Wagner K, Merdes G, Eggert S, Kins S (2014) Shedding of APP limits its synaptogenic activity and cell adhesion properties. Front Cell Neurosci 8:410.

Stieren ES, El Ayadi A, Xiao Y, Siller E, Landsverk ML, Oberhauser AF, Barral JM, Boehning D (2011) Ubiquilin-1 is a molecular chaperone for the amyloid precursor protein. J Biol Chem 286:35689–98.

Sun Y, Jiang X, Price BD (2010) Tip60: connecting chromatin to DNA damage signaling. Cell Cycle 9:930–6.

Svedružić ZM, Popović K, Smoljan I, Sendula-Jengić V (2012) Modulation of γ-secretase activity by multiple enzyme-substrate interactions: implications in pathogenesis of Alzheimer's disease. PLoS One 7:e32293.

Takalo M, Haapasalo A, Natunen T, Viswanathan J, Kurkinen KM, Tanzi RE, Soininen H, Hiltunen M (2013) Targeting ubiquilin-1 in Alzheimer's disease. Expert Opin Ther Targets 17:795–810.

Tanzi RE, Haines JL, Watkins PC, Stewart GD, Wallace MR, Hallewell R, Wong C, Wexler NS, Conneally PM, Gusella JF (1988) Genetic linkage map of human chromosome 21. Genomics 3:129–36.

Tapiola T, Pennanen C, Tapiola M, Tervo S, Kivipelto M, Hänninen T, Pihlajamäki M, Laakso MP, Hallikainen M, Hämäläinen A, Vanhanen M, Helkala EL, Vanninen R, Nissinen A, Rossi R, Frisoni GB, Soininen H (2008) MRI of hippocampus and entorhinal cortex in mild cognitive impairment: a follow-up study. Neurobiol Aging 29:31–8.

Tasaki T, Kwon YT (2007) The mammalian N-end rule pathway: new insights into its components and physiological roles. Trends Biochem Sci 32:520–8.

Tasaki T, Mulder LCF, Iwamatsu A, Lee MJ, Davydov IV, Varshavsky A, Muesing M, Kwon YT (2005) A family of mammalian E3 ubiquitin ligases that contain the UBR box motif and recognize N-degrons. Mol Cell Biol 25:7120–36.

Tasaki T, Sriram SM, Park KS, Kwon YT (2012) The N-end rule pathway. Annu Rev Biochem 81:261–89.

Taylor JM, Song YJ, Huang Y, Farrer MJ, Delatycki MB, Halliday GM, Lockhart PJ (2007) Parkin co-regulated gene (PACRG) is regulated by the ubiquitin-proteasomal system and is present in the pathological features of parkinsonian diseases. Neurobiology of disease 27:238–47.

Thinakaran G, Koo EH (2008) Amyloid precursor protein trafficking, processing, and function. J Biol Chem 283:29615–9.

Tsvetkov P, Reuven N, Shaul Y (2009) The nanny model for IDPs. Nat Chem Biol 5:778–81.

Tyan SH, Shih AY, Walsh JJ, Maruyama H, Sarsoza F, Ku L, Eggert S, Hof PR, Koo EH, Dickstein DL (2012) Amyloid precursor protein (APP) regulates synaptic structure and function. Mol Cell Neurosci 51:43–52.

van der Veen AG, Ploegh HL (2012) Ubiquitin-like proteins. Annu Rev Biochem 81:323–57.

Van Nostrand WE, Schmaier AH, Neiditch BR, Siegel RS, Raschke WC, Sisodia SS, Wagner SL (1994) Expression, purification, and characterization of the kunitz-type proteinase inhibitor domain of the amyloid beta-protein precursor-like protein-2. Biochim Biophys Acta 1209:165–70.

Varshavsky A (1992) The N-end rule. Cell 69:725–35.

Varshavsky A (2011) The N-end rule pathway and regulation by proteolysis. Protein Science 20:1298–1345.

Varshavsky A, Byrd C (1996) The N-end rule: Functions, mysteries, uses. Molecular Biology of the Cell 7:2946–2946.

Verma R, Deshaies RJ (2000) A proteasome howdunit: the case of the missing signal. Cell 101:341–4.

Vingtdeux V, Hamdane M, Begard S, Loyens A, Delacourte A, Beauvillain JC, Buee L, Marambaud P, Sergeant N (2007) Intracellular pH regulates amyloid precursor protein intracellular domain accumulation. Neurobiol Dis 25:686–96.

Viswanathan J, Haapasalo A, Kurkinen KMA, Natunen T, Mäkinen P, Bertram L, Soininen H, Tanzi RE, Hiltunen M (2013) Ubiquilin-1 modulates γ-secretase-mediated ε-site cleavage in neuronal cells. Biochemistry 52:3899–912.

von Koch CS, Zheng H, Chen H, Trumbauer M, Thinakaran G, van der Ploeg LH, Price DL, Sisodia SS (1997) Generation of APLP2 KO mice and early postnatal lethality in APLP2/APP double KO mice. Neurobiol Aging 18:661–9.

von Rotz RC, Kohli BM, Bosset J, Meier M, Suzuki T, Nitsch RM, Konietzko U (2004) The APP intracellular domain forms nuclear multiprotein complexes and regulates the transcription of its own precursor. J Cell Sci 117:4435–48.

Walsh DM, Fadeeva JV, LaVoie MJ, Paliga K, Eggert S, Kimberly WT, Wasco W, Selkoe DJ (2003) gamma-Secretase cleavage and binding to FE65 regulate the nuclear translocation of the intracellular C-terminal domain (ICD) of the APP family of proteins. Biochemistry 42:6664–73.

Wang P, Yang G, Mosier DR, Chang P, Zaidi T, Gong YD, Zhao NM, Dominguez B, Lee KF, Gan WB, Zheng H (2005) Defective neuromuscular synapses in mice lacking amyloid precursor protein (APP) and APP-Like protein 2. J Neurosci 25:1219–25.

Wasco W, Bupp K, Magendantz M, Gusella JF, Tanzi RE, Solomon F (1992) Identification of a mouse brain cDNA that encodes a protein related to the Alzheimer disease-associated amyloid beta protein precursor. Proc Natl Acad Sci USA 89:10758–62.

Wasco W, Gurubhagavatula S, Paradis MD, Romano DM, Sisodia SS, Hyman BT, Neve RL, Tanzi RE (1993) Isolation and characterization of APLP2 encoding a homologue of the Alzheimer's associated amyloid beta protein precursor. Nat Genet 5:95–100.

Watanabe T, Hikichi Y, Willuweit A, Shintani Y, Horiguchi T (2012) FBL2 regulates amyloid precursor protein (APP) metabolism by promoting ubiquitination-dependent APP degradation and inhibition of APP endocytosis. J Neurosci 32:3352–65.

Weyer SW, Klevanski M, Delekate A, Voikar V, Aydin D, Hick M, Filippov M, Drost N, Schaller KL, Saar M, Vogt MA, Gass P, Samanta A, Jaschke A, Korte M, Wolfer DP, Caldwell JH, Muller UC (2011) APP and APLP2 are essential at PNS and CNS synapses for transmission, spatial learning and LTP. EMBO J 30:2266–80.

Wiley JC, Hudson M, Kanning KC, Schecterson LC, Bothwell M (2005) Familial Alzheimer's disease mutations inhibit gamma-secretase-mediated liberation of beta-amyloid precursor protein carboxy-terminal fragment. J Neurochem 94:1189–201.

Wimo A, Prince M (2010) World Alzheimer Report 2010 - the global economic impact of dementia. Technical report, Alzheimer's Disease International.

Winston JT, Koepp DM, Zhu C, Elledge SJ, Harper JW (1999) A family of mammalian F-box proteins. Curr Biol 9:1180–2.

Wolfe MS (2007) When loss is gain: reduced presenilin proteolytic function leads to increased Abeta42/Abeta40. talking point on the role of presenilin mutations in Alzheimer disease. EMBO Rep 8:136–40.

Yanagida K, Okochi M, Tagami S, Nakayama T, Kodama TS, Nishitomi K, Jiang J, Mori K, Tatsumi S, Arai T, Ikeuchi T, Kasuga K, Tokuda T, Kondo M, Ikeda M, Deguchi K, Kazui H, Tanaka T, Morihara T, Hashimoto R, Kudo T, Steiner H, Haass C, Tsuchiya K, Akiyama H, Kuwano R, Takeda M (2009) The 28-amino acid form of an APLP1-derived Abeta-like peptide is a surrogate marker for Abeta42 production in the central nervous system. EMBO Mol Med 1:223–35.

Yang Y, Kitagaki J, Dai RM, Tsai YC, Lorick KL, Ludwig RL, Pierre SA, Jensen JP, Davydov IV, Oberoi P, Li CCH, Kenten JH, Beutler JA, Vousden KH, Weissman AM (2007) Inhibitors of ubiquitin-activating enzyme (E1), a new class of potential cancer therapeutics. Cancer Res 67:9472–81.

Zhang YW, Wang R, Liu Q, Zhang H, Liao FF, Xu H (2007) Presenilin/gamma-secretase-dependent processing of beta-amyloid precursor protein regulates EGF receptor expression. Proc Natl Acad Sci USA 104:10613–8.

Zheng H, Jiang M, Trumbauer ME, Sirinathsinghji DJ, Hopkins R, Smith DW, Heavens RP, Dawson GR, Boyce S, Conner MW, Stevens KA, Slunt HH, Sisoda SS, Chen HY, Van der Ploeg LH (1995) beta-Amyloid precursor protein-deficient mice show reactive gliosis and decreased locomotor activity. Cell 81:525–31.

Zheng H, Koo EH (2011) Biology and pathophysiology of the amyloid precursor protein. Molecular neurodegeneration 6:27.